# MeV gamma-ray astronomy with COMPTEL reloaded

Andy Strong, Werner Collmar
MPE Garching

eAstrogam Workshop
Padova, 28 Feb – 2 Mar 2017
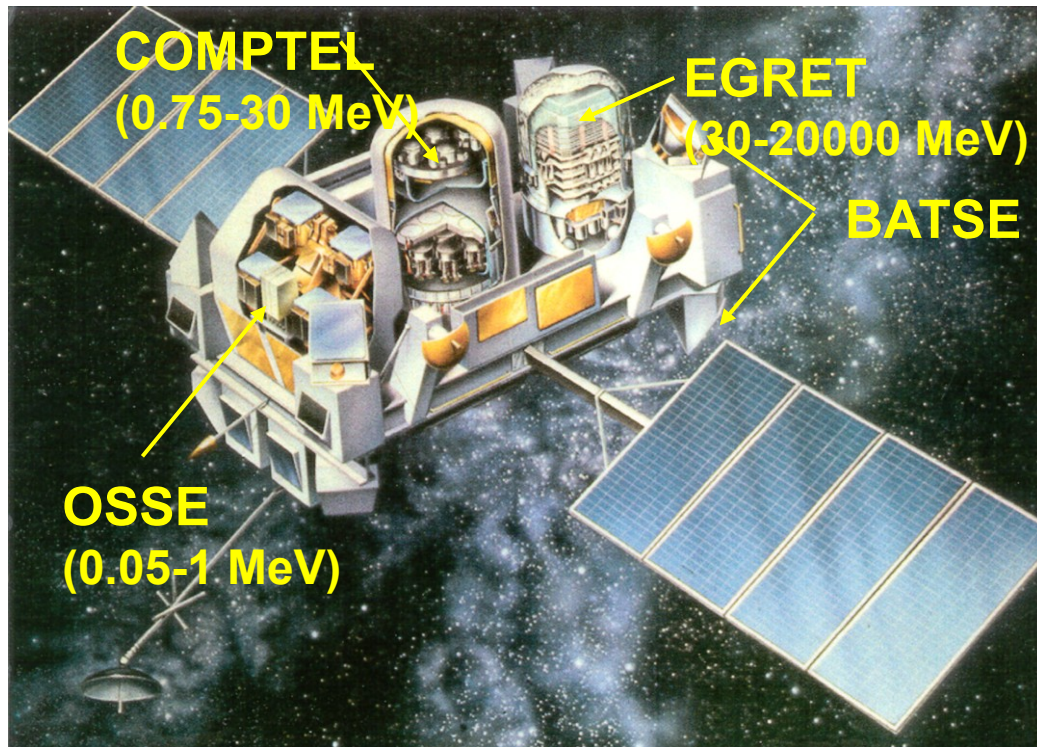
# MeV gamma-ray astronomy with COMPTEL reloaded

Andy Strong, Werner Collmar
MPE Garching

eAstrogam Workshop
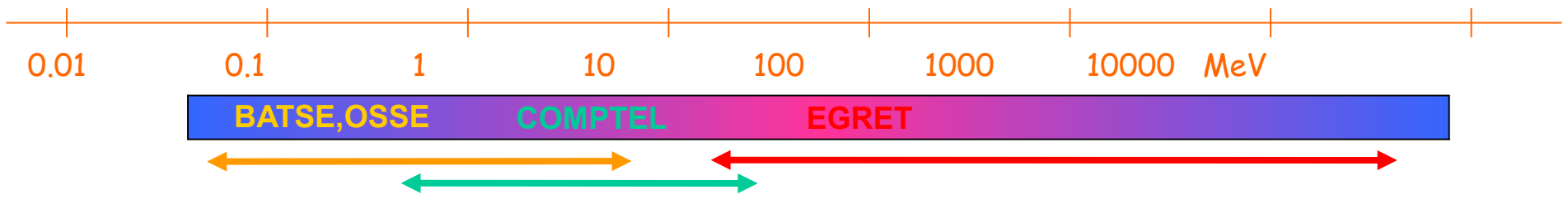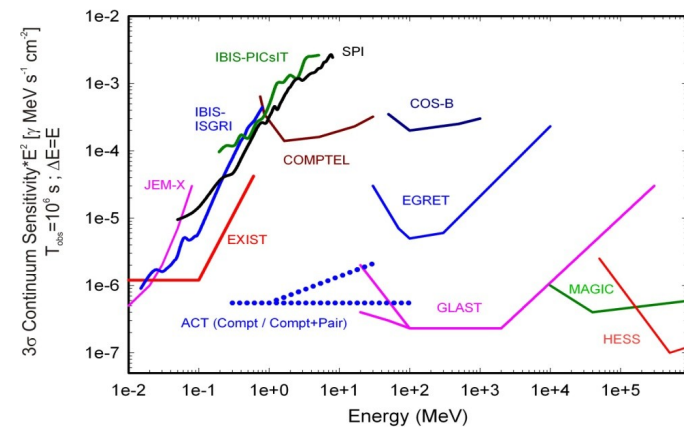Padova, 28 Feb – 2 Mar 2017

# COMPTEL on CGRO



COMPTEL
(0.75-30 MeV)

EGRET
(30-20000 MeV)

BATSE

OSSE
(0.05-1 MeV)

**COMPTEL** (Compton Telescope)
- mission: Apr. 91 – June 2000
- energy range: 0.75 – 30 MeV
- mounted parallel to EGRET
- "first-generation" experiment
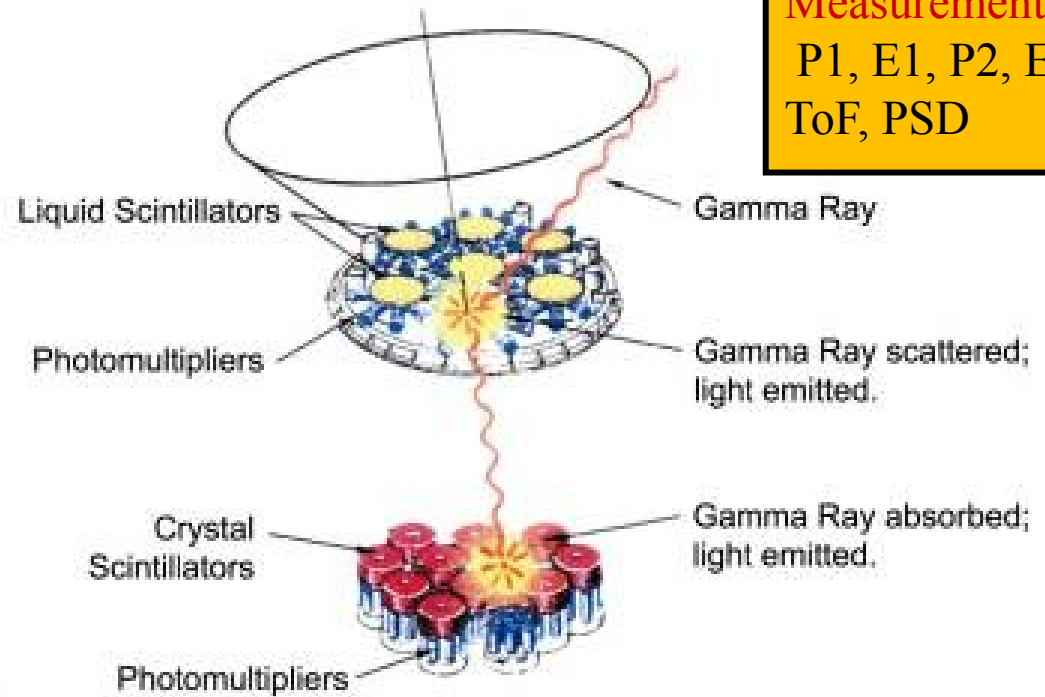- **pioneered MeV band**





| 0.01 | 0.1 | 1 | 10 | 100 | 1000 | 10000 | MeV |

BATSE,OSSE    COMPTEL    EGRET

# COMPton TELescope "COMPTEL"

2.60 m

1.70 m

**Detection Principle**

Measurements:
P1, E1, P2, E2
ToF, PSD

Liquid Scintillators — 

Photomultipliers — 

Crystal Scintillators — 

Photomultipliers — 

Gamma Ray

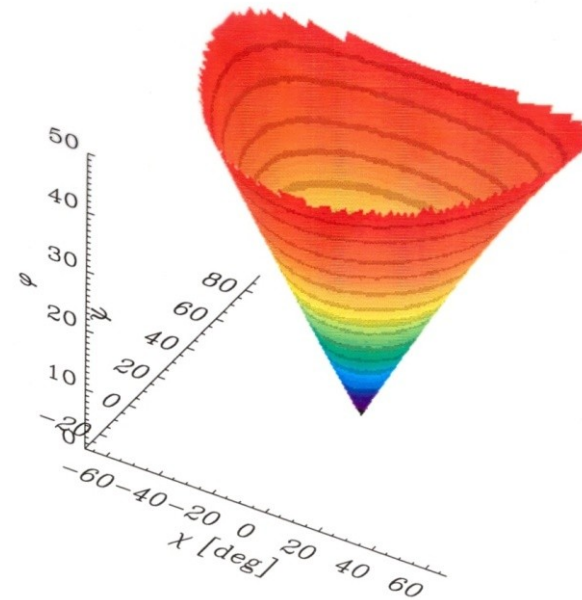Gamma Ray scattered; light emitted.

Gamma Ray absorbed; light emitted.

# COMPTEL Imaging Technique



Imaging Technique

Compton Telescope

$(\chi, \psi)$
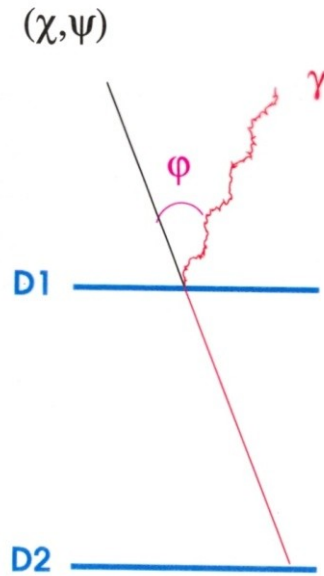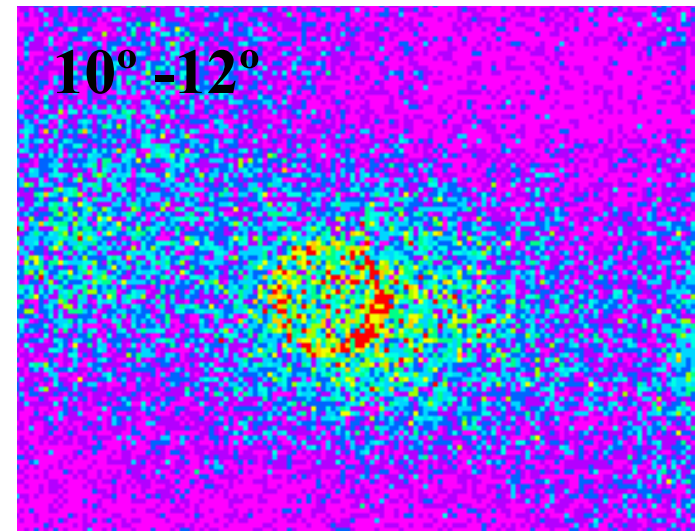
3D Dataspace & Spherical Distortion

# COMPTEL Event Data (Crab, 10 – 30 MeV)



4º -6º
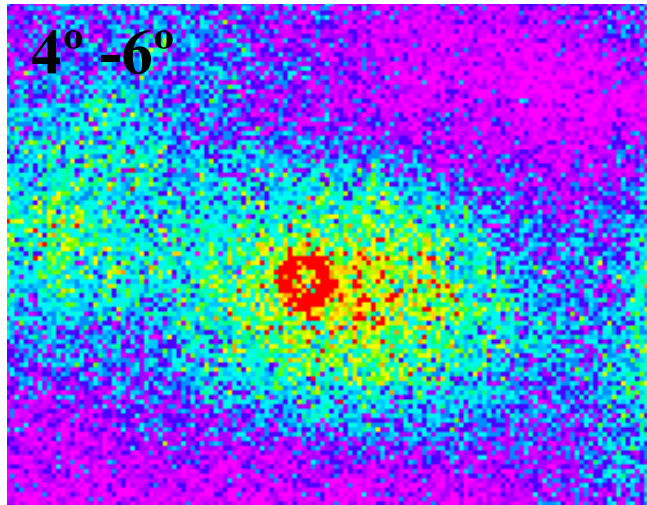
**Event File:
Layers in
Scatter Angle**

6º -8º

8º -10º

10º -12º
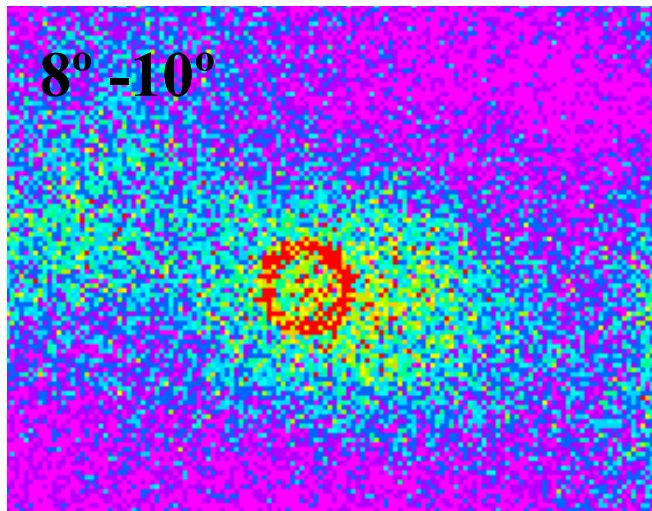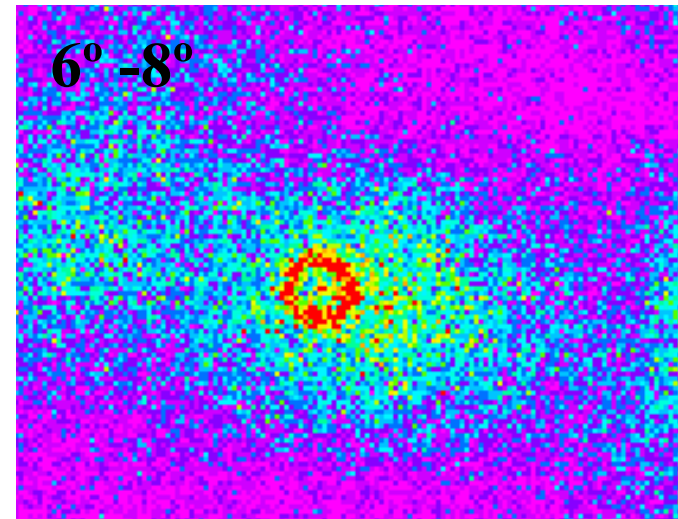
# COMPTEL Principle ("Event Circles")
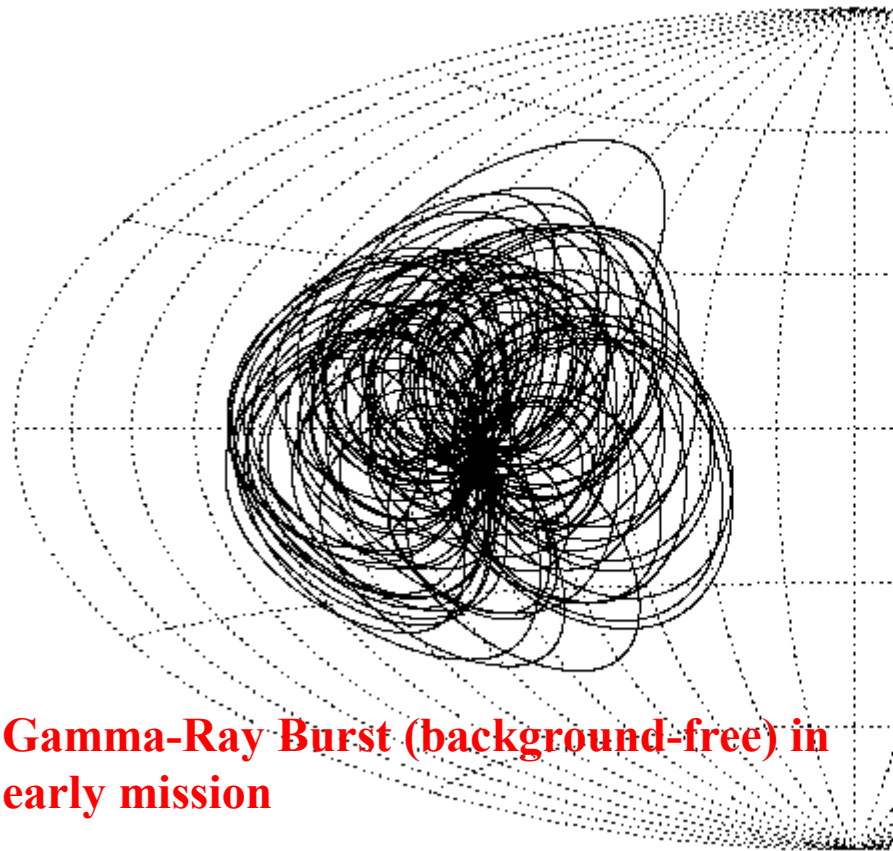
**Energy Range:** 0.75 – 30 MeV

**Field-of-View:** ~1sr (50% at 25°)

**Angular Resol.:** 2.4° at 1 MeV
**(1σ)** 1.3° at 10 MeV

**Energy Resol.:** 8.7% at 1 MeV
**(FWHM)** 5% at 10 MeV

**Effective Area:** 20 – 50 cm2

**Localisation:** ~0.5° (flux depend.)

Gamma-Ray Burst (background-free) in early mission

# COMPTEL ALL-Mission All-Sky Exposure



CGRO/COMPTEL All-Mission Exposure Map
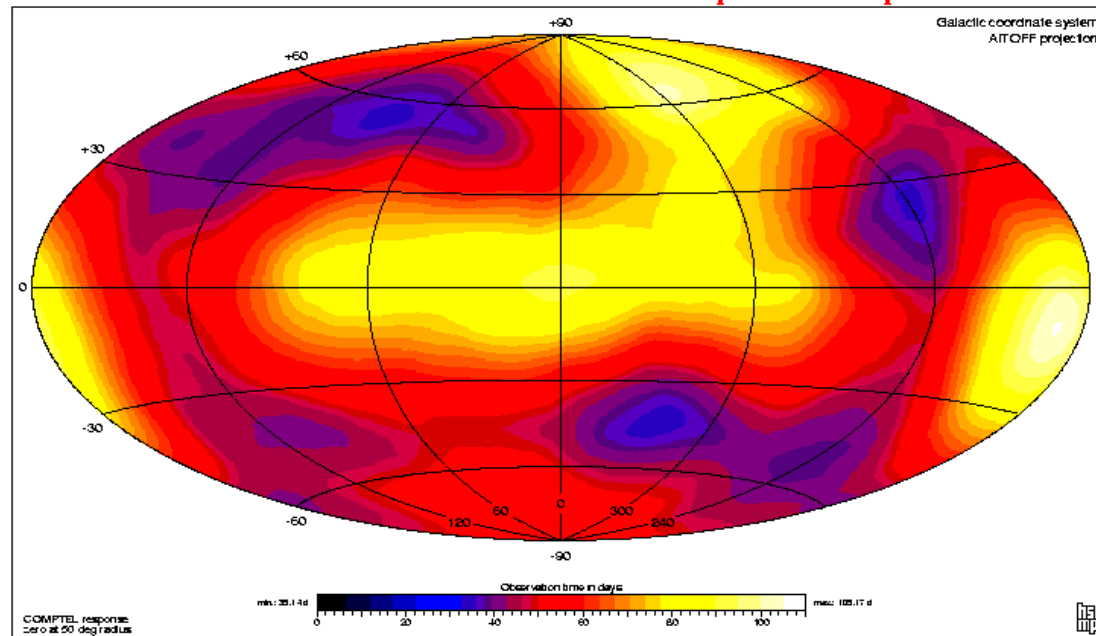
# Past COMPTEL Diffuse All-Sky Maps

Phase 1+2+3    10–30  MeV



$^{26}$Al



COMPTEL 1991–2000, ME 7
(Plüschke et al. 2001)
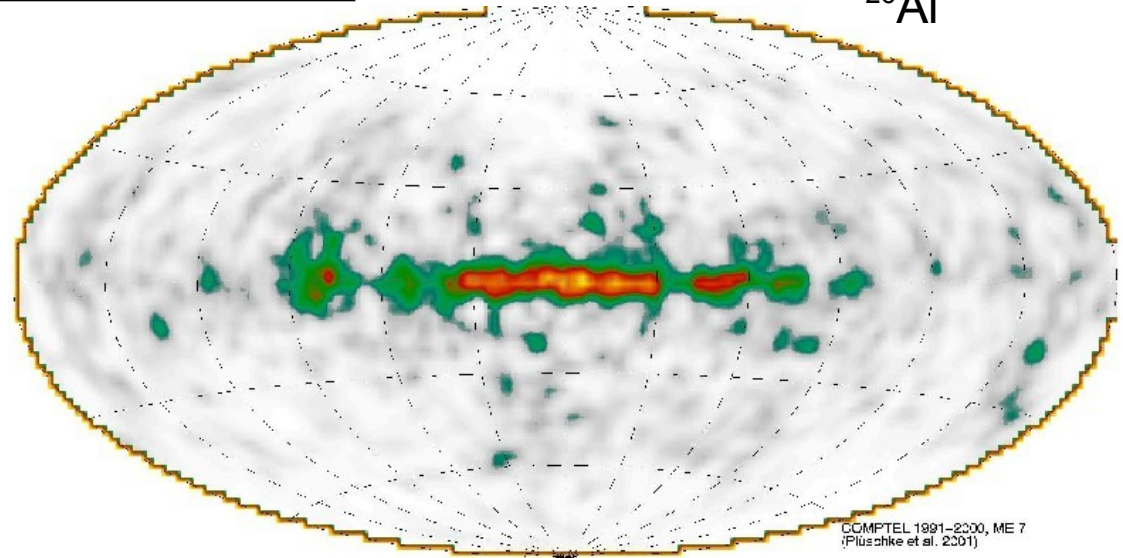
# Summary First COMPTEL Source Catalog



(Schönfelder et al. 2000)

Galactic coordinate system
AITOFF projection

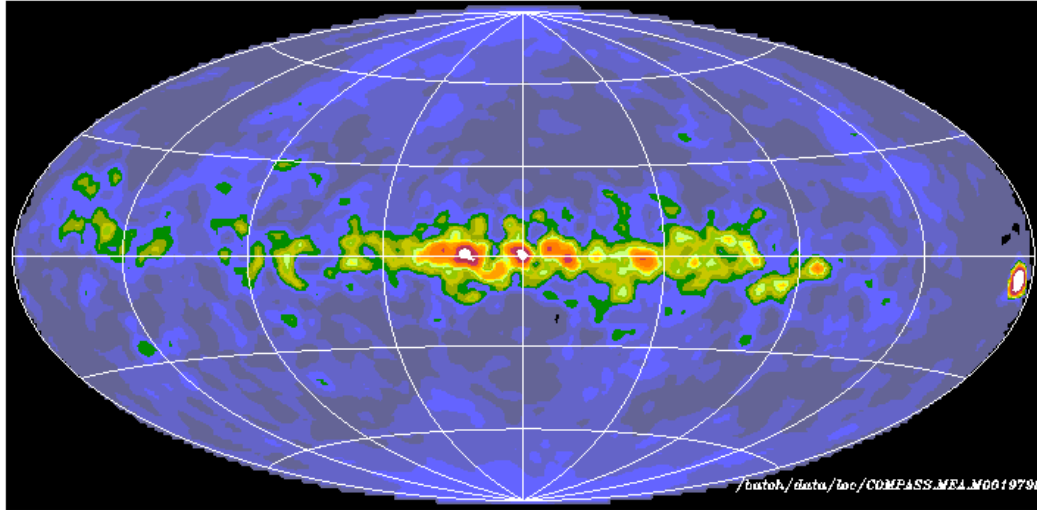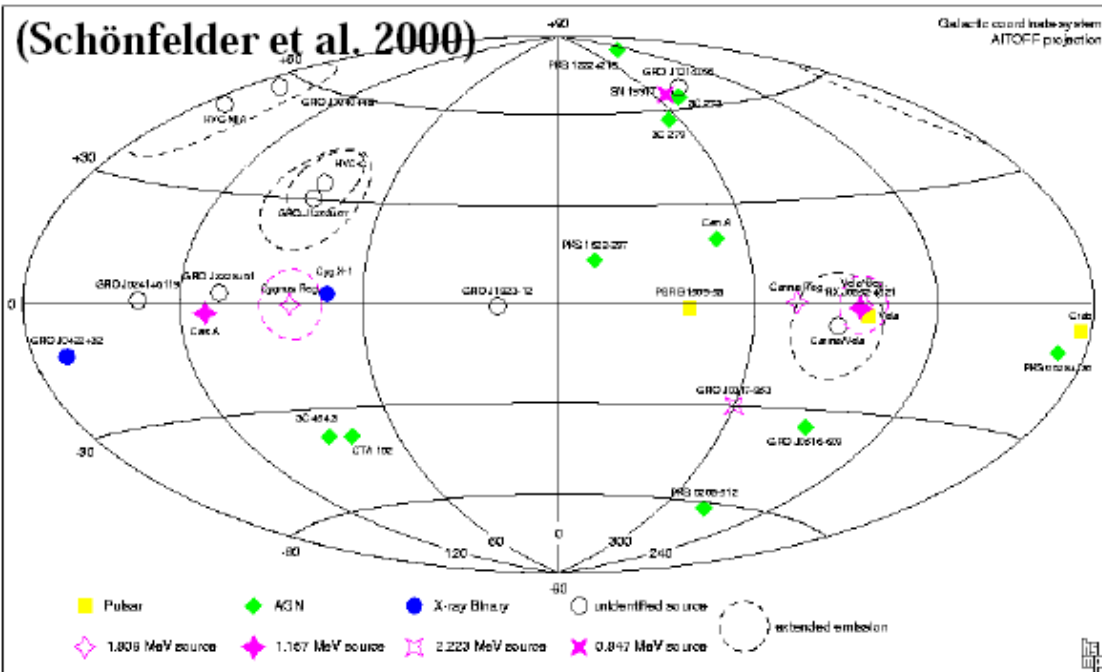| Source Type | # |
|---|---|
| Pulsars | 3 |
| Stellar BH | 2 |
| SNR (continuum) | 1 |
| AGN | 10 |
| Unidentified Sources | |
| - \|b\| < 10° | 4 |
| - \|b\| > 10° | 5 |
| γ-line sources | |
| - 1.809 MeV ($^{26}$Al) | 3 |
| - 1.157 MeV ($^{44}$Ti) | 2 |
| -0.847/1.238 MeV ($^{56}$Co) | 1 |
| - 2.223 MeV (n-capt.) | 1 |

- **contains published results of first 5.5 years (April ´91 – October ´96)**
- **32 Sources (different nature)**
- **31 GRBs / 21 solar flares**
- **upper limits for various types of objects (e.g. AGN, gal. BHs)**

# COMPTEL Analyses in 21. Century

## Why?

- 1. COMPTEL Catalog covers only part of the mission

- COMPTEL science not "fully" exploited
  - late-mission data not „really" explored
  - no whole-mission maps (apart 26Al)
  - no systematic source searches
  - no whole-mission analyses for signif. sources (excep. Crab)

- no more sensitive MeV mission for years

- improved computer power available

## How?

- software to automize the analyses
- systematic source searches by all-sky analyses (incl. diffuse model handling) for
  - different time periods
  - different energy bands (std.: 0.75-1, 1-3, 3-10,10-30 MeV; revised bands )
- goal: 2. COMPTEL Source Catalog
  - several other scientific issues

- effort to improve COMPTEL sensitivity

# NEW All-Mission All-Sky Point Source Map (1 –3 MeV)

(extragalactic / galactic / unknown sources)
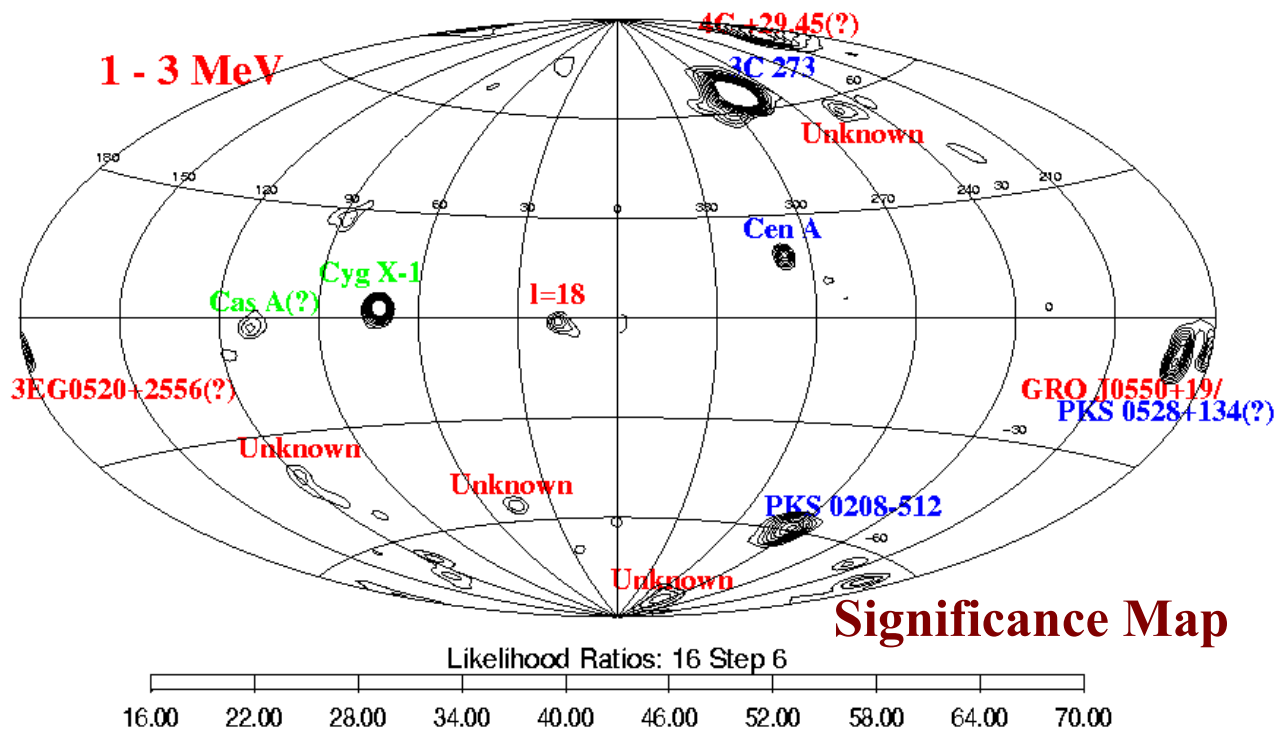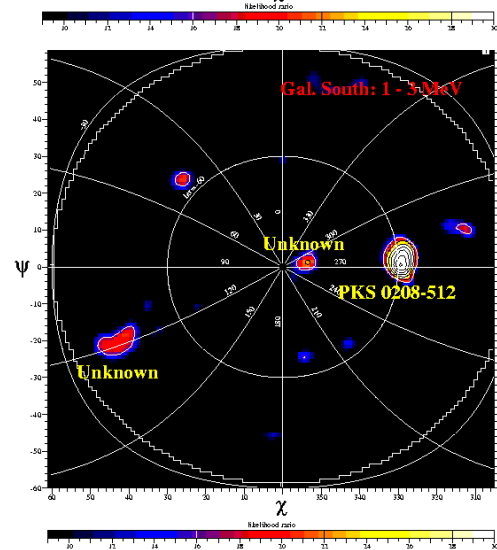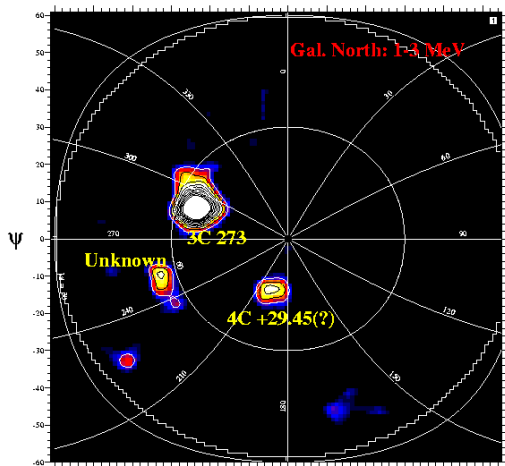
# NEW All-Mission All-Sky Point Source Map (3 - 10 MeV)

(extragalactic / galactic / unknown sources)
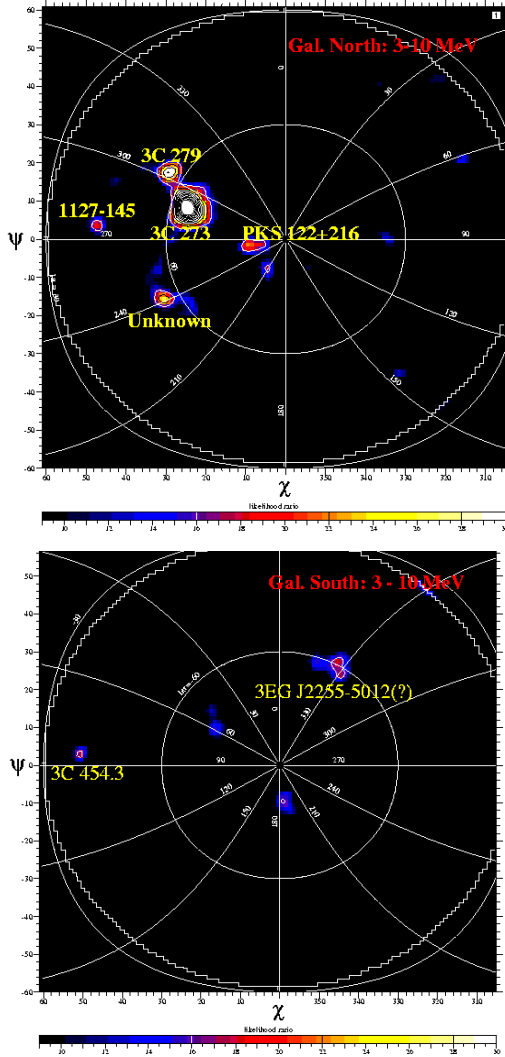
# NEW All-Mission All-Sky Point Source Map (10 - 30 MeV)
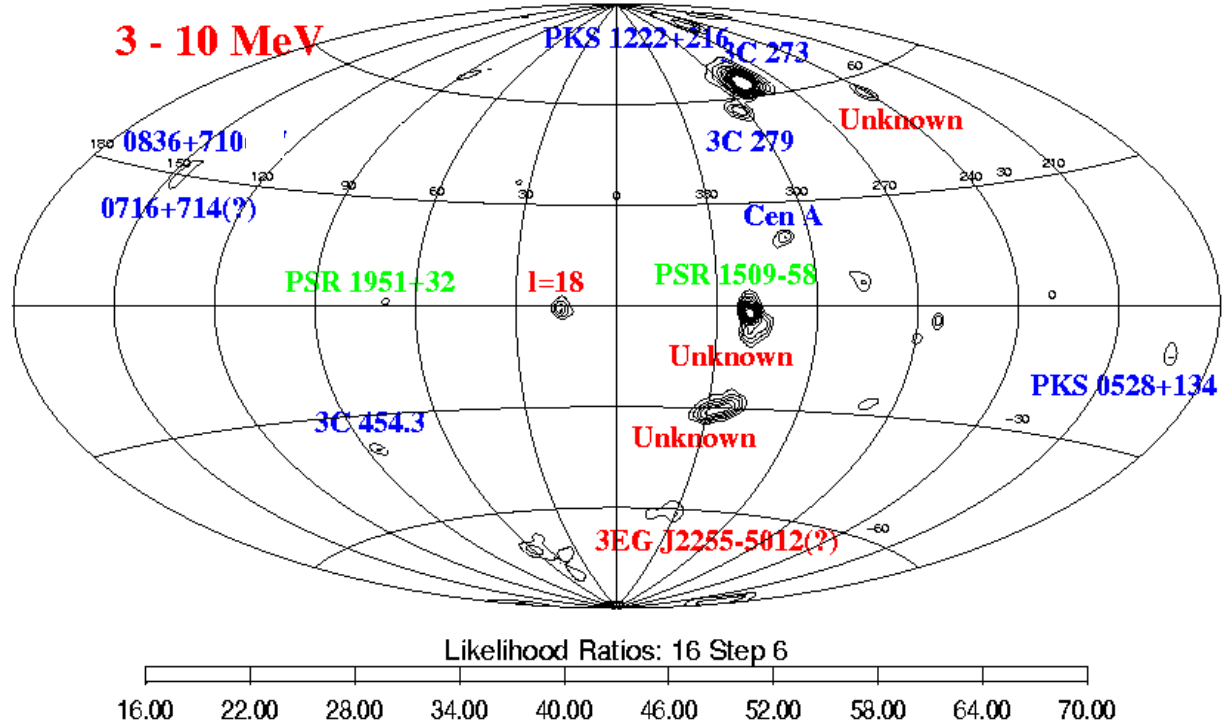
(extragalactic / galactic / unknown sources)
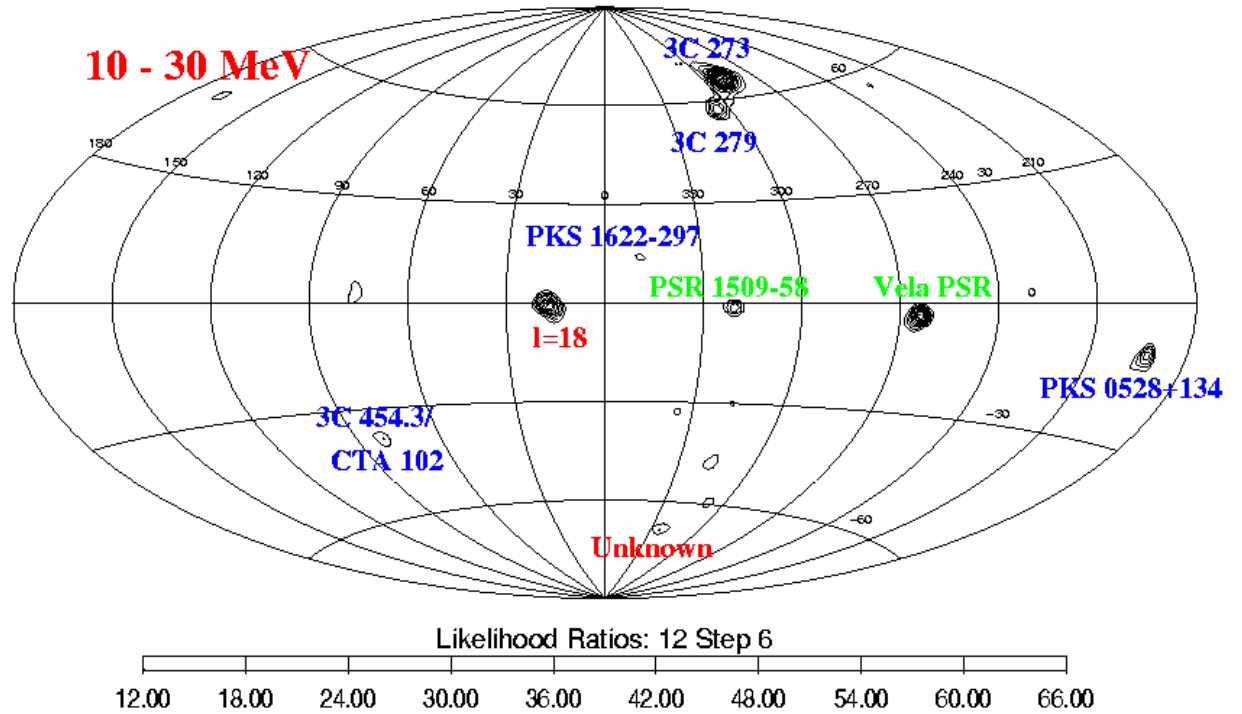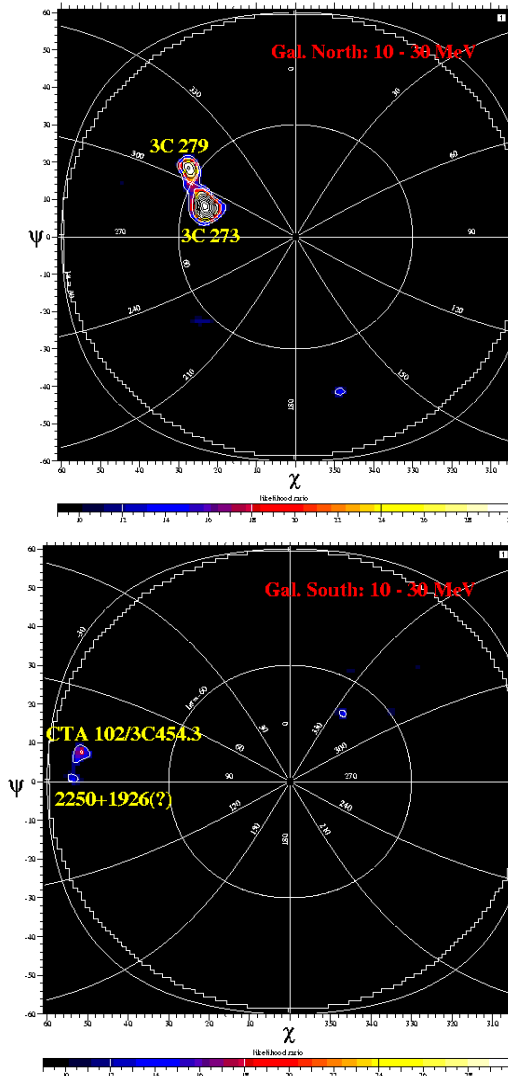


≥ 45 Sources

# Updated COMPTEL AGN List

| Source | z | Type | Det. Conf. |
|---|---|---|---|
| Cen A | 0.002 | Radio G. | high |
| Mkn 421 | 0.030 | BL Lac | low |
| 3C 273 | 0.158 | FSRQ | high |
| 0716+714 | 0.31 | BL Lac | low |
| PKS 1222+216 | 0.432 | FSRQ | medium |
| 3C 279 | 0.536 | FSRQ | high |
| 1622-297 | 0.815 | FSRQ | high |
| 3C 454.3 | 0.859 | FSRQ | high |
| PKS 0208-512 | 0.999 | FSRQ | high |
| CTA 102 | 1.037 | FSRQ | low |
| GRO J0516-609 | 1.09 | FSRQ | medium |
| 1127-145 | 1.184 | FSRQ | medium |
| PKS 0528+134 | 2.06 | FSRQ | high |
| 0836+710 | 2.17 | FSRQ | medium |
| PKS 1830-210 | 2.51 | FSRQ | high |

# TOF : time-of-flight: background rejection

Original "TOF-IV": per D1, D2 detector
New      "TOF-VI": resolves position in detectors (Georg Weidenspointner (MPE),  PhD thesis)
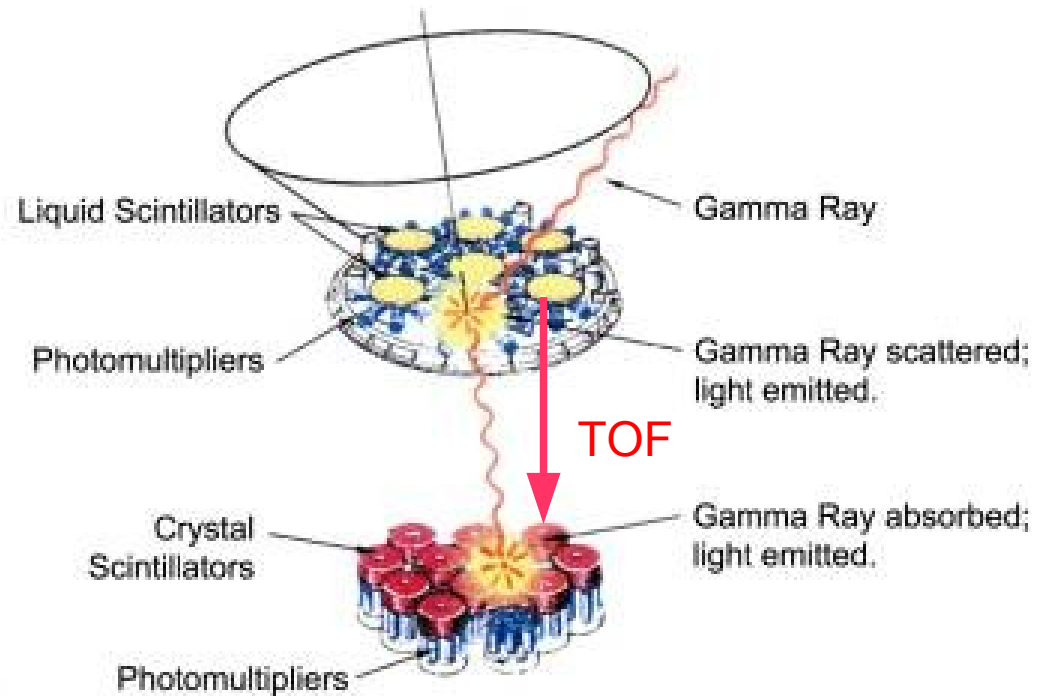
# Comparison TOF-IV – TOF-VI
## Crab 10 – 30 MeV
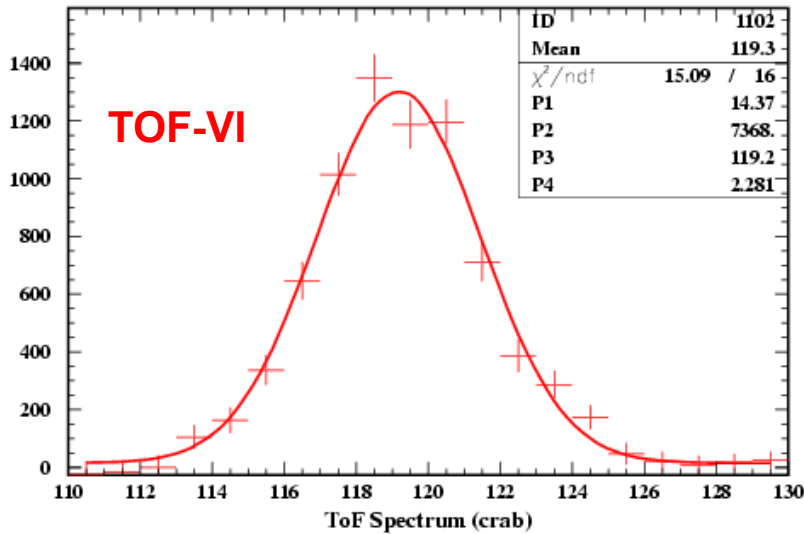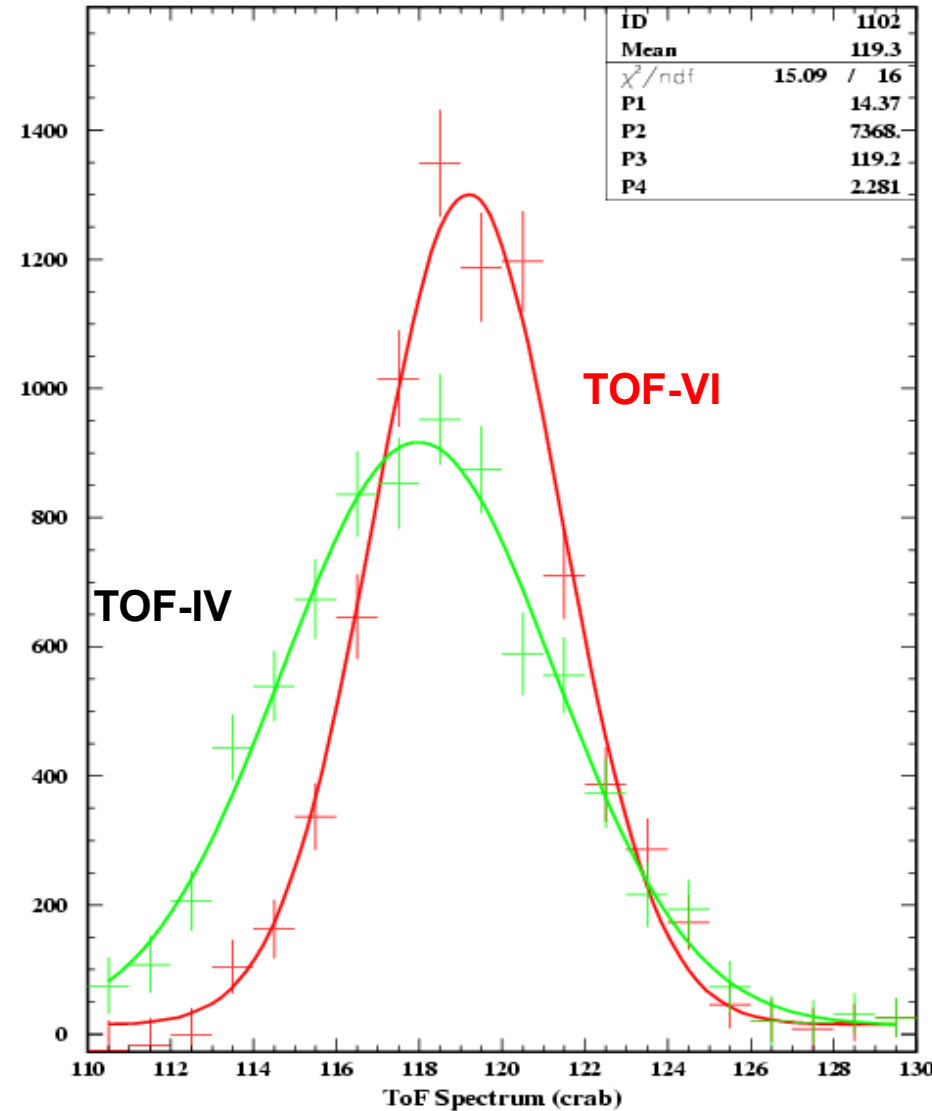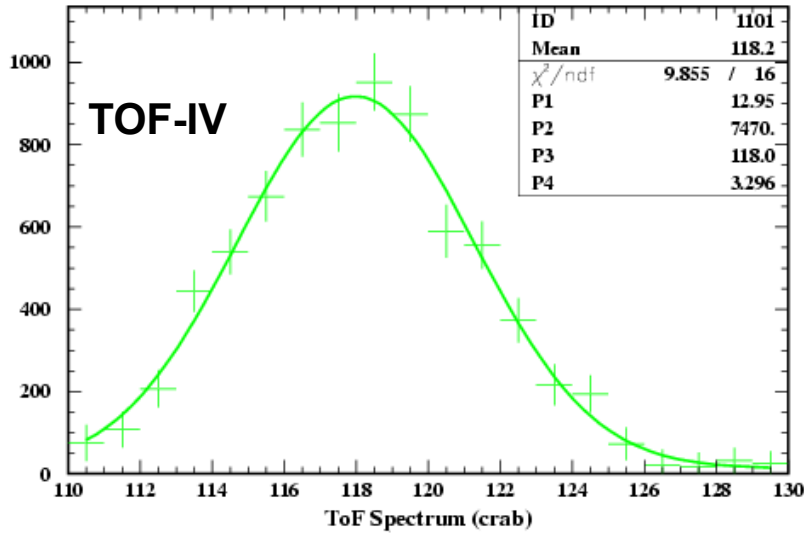
TOF channels (related to actual flight time)

# Analysis Method of COMPTEL ToF-VI Data



crab(29,ToFVI) (8658.68-99999, 9000-30000, 4-36, 115-125.5, 63-93, 0-999,-999-99)

Crab 9 – 30 MeV

| Entries | 155769 |
|---|---|
| $\chi^2$/ndf | 94.12 / 53 |
| P1 | 877.2 |
| P2 | 0.2092E+05 |
| P3 | -5.048 |
| P4 | 8.277 |
| P5 | 4657. |
| P6 | 0.2000 |
| P7 | 1.200 |
| P8 | -34.36 |

total

Crab

Background fit

Compton angle - true angle
degrees
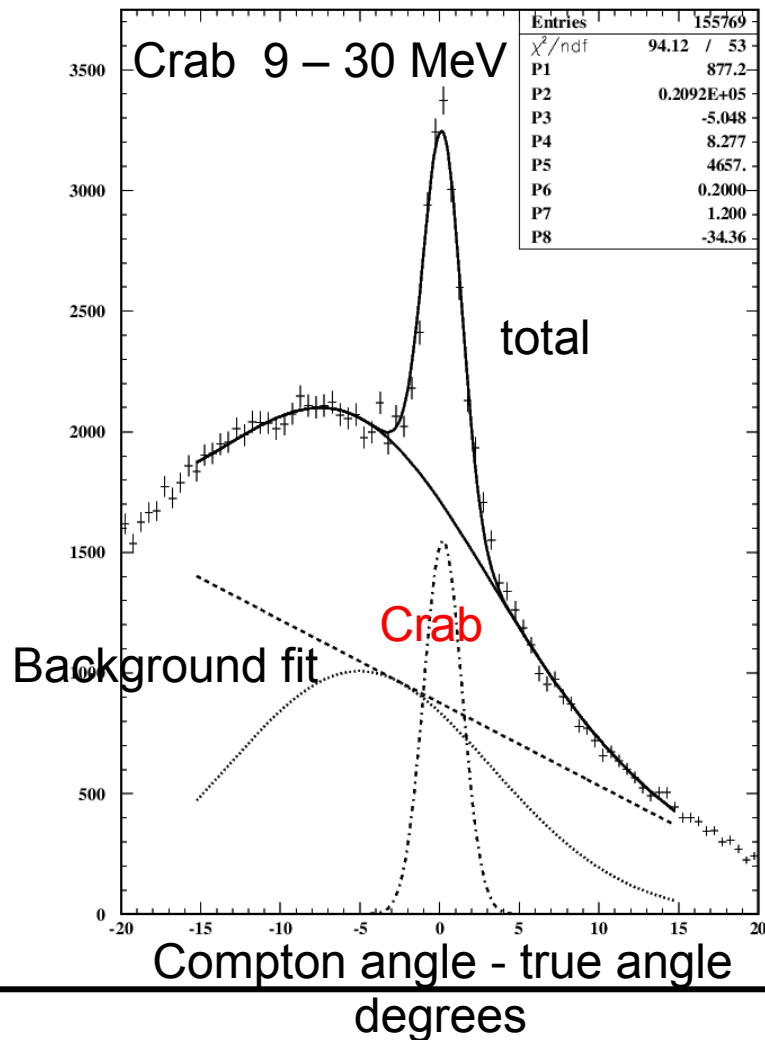
**Methode:**

● Unterteilung in "Quelle" und "Hintergrund" durch Modell-Fits

● Modell: Mathematische Funktionen

● Quelle: "Gauß-Funktion"

● Hintergrund: "Gauß" + "Gerade"

● Ziel: Optimierung "Quelle" zu "Hintergrund"

● Quantitative Ergebnisse
1156086 / 8540.3 / 15197.5 / 0.45 / 51.33

# COMPTEL Comparison (9 – 30 MeV)



ToF-IV
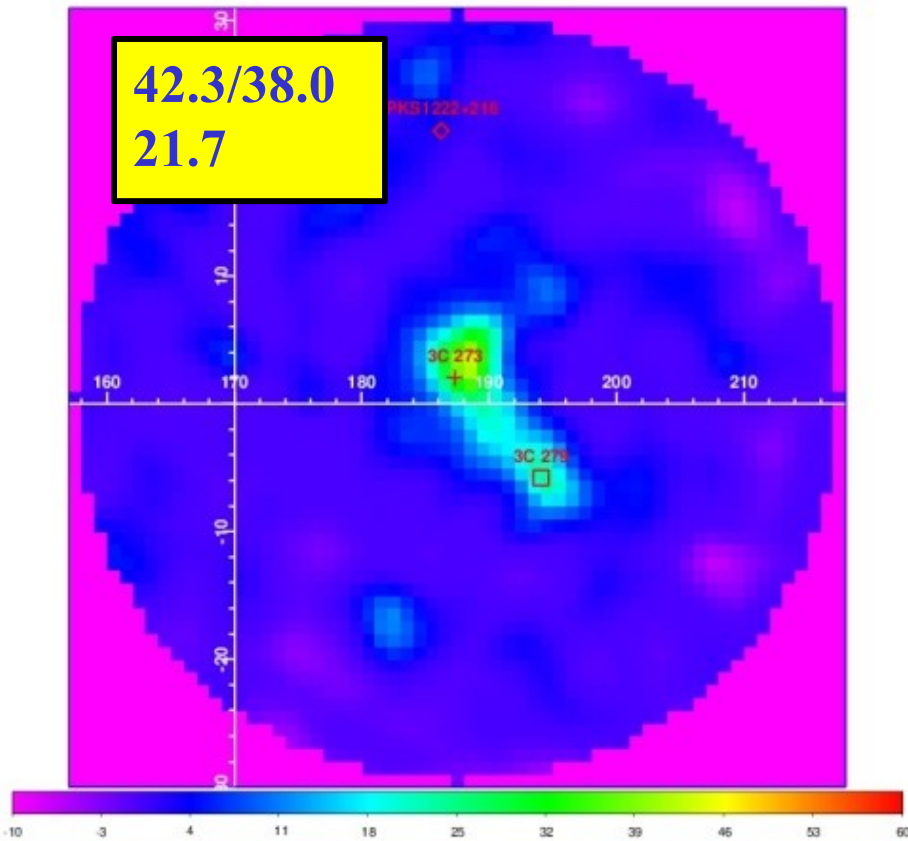
ToF-VI

# COMPTEL Comparison (4.3 – 9 MeV)

ToF-IV

ToF-VI

# COMPTEL reloaded: new initiatives in heritage MeV gamma-ray astronomy

A. W. Strong[1], W. Collmar[1], T. A. Enβlin[2], M .Reinecke[2], D. Pumpe[2], F. Guglielmetti[2]

1. MPE Garching    2. MPA Garching

Max-Planck-Institut für extraterrestrische Physik

Max-Planck-Institut für Astrophysik

## ABSTRACT

The COMPTEL gamma-ray telescope on NASA's Compton Gamma Ray Observatory (CGRO) operated from 1991 to 2000. It was a double-scatter Compton instrument covering the energy range 0.75-30 MeV, both in continuum  and lines. Full-sky maps and a source catalogue were 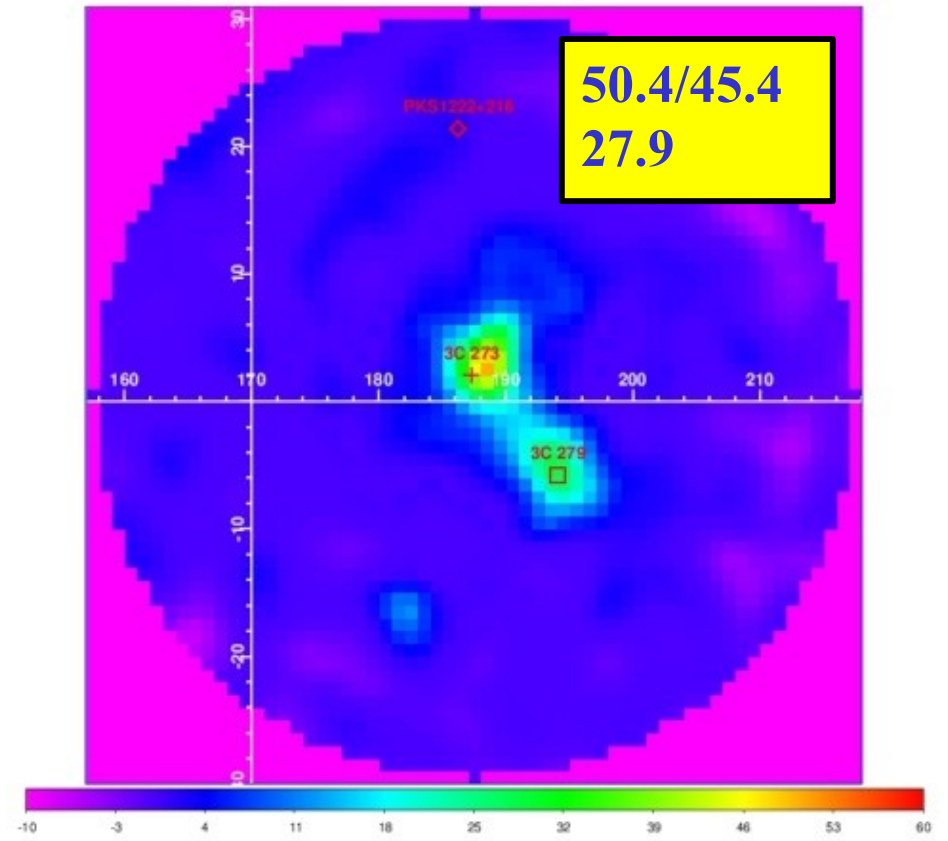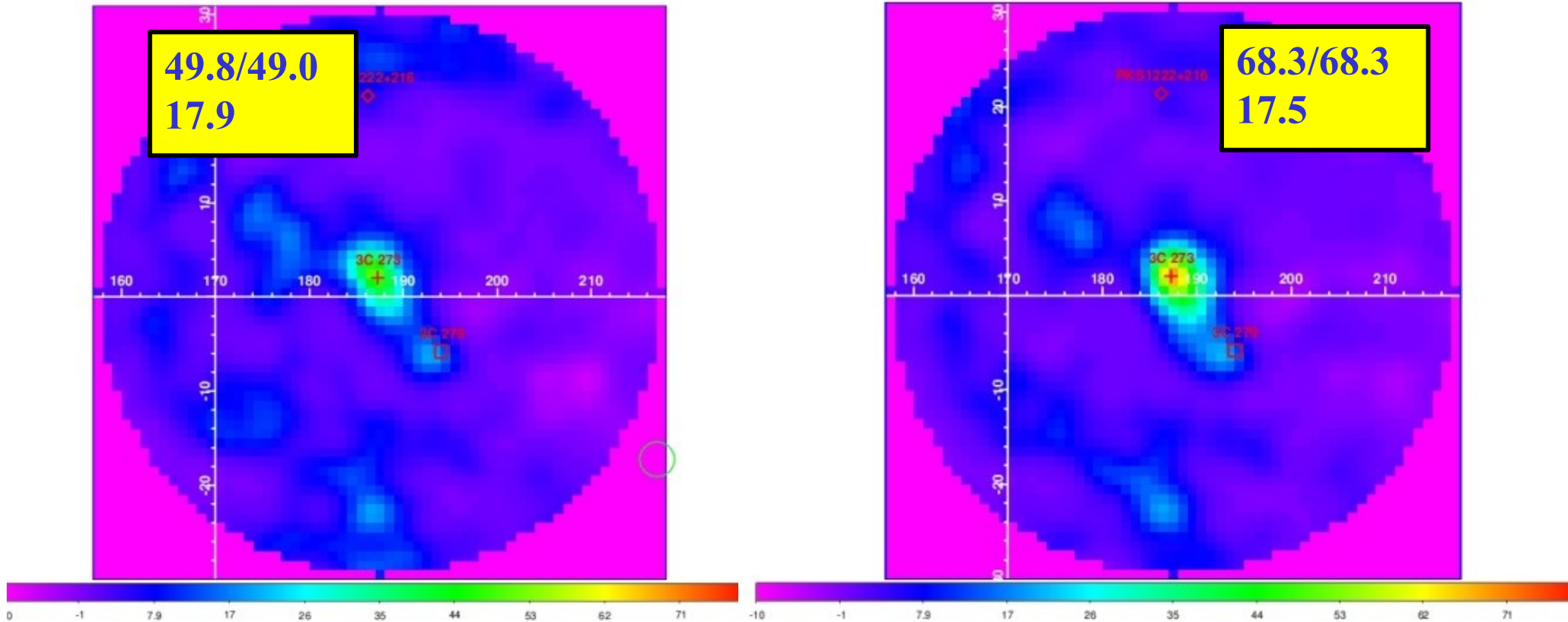the main outcome of the mission. While the Fermi-LAT instrument has now vastly enhanced our knowledge of the gamma-ray sky at higher energies, the MeV range remains devoid of new missions, so that the heritage COMPTEL data is an essential resource. Data analysis has continued at MPE Garching, with improved event processing and selections. The original skymapping method using Maximum Entropy has been adapted to current technology. A new initiative for skymapping using state-of-the-art Bayesian techniques has been started at MPA Garching; this involves Information Field Theory with the D³PO system.

## INSTRUMENT

**COMPTEL on CGRO**
**(1991 - 2000)**



## DETECTION TECHNIQUE

The double-Compton scattering detection technique means that each photon is associated with an annulus on the sky, with known centre, radius and shape; this makes deconvolution essential for imaging. One method is Maximum Entropy (Maxent), which has been used to make all-sky images. The large instrumental background is a further challenge for any COMPTEL analysis.

PRINCIPLE OF MEASUREMENT

*(Ryan & Lockwood, 1989)*



$$\text{if } E'_\gamma + E''_e$$
$$\Rightarrow$$
$$E_\gamma = E'_e + E'_\gamma$$
$$\cos \phi = 1 - \frac{m_0 c^2}{E''_e} + \frac{m_0 c^2}{E'_e + E''_e}$$
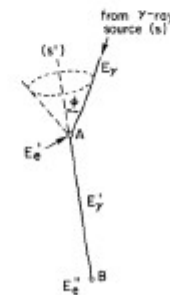
## Original Maxent images (A)

In the original work (Strong et al. 1998) the MEMSYS5 Bayesian 'Classic' Maxent package was used (Skilling, 1989). It employed a template for the instrumental background taken from high Galactic latitudes where the celestial signal is small. In the original work 240 COMPTEL observations were used, and the data and instrumental response were treated in the instrumental coordinate system. Because of the large computing requirements the computation was performed on 240 CPUs of a Cray supercomputer which was state-of-the-art at the time.
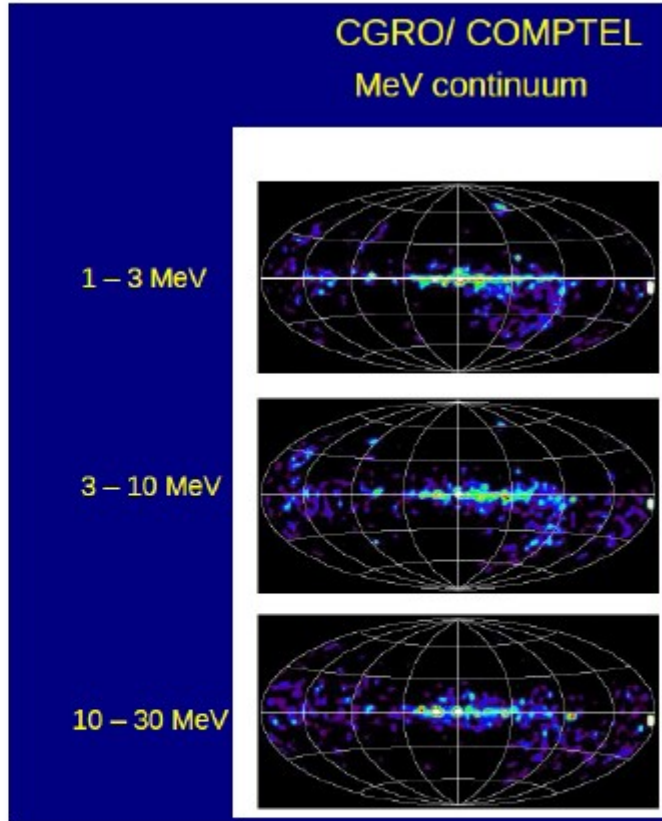
### Classic Maxent
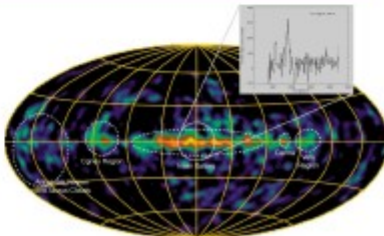
Entropic prior on image:

$$\Phi(S) \propto \exp(\alpha S)$$

Posterior of image:

$$\Pr(h, \alpha, D) = \Pr(\alpha) \Pr(h \mid \alpha) \Pr(D \mid h)$$
$$= \Pr(\alpha) \frac{\exp(\alpha \mathcal{S}(h) - \mathcal{L}(h))}{Z_{\mathcal{S}}(\alpha) Z_{\mathcal{L}}}$$



**(A)**

**CGRO/ COMPTEL**
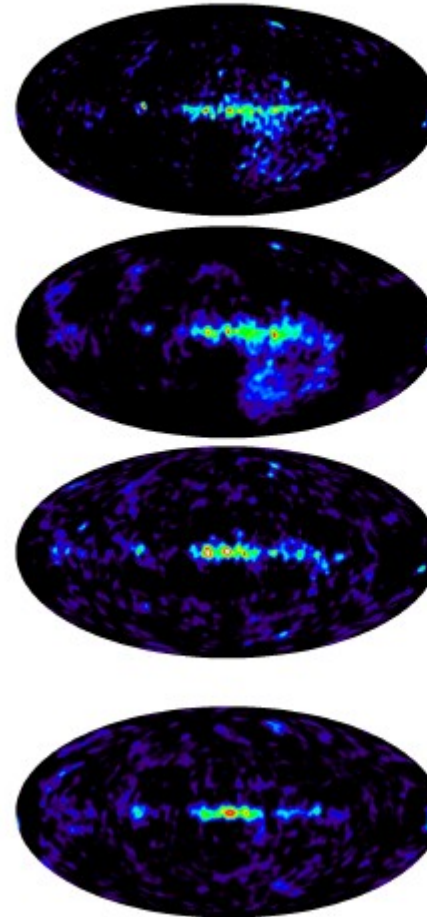**MeV continuum**

1 – 3 MeV

3 – 10 MeV

10 – 30 MeV

1.8 MeV – $^{26}$Al

**(B)**

## New Maxent images (B)

In view of the importance of the COMPTEL data, we have recently revisited imaging with current software and hardware technology. The original code was adapted to use the *HEALPix* sky representation for a uniform sky coverage both in data and image space instead of the original straight (l,b) system. This also allows fast convolution/correlation on the sphere, replacing the original "brute-force" method. This already gives an enormous speed gain, and running in on a multicore machine produces images in hours (compared to weeks on the original Cray implementation). A finer pixelization (0.5° instead of the original 1°) is hence possible. The *HEALPix* format enhances the value of the images and the speed allows investigation of more imaging parameters, data selection etc.

The new images are fully consistent with the original ones, with the Galactic plane clearly visible, and in addition the well-known sources including the Crab, Vela, Cyg X-1, LS5039, 3C273, 3C279, PKS0528+134 and the Galactic Centre. (Note: the excess at lower right is due to Earth atmospheric emission)

In addition we have produced a 1.8 MeV $^{26}$Al line map which can be compared with the standard Maxent image (Plüschke et al. 2001).

New version of imaging software with Martin Reinecke, MPA Garching

COMPTEL response is very particular!

Each photon has its own annulus on the sky depending on
 energy deposits in upper and lower detectors (Compton formula).

Makes direct imaging (a` la Fermi-LAT) impossible.

Point-source analysis done with *likelihood method*.
Test for a point-source at each point on sky.

Extended emission requires more sophisticated approach.
Ideal candidate for indirect imaging (deconvolution)
*Maximum entropy* was ideally suited for this.

Bayesian method, prior = image entropy, parameters = pixel fluxes
Background fitted simultaneously.
3D dataspace: l, b, phibar (Compton formula)
Data in instrument system, each observation preserved (341 observations)

# COMPTEL Maximum Entropy Imaging

Original (by AWS) in 1998 using Cray supercomputer
MEMSYS5 Package (John Skilling)

New developments:

<u>Imaging software</u> (with Martin Reinecke, Torsten Ensslin @ MPA Garching)

HealPix equal-area all-sky projection  for both data and image
Fast convolution on sphere (COMPTEL PSF annuli up to ~$30^{\circ}$ )
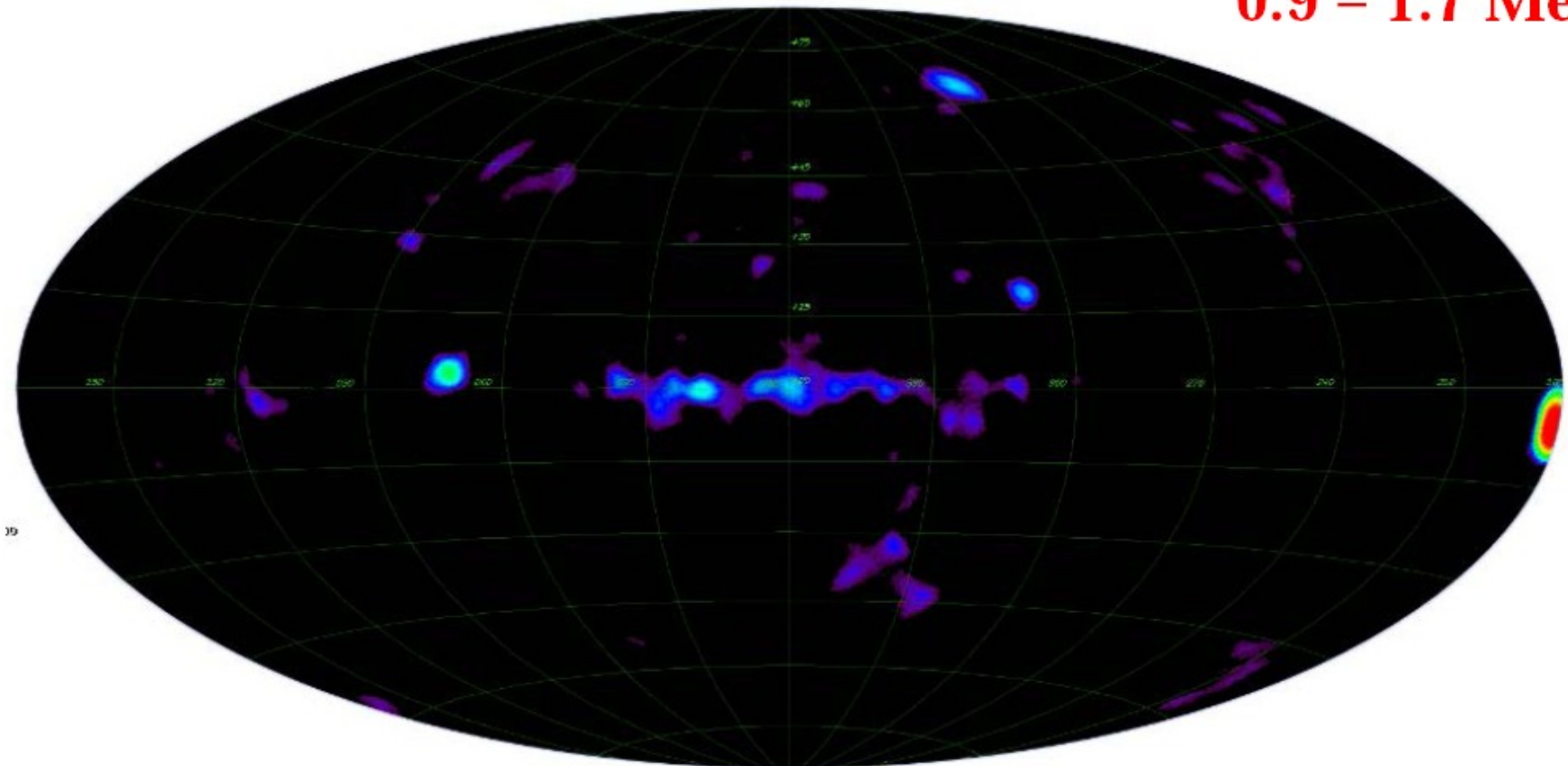Parallel architecture

<u>Data</u> (Werner Collmar @ MPE Garching)

New event processing, better background rejection with TOF and PSD
New energy ranges to avoid background lines and better spectral coverage
Full data set from whole mission

# Current Developments: All-Sky Imaging

preliminary

0.9 – 1.7 MeV



Werner Collmar, MPE Garching

1.7 – 4.3 MeV
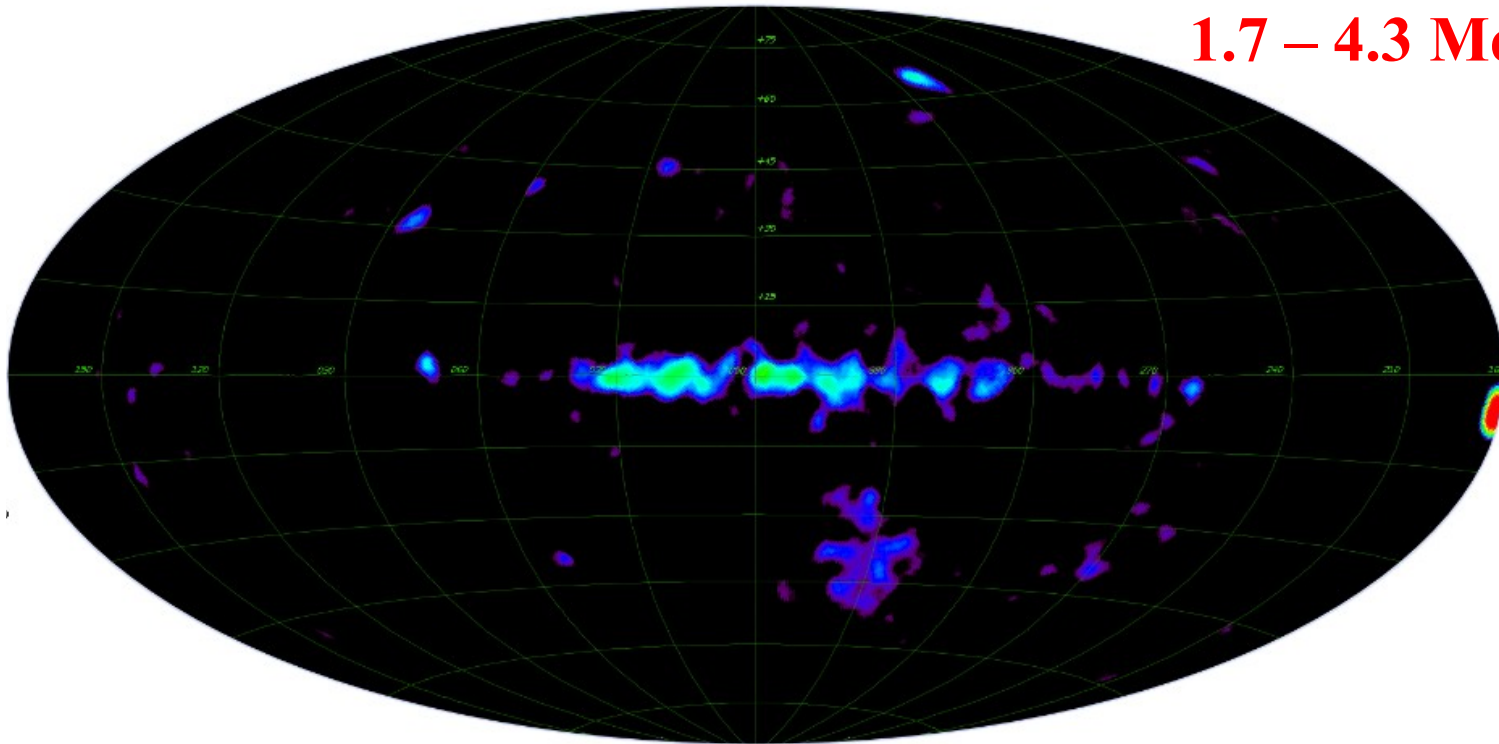
4.3 – 9.0 MeV
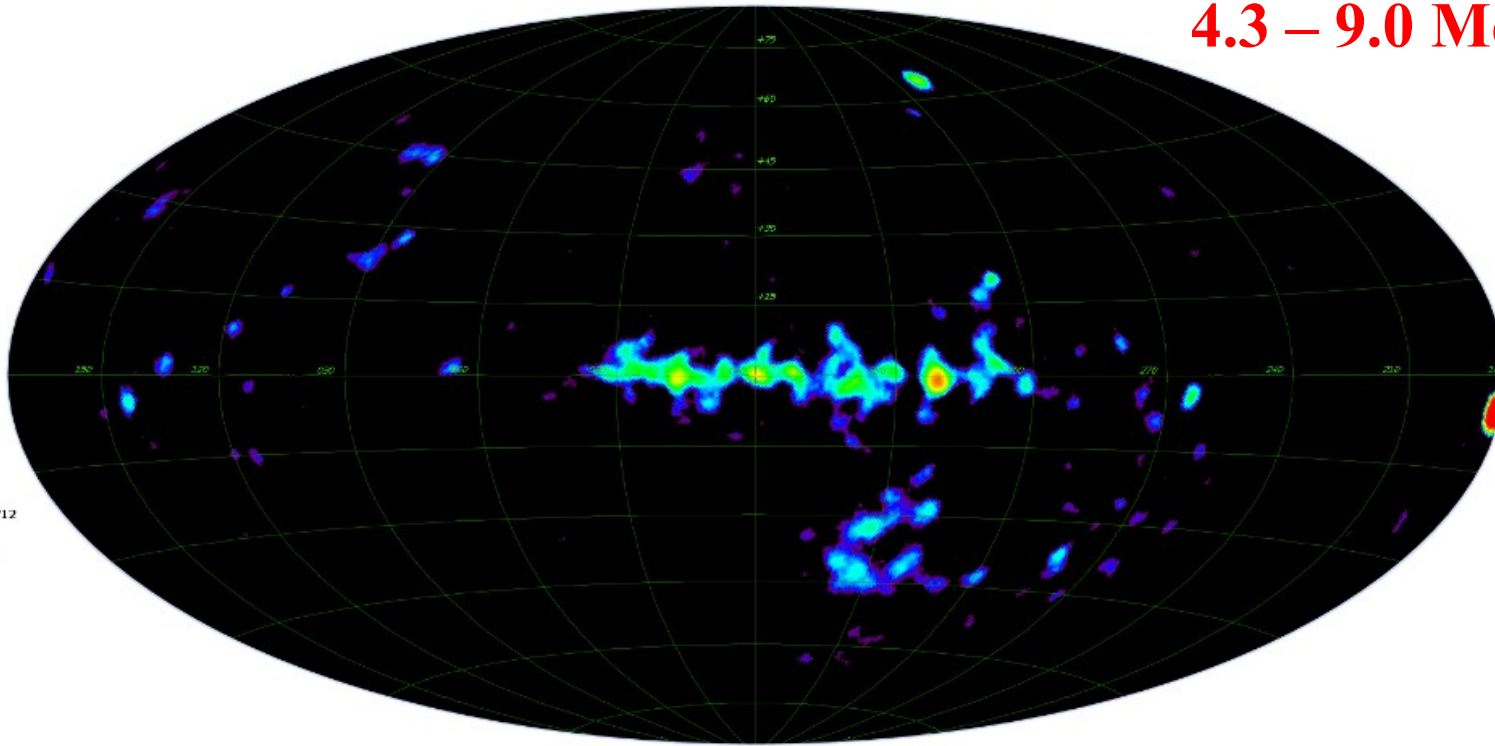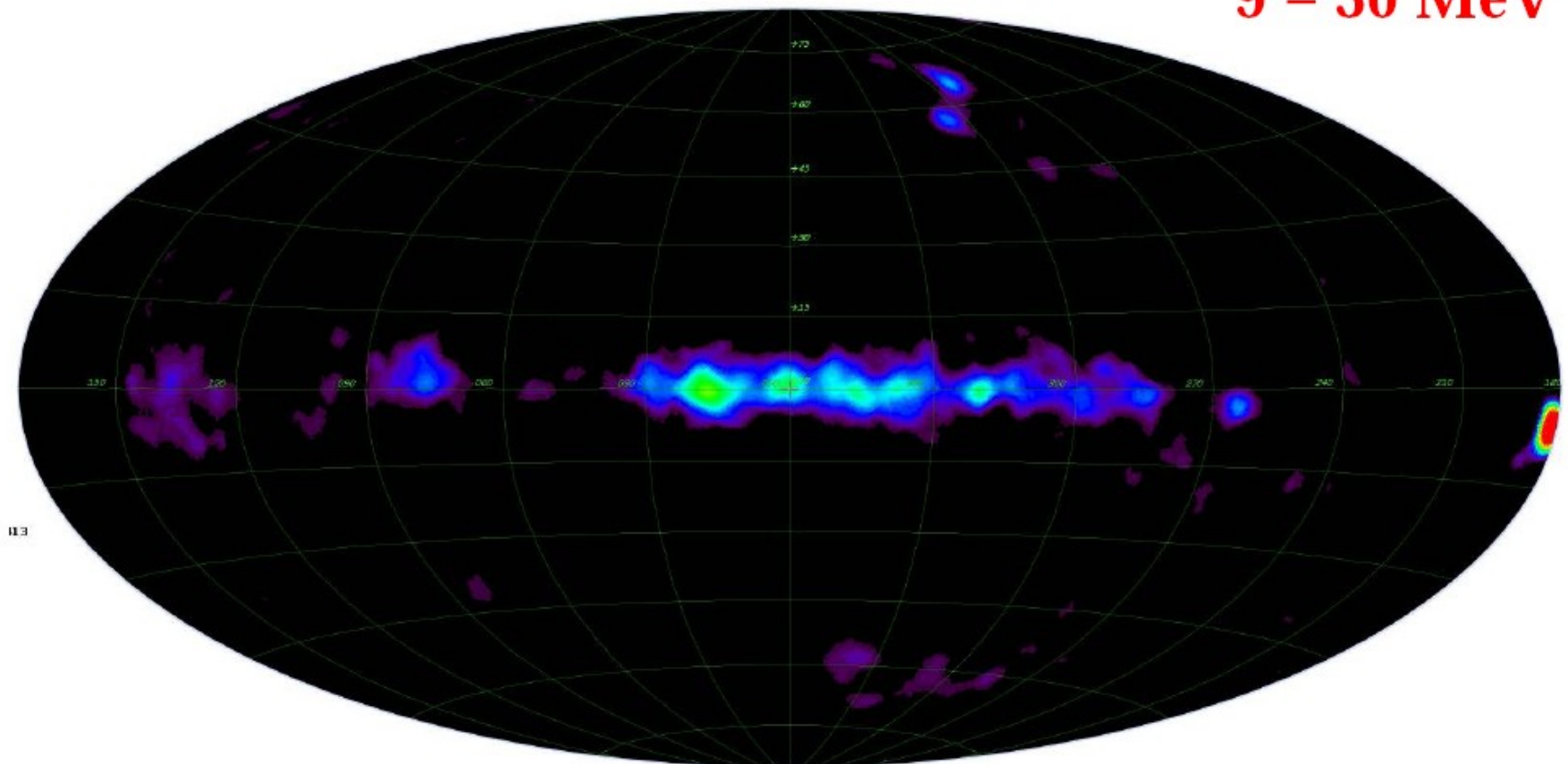
preliminary

9 – 30 MeV



Werner Collmar, MPE Garching
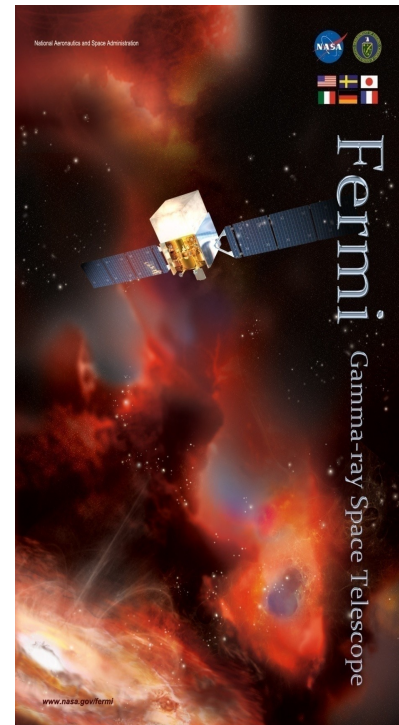
Fermi-LAT 25 – 40 MeV
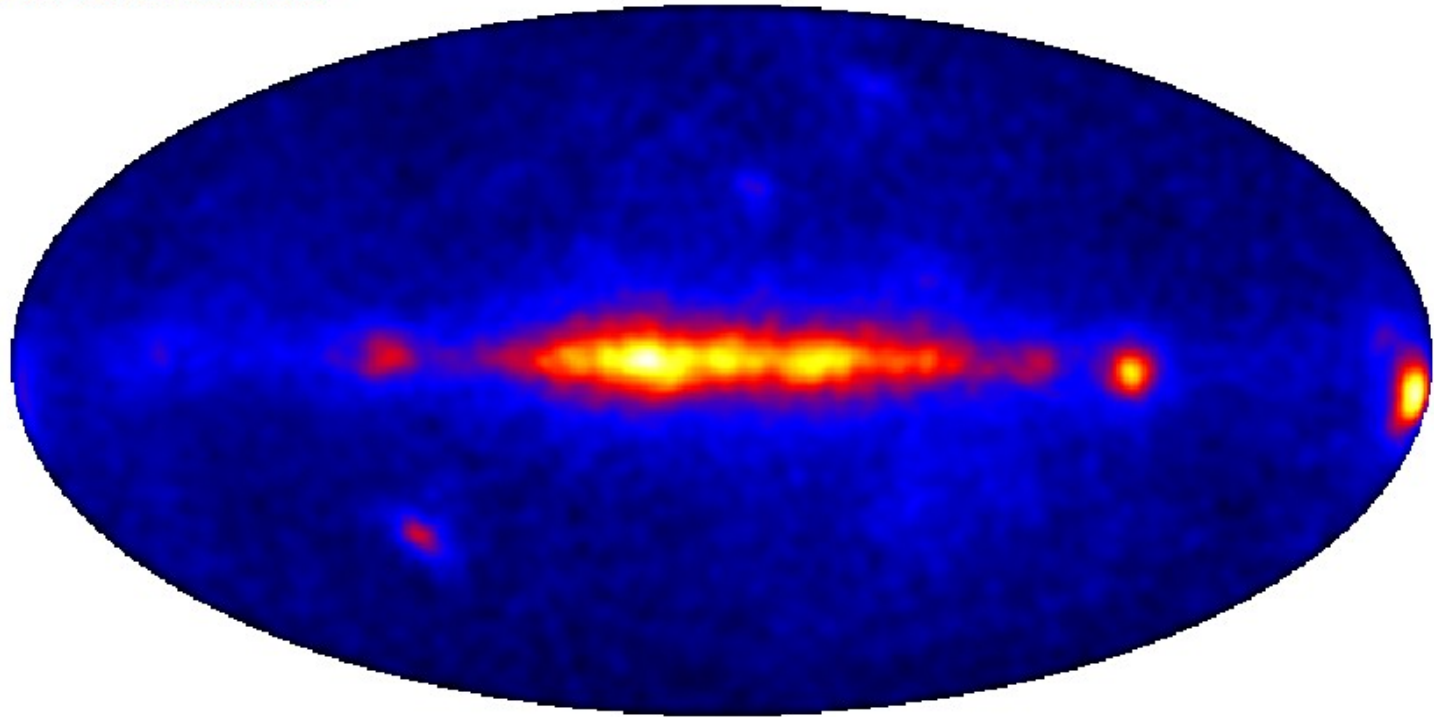
PRELIMINARY

NB low angular and energy resolution !
*Nominal energy range*: photons may originate from range 10 to <100 MeV.
 But valuable to bridge the MeV gap.

# Fermi-LAT 25-40 MeV

PRELIMINARY
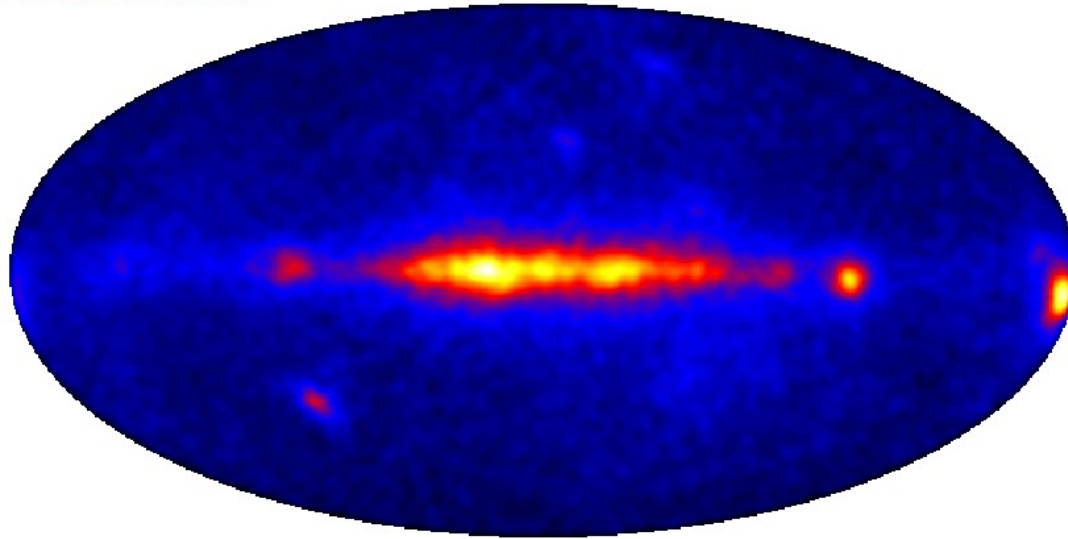


meets

# COMPTEL 10-30 MeV

**Comparison with Fermi-LAT**

Fermi-LAT energy range extends to lower energies with Pass 8, and this allows a comparison with COMPTEL.

(from A. Strong on behalf of Fermi-LAT Collaboration, talk at MeV Conference, APC Paris 2012)

**References**
Collmar, W., Zhang S., 2014, A&A 565, A38
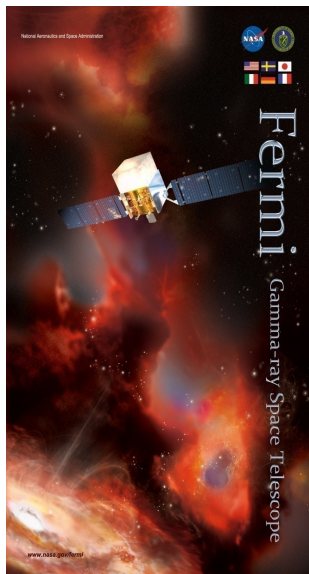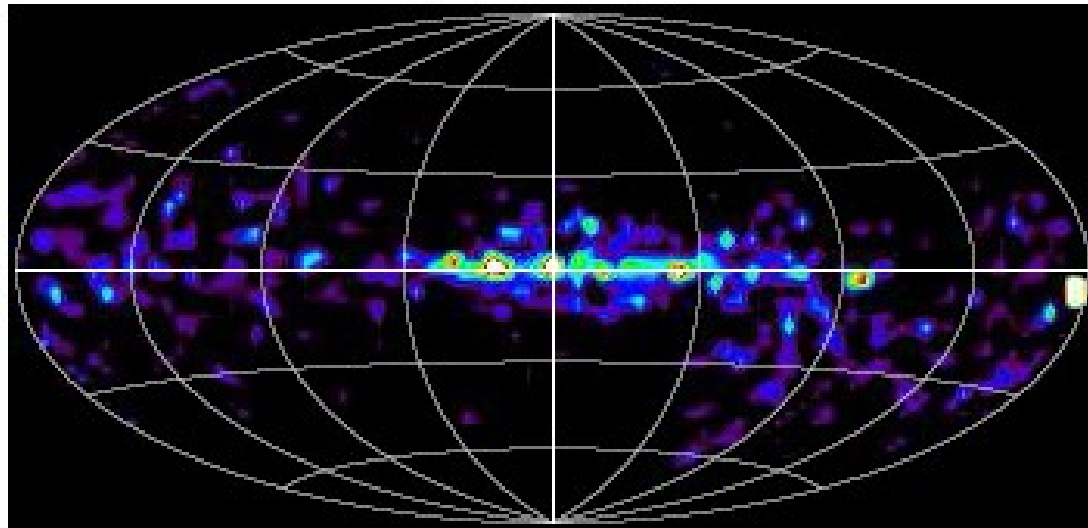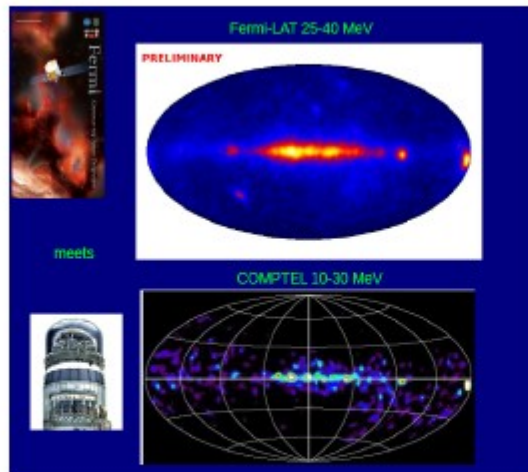Plüschke, S., Diehl, R., Schönfelder, V., et al. 2001, in Exploring the Gamma-Ray Universe, ESA SP, 459, 55
Selig, M., et al., 2015, A&A 581, A126
Skilling, J. , 1989 in Maximum Entropy and Bayesian Methods, (Dordrecht: Kluwer), ISBN-0-7923-0224-9, 45
Strong, A.W. et al. 1998, Proc. 3rd INTEGRAL Workshop, arXiv:astro-ph/9811211; Astrophys. Lett. Commun. 39, 209

**OUTLOOK**

**New COMPTEL photon data processing**

COMPTEL data analysis continues at MPE (Collmar & Zhang 2014). The event processing and selection is also under study at MPE with improved time-of-flight calculation and other enhancements to reduce the instrumental background. More observations are also now available than for the skymaps shown above. This new data will be used to generate updated images in the near future.

**Future methods**

While Maxent has been very successful for image COMPTEL data, further advances in data analysis have been made in the last decade. Information Field Theory (IFT) as implemented in the NIFTY and D³PO software has been applied to Fermi-LAT data (Selig et al. 2015), see talk 'Gamma-ray analysis with D³PO' at this symposium. Application of this method to COMPTEL is in progress.

# GRO J1823-12 (LS 5039 ?)
## Orbit-averaged Analysis



1 – 3 MeV

10 - 30 MeV

3 - 10 MeV

Error location Contours
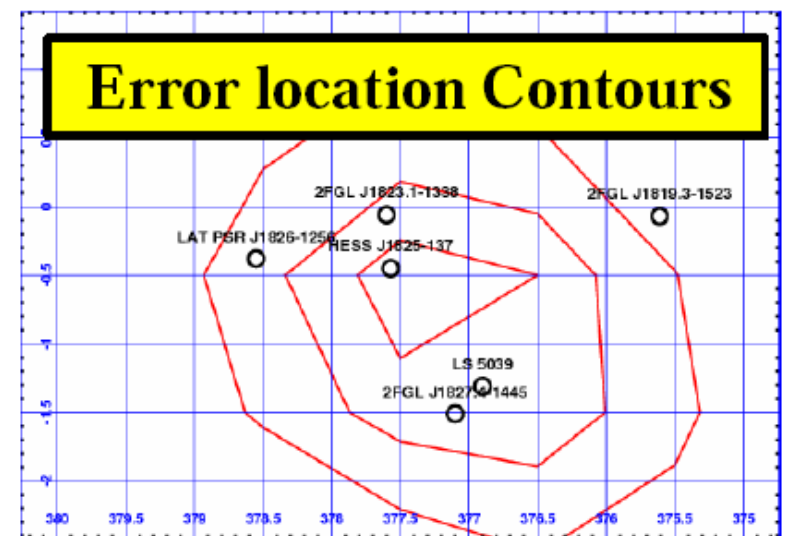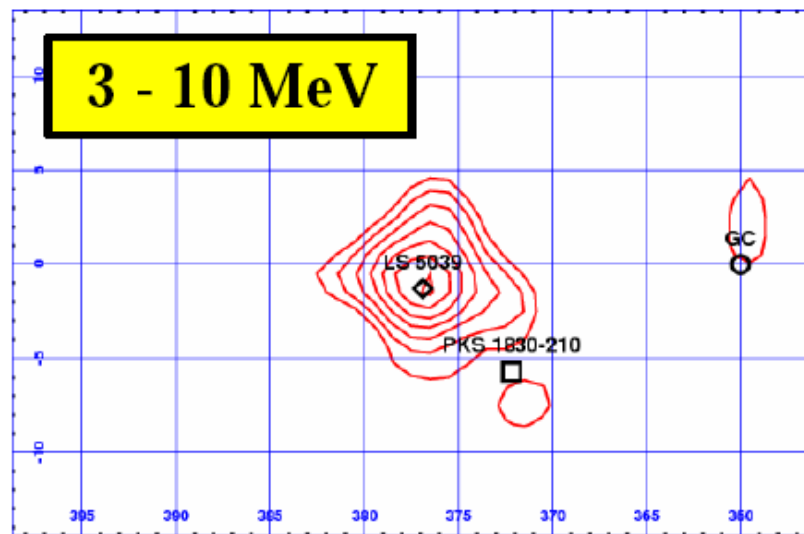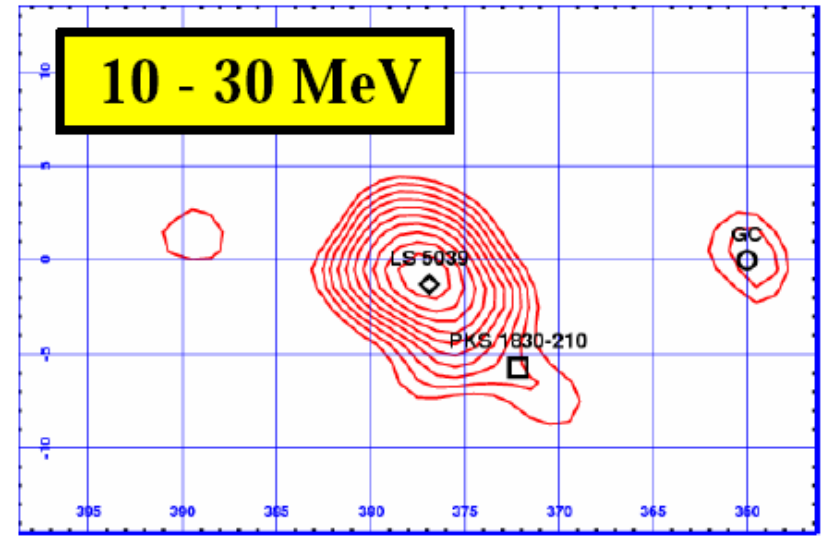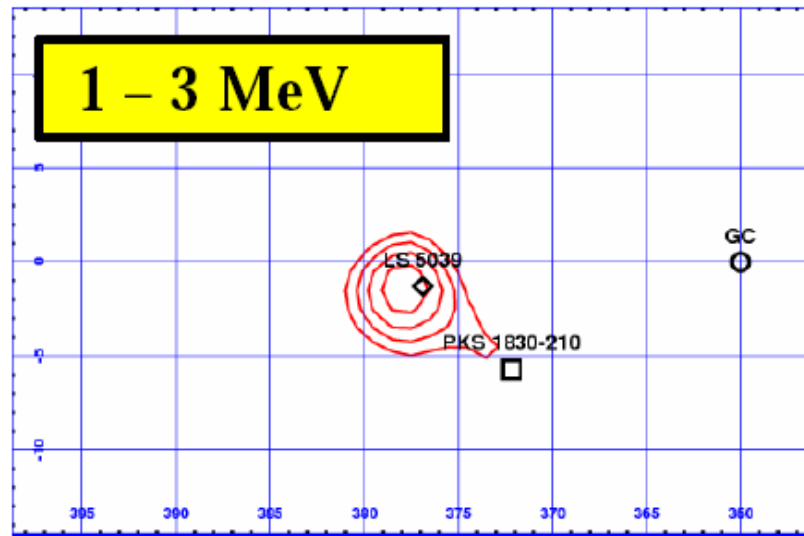
# GRO J1823-12 (LS 5039)
## Orbital Lightcurve (Ephemeris: Casares et al. 2005)
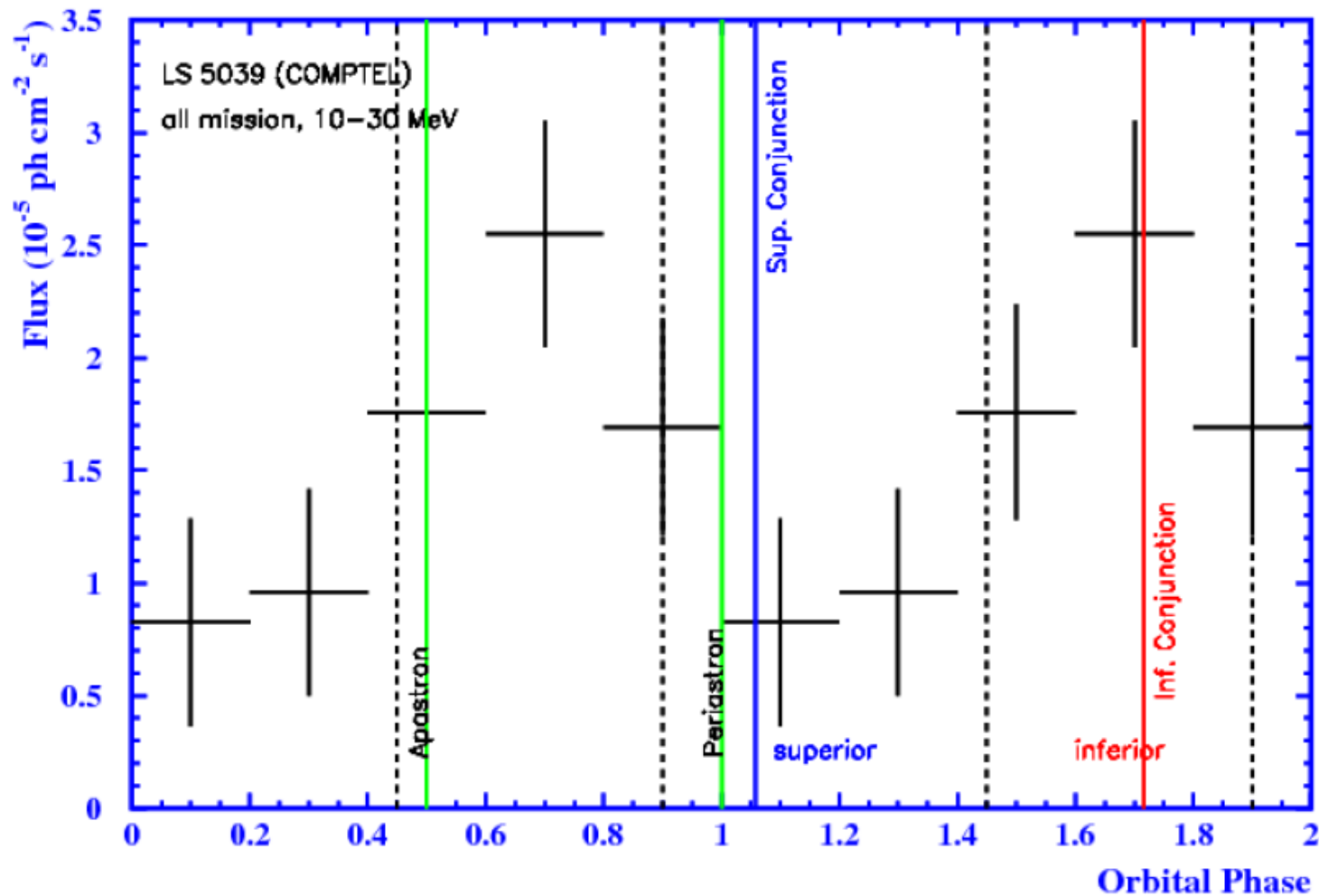
# LS 5039 High-Energy Light Curves



**1 – 10 keV: Suzaku**
**(Takahashi et al. 2009)**

**25 – 200 keV: INTEGRAL**
**(Hoffmann et al. 2009)**

**10 – 30 MeV: COMPTEL**
**(Collmar et al. 2014 )**

**> 100 MeV: Fermi/LAT**
**(Abdo et al. 2009)**

**at 1 TeV: HESS**
**(Aharonian et al. 2006)**

# LS 5039 High-Energy SED

# LS 5039 Modelling

### INVERSE COMPTON SCATTERING MODEL FOR X-RAY EMISSION OF THE GAMMA-RAY BINARY LS 5039

M. S. Yamaguchi and F. Takahara

Department of Earth and Space Science, Graduate School of Science, Osaka University,

Toyonaka, Osaka, 560-0043, Japan

Received _____ ;   accepted _____

### 5. Summary

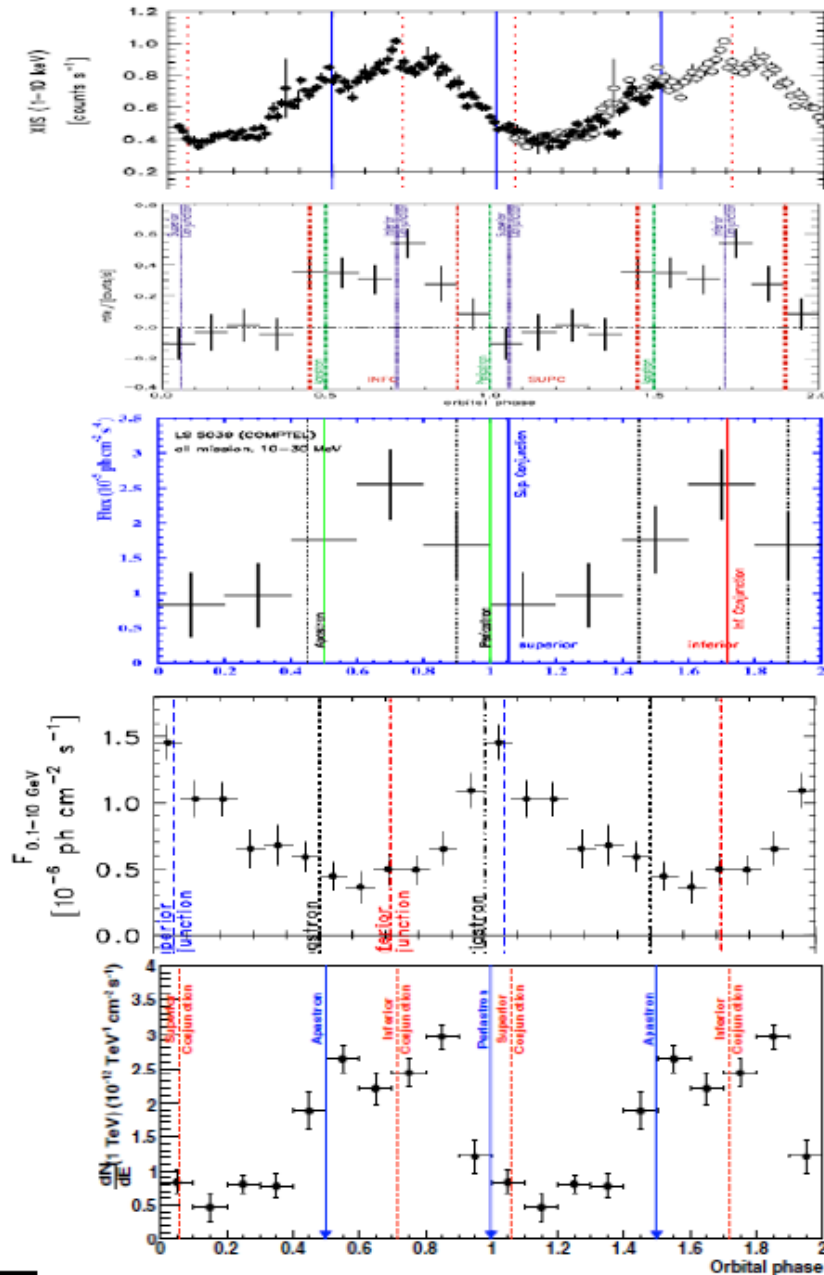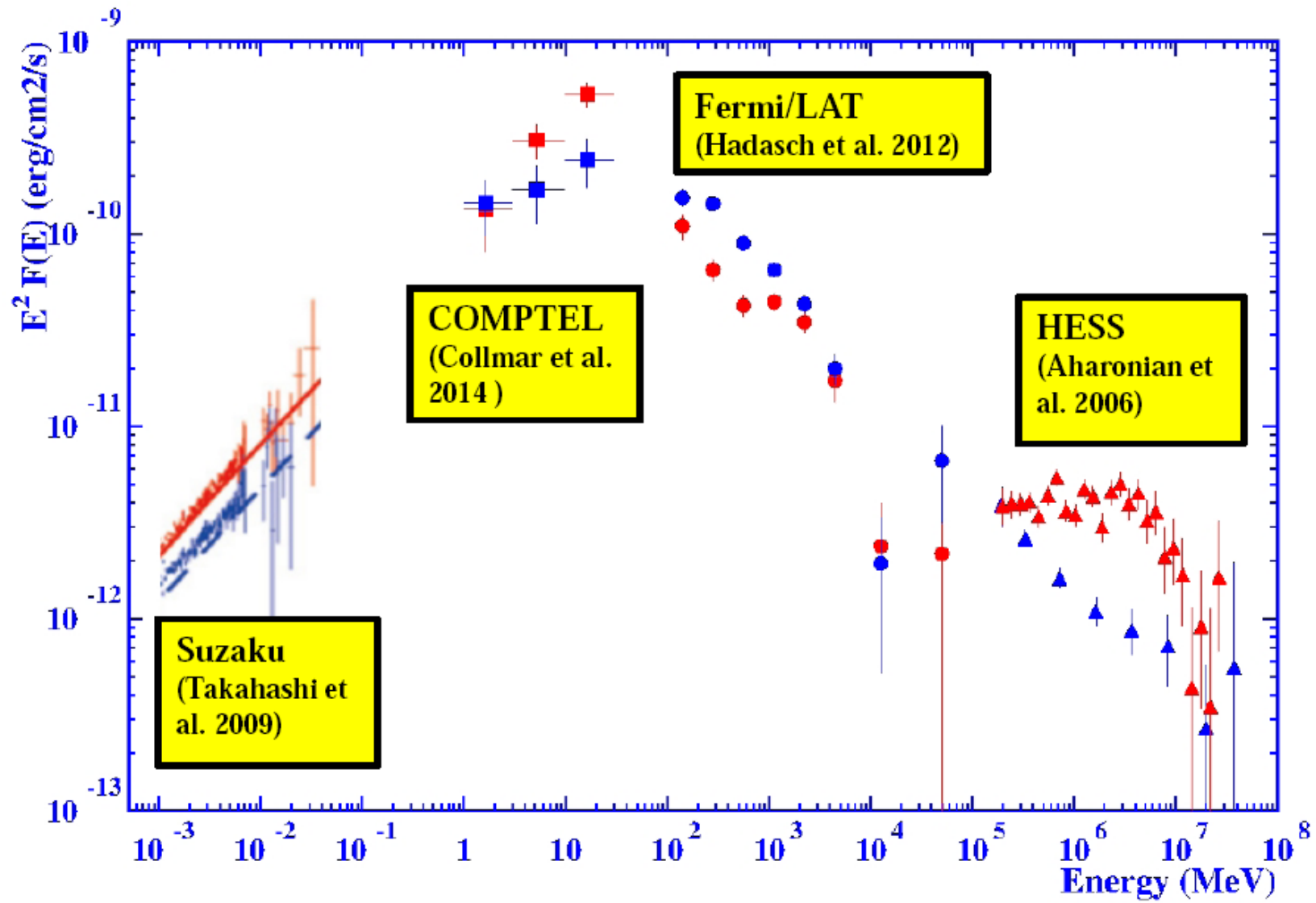We assume that X-ray emission from LS 5039 is due to the IC scattering of electrons with $\gamma \sim 10$. We calculate the anisotropic IC emission from electrons with the Lorentz factor $5 < \gamma < 3 \times 10^8$ in the Thomson regime. As a result, we have found that we can reproduce *Suzaku* flux if the minimum Lorentz factor of injected electrons $\gamma_{min} \sim 10^3$. Moreover, the X-ray light curve is well reproduced if a simple relation $\gamma_{min} \propto F_{GeV}$ is satisfied, where $F_{GeV}$ represents the GeV flux. We have obtained these results based on YT10, where the index and the coefficient of the power-law distribution for injected electrons do not change with respect to the orbital phase. We may obtain different results when we adopt the model in which the index and the coefficient vary, but *Suzaku* data can be reproduced by adjusting these parameters, because the X-ray flux variation is primarily determined by the number of low energy electrons. Thus, we suggest that the X-ray emission obtained with *Suzaku* can be explained by the IC emission. However, we need more investigation for explaining the *Fermi* data. This model will be justified or rejected by future observations in the MeV range.
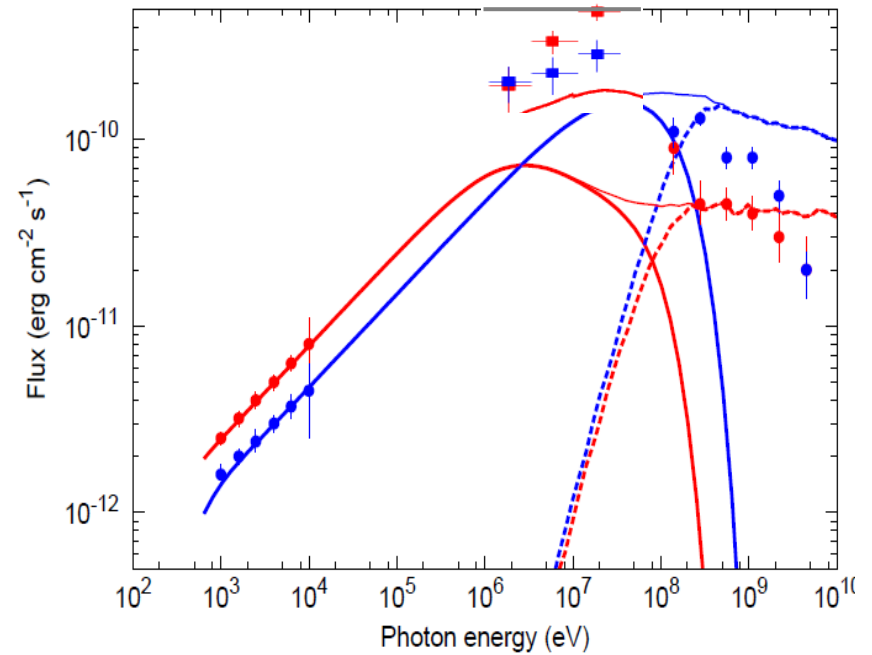
**Sorry!**

# Current Developments: All-Sky Imaging

preliminary

0.9 – 1.7 MeV

# Current Developments: All-Sky Imaging

preliminary

0.9 – 1.7 MeV



Fermi-LAT
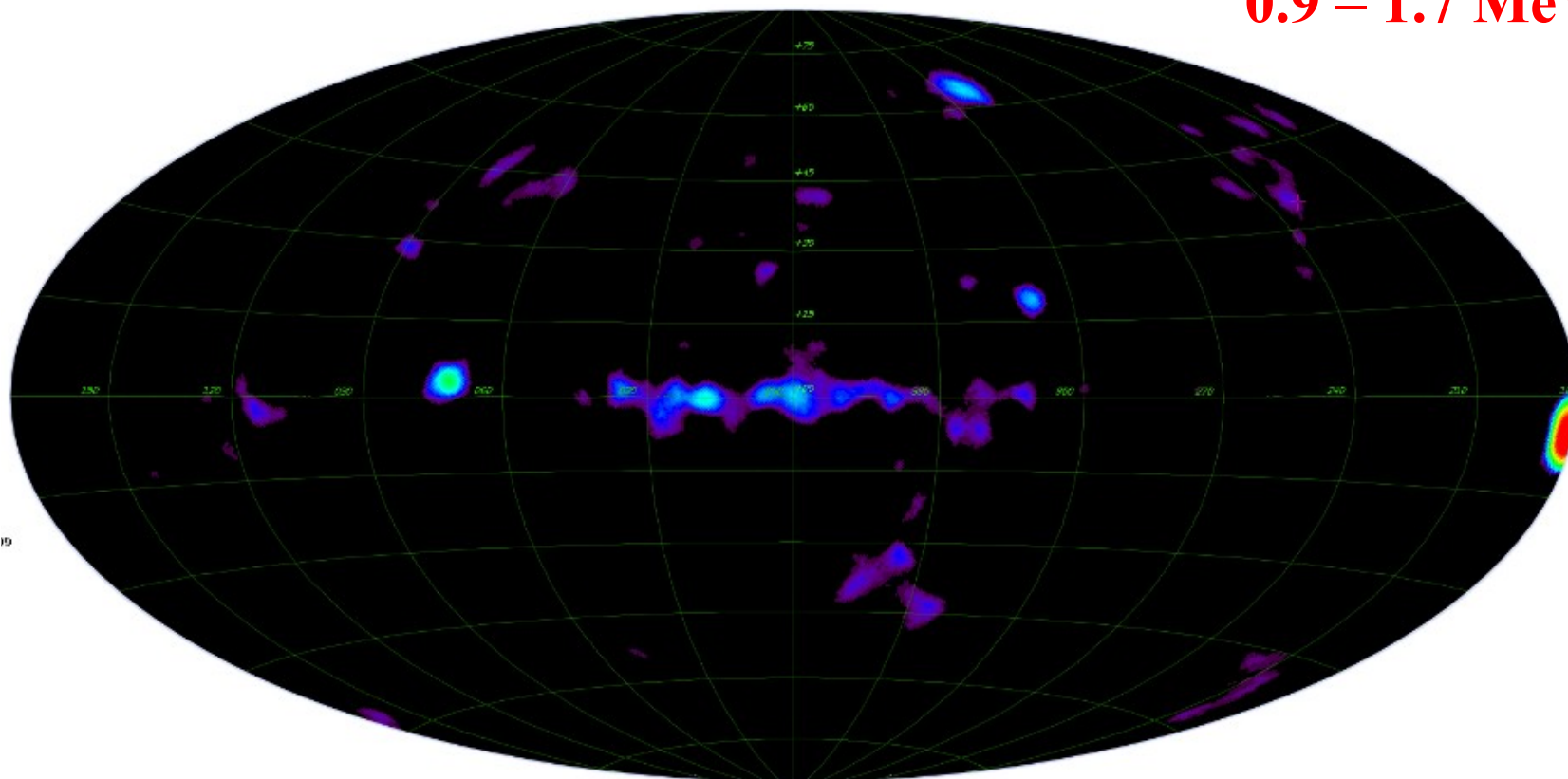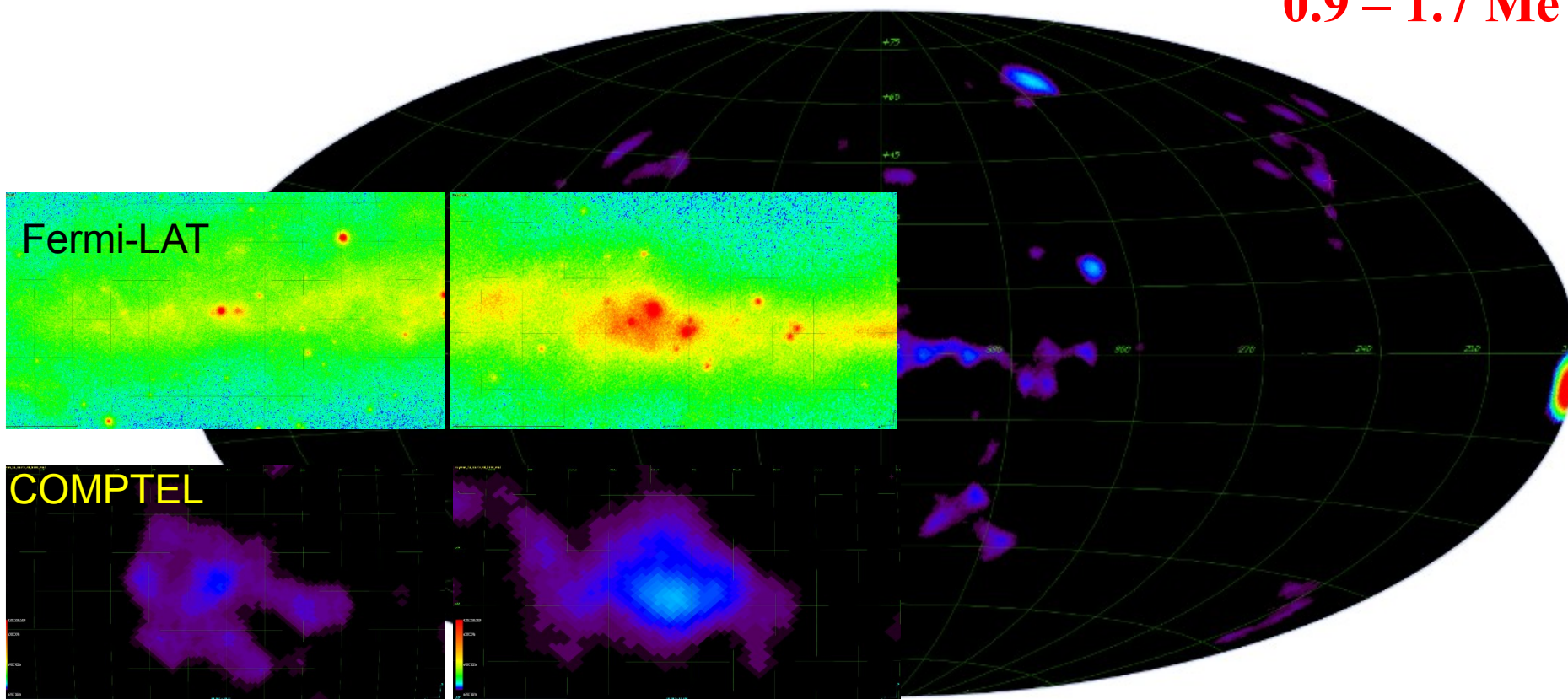
COMPTEL

LSI+61° 303?

γ Cyg ?

# Summary

- COMPTEL opened the soft γ-ray sky (0.75 – 30 MeV) for science

- Crab (total) by far brightest MeV source,
  others at 100 mCrab (e.g. 3C 273) and below

- after '1st COMPTEL Catalog' the "MeV sky" was still populating
  with sources: 4 blazars, 4 unidentified sources, further candidates
  → > 40 Sources

- COMPTEL data are still the most sensitive existing MeV data,
  parts (in particular late mission) are still unexplored

- Recent developments
  - calibrate reprocessed COMPTEL data (sensitiv. improvements)
  - apply polarization capability (GRBs, solar flares, binaries)
  - apply "modern" imaging techniques (e.g. incl. "HEALPIX")
    by using modern computer power

- Good News: COMPTEL data are still there …
  … and even ready again to be looked at

- Science aspect: the 'pion bump'

# The origin of Cosmic-Rays from SNRs: confirmations and challenges after the first direct proof.

M.Cardillo[a,*], M.Tavani[b,c,d], A.Giuliani[e]

[a] INAF-Osservatorio Astrofisico di Arcetri, Largo E.Fermi 5, 50125, Florence (Italy)
[b] INAF/IAPS, I-00133 Roma, Italy
[c] Dip. di Fisica, Univ. Tor Vergata, I-00133 Roma, Italy
[d] CIFS-Torino, I-10133 Torino, Italy
[e] INAF/IASF-Milano, I-20133 Milano, Italy

## Abstract

Until now, providing an experimental unambiguous proof of Cosmic Ray (CR) origin has been elusive. The SuperNova Remnant (SNR) study showed an increasingly complex scenario with a continuous elaboration of theoretical models. The middle-aged supernova remnant (SNR) W44 has recently attracted attention because of its relevance regarding the origin of Galactic cosmic-rays. The gamma-ray missions AGILE and Fermi have established, for the first time for a SNR, the spectral continuum below 200 MeV which can be attributed to neutral pion emission. Our work is focused on a global re-assessment of all available data and models of particle acceleration in W44 and our analysis strengthens previous studies and observations of the W44 complex environment, providing new information for a more detailed modeling. However, having determined the hadronic nature of the gamma-ray emission on firm ground, a number of theoretical challenges remains to be addressed in the context of CR acceleration in SNRs.

**SNRs : several with claimed 'pion-peak'**

But beware, this is at $m(\pi^0)/2 = 67.5$ MeV, so Fermi hardly covers it.

NB multiplying by $E^2$ is good but shifts the peak to higher energies, do not see the 'bump'

May be instead an indication for break in proton spectrum.

Sample spectrum: W44, Cardillo etal 2014. Model proton spectrum has break at 20 GeV.
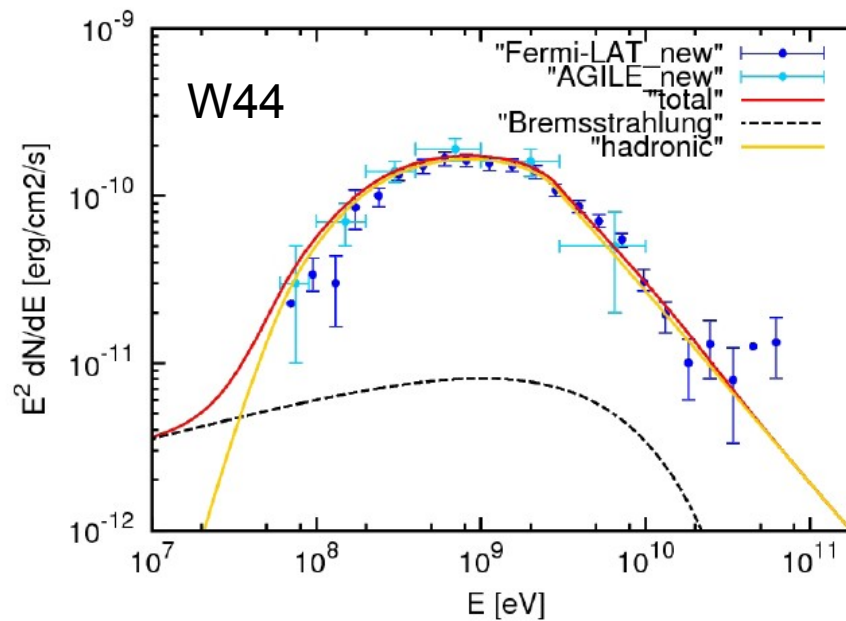
NASA SP-249

# Cosmic
# Gamma
# Rays

NATIONAL AERONAUTICS AND SPACE ADMINISTRATION

We have thus proved an important kinematic property regarding the energy range of secondary $\gamma$-rays that are the product of two-body decays; viz,

<div align="right">(1–225)</div>

> The geometric mean of the energy range of secondary $\gamma$-rays which are produced in all two-body decays is equal to the energy of the $\gamma$-rays in the rest system of the decaying primary $\mu$ and is independent of the energy of the primary particle.

these $\gamma$-rays,
num energies.

spectrum. We therefore deduce a second important kinematic property, which holds for two-body decays that produce $\gamma$-rays isotropically in the rest system of the decaying primary; viz,

> The energy spectra of $\gamma$-rays produced isotropically in the rest system of the decaying primary will be symmetric on a logarithmic plot with respect to $E_\gamma = \mu$ and will peak at $E_\gamma = \mu$.

Isotropic decay in CM
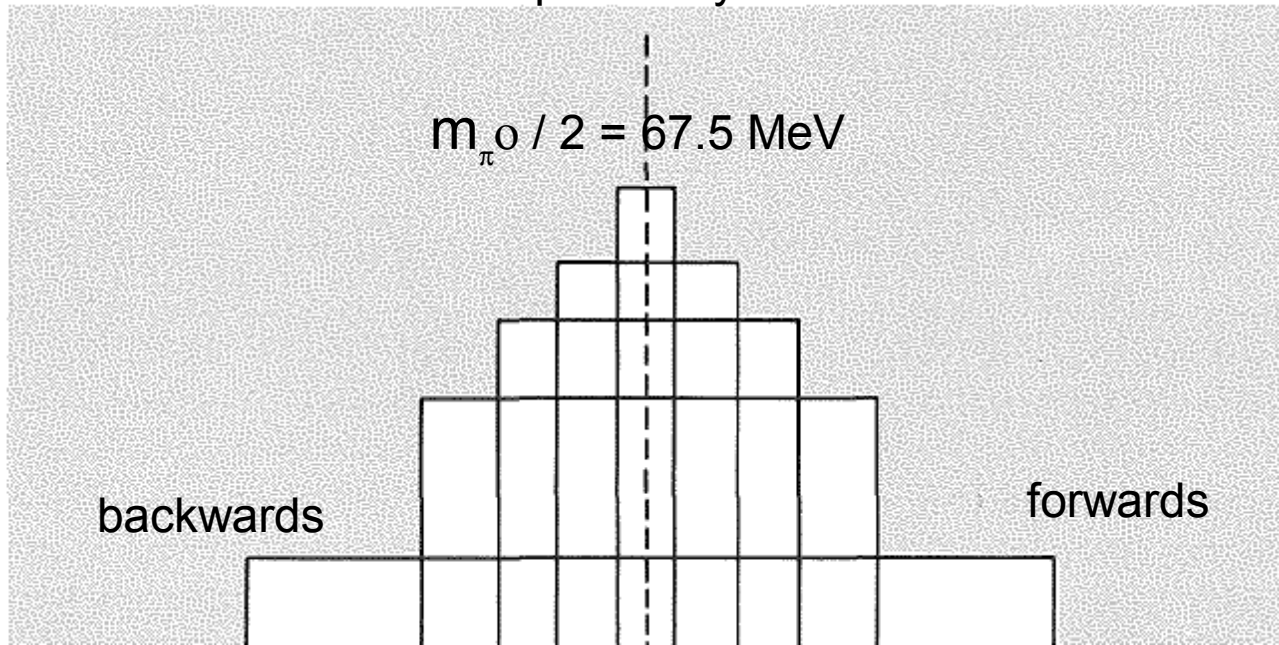
This result, combined with equations (5–26) and (5–27), yields the conclusion that $\epsilon$ increases monotonically with $\delta$. Since $F[\epsilon]$ is a monotonically decreasing functional of $\epsilon$, it follows that $F[\delta]$ is a monotonically decreasing functional of $\delta$. Thus, $F[\delta]$ is a maximum at $\delta = 0$ and decreases more and more with increasing $\delta$. It follows that $F(E_\gamma)$ is a maximum at $\ln E_\gamma = \nu$; i.e., at $E_\gamma = \frac{1}{2} m_\pi$ and that this is, in fact, the only maximum. Note that these results were reached by less rigorous arguments in our general discussion in section 1–6.
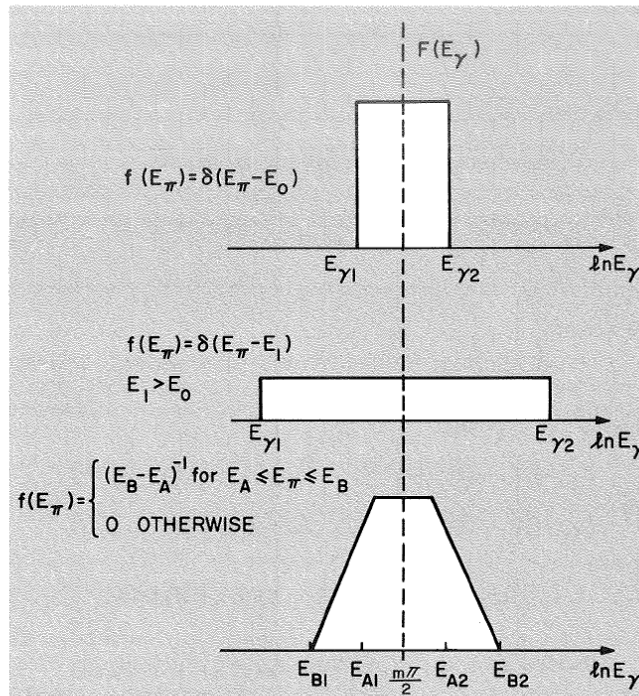
FIGURE 5–3.—Some ideal $\gamma$-ray spectra resulting from the decay of some ideal spectra of neutral pions.

**SNRs : several with claimed 'pion-peak'**

But beware, this is at $m(\pi^o)/2 = 67.5$ MeV, so Fermi hardly covers it.

NB multiplying by $E^2$ is good but shifts the peak to higher energies, do not see the 'bump'

May be instead an indication for break in proton spectrum.

Sample spectrum: W44, Cardillo et al 2014. .
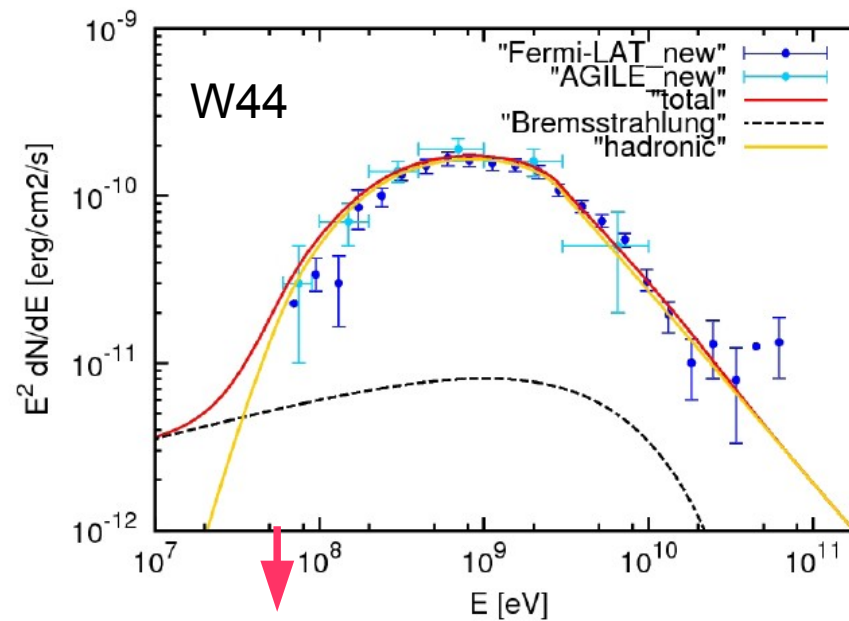


$m_\pi o / 2 = 67.5$ MeV

**SNRs : several with claimed 'pion-peak'**

But beware, this is at $m(\pi^0)/2 = 67.5$ MeV, so Fermi hardly covers it.

NB multiplying by $E^2$ is good but shifts the peak to higher energies, do not see the 'bump'

May be instead an indication for break in proton spectrum.

Need Fermi extension to lower energies, coming with Pass 8.

Sample spectrum: W44, Cardillo etal 2014. Model proton spectrum has break at 20 GeV.
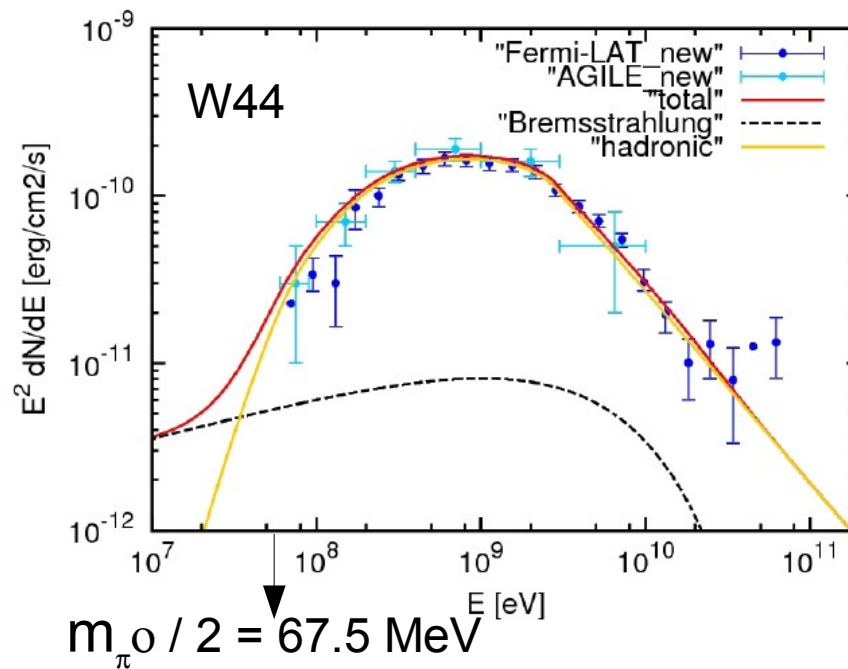


Spectrum X $E^2$

Shifts the peak
to higher energy
but Fermi cannot
see a peak which is
below it's range!

# Sample spectrum: W44, Cardillo etal 2014. Model proton spectrum has break at 20 GeV.



Spectrum X $E^2$

Shifts the peak
to higher energy
but Fermi cannot
see a peak which is
below it's range!

Spectrum times $E^2$

Sample spectrum: W44, Cardillo etal 2014. Model proton spectrum has break at 20 GeV.



Spectrum X $E^2$

Shifts the peak
to higher energy
but Fermi cannot
see a peak which is
below it's range!

Spectrum times $E^2$

Spectrum without $E^2$
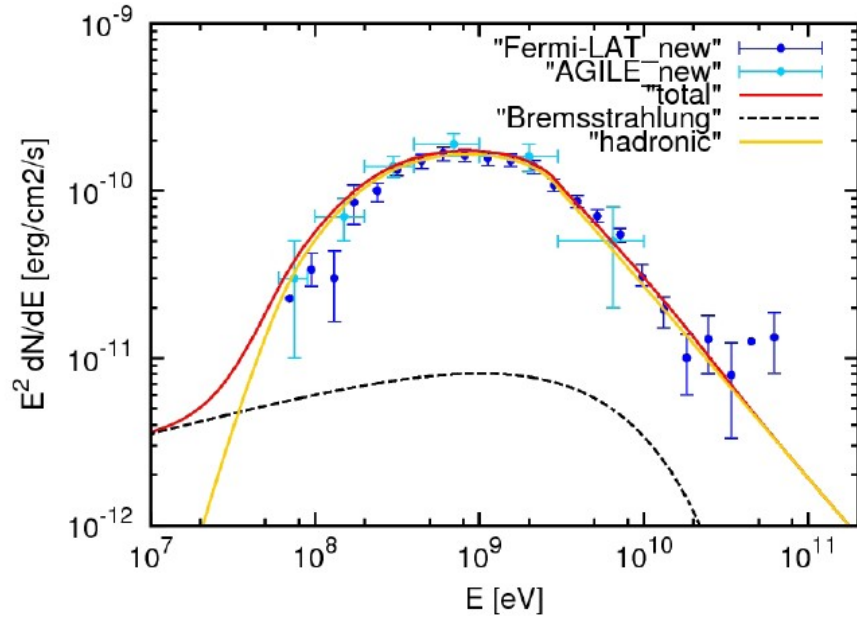


MeV cm$^{-2}$ s$^{-1}$

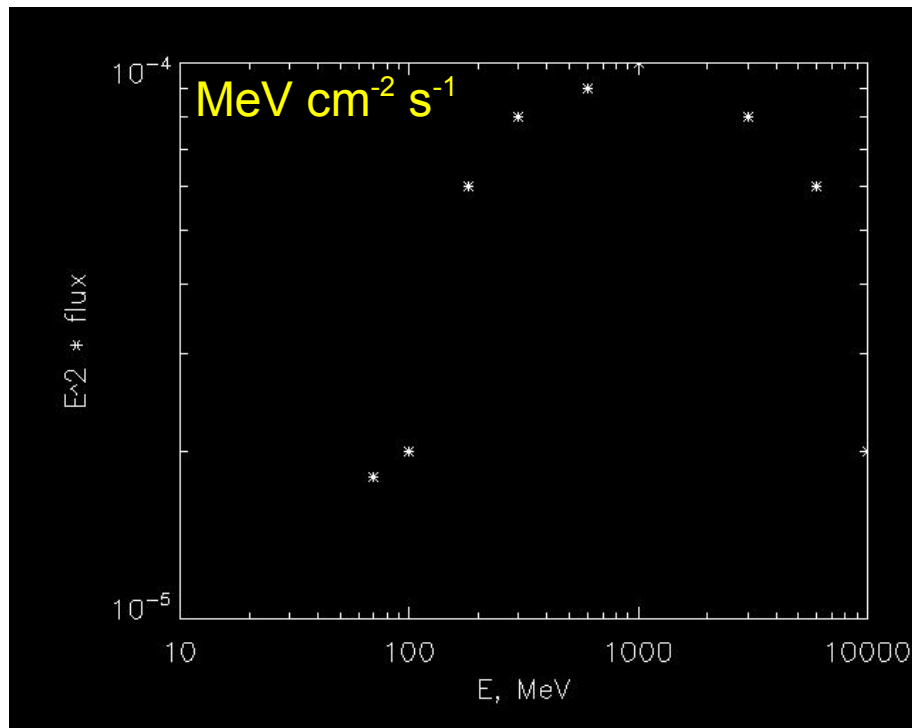cm$^{-2}$ s$^{-1}$ MeV$^{-1}$

# Sample spectrum: W44, Cardillo etal 2014. Model proton spectrum has break at 20 GeV.
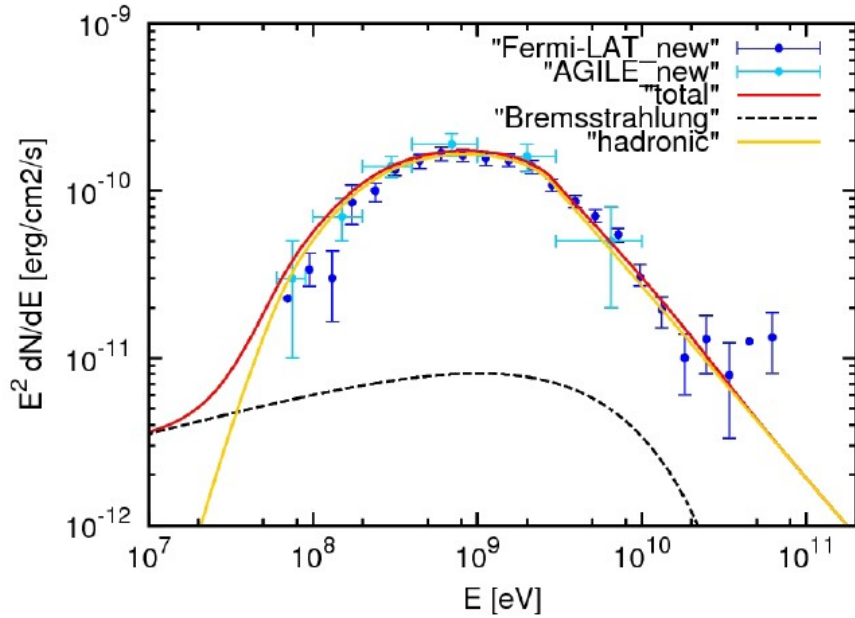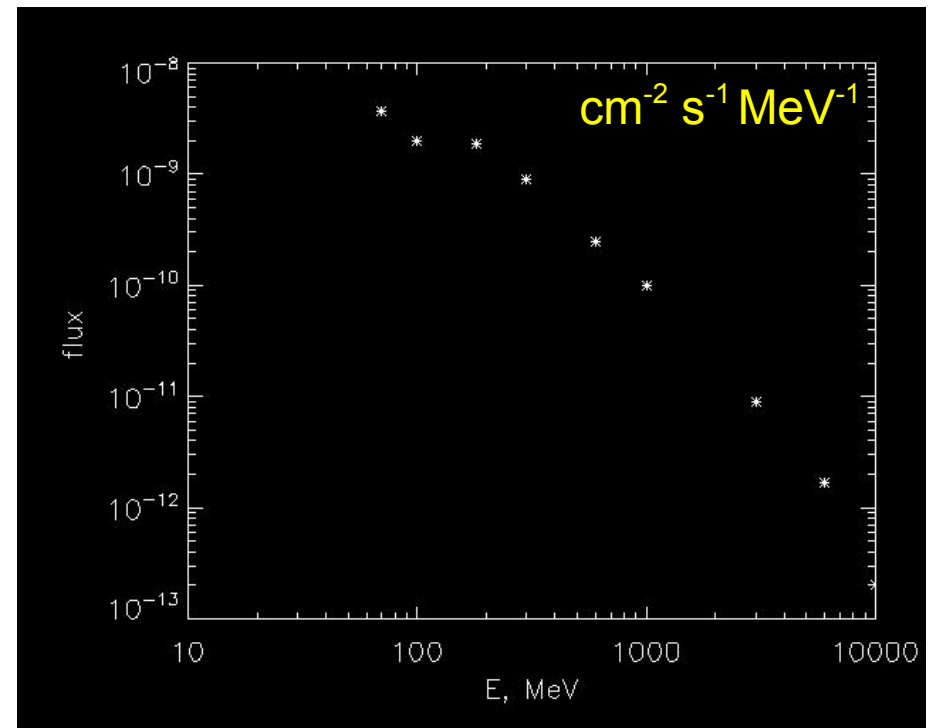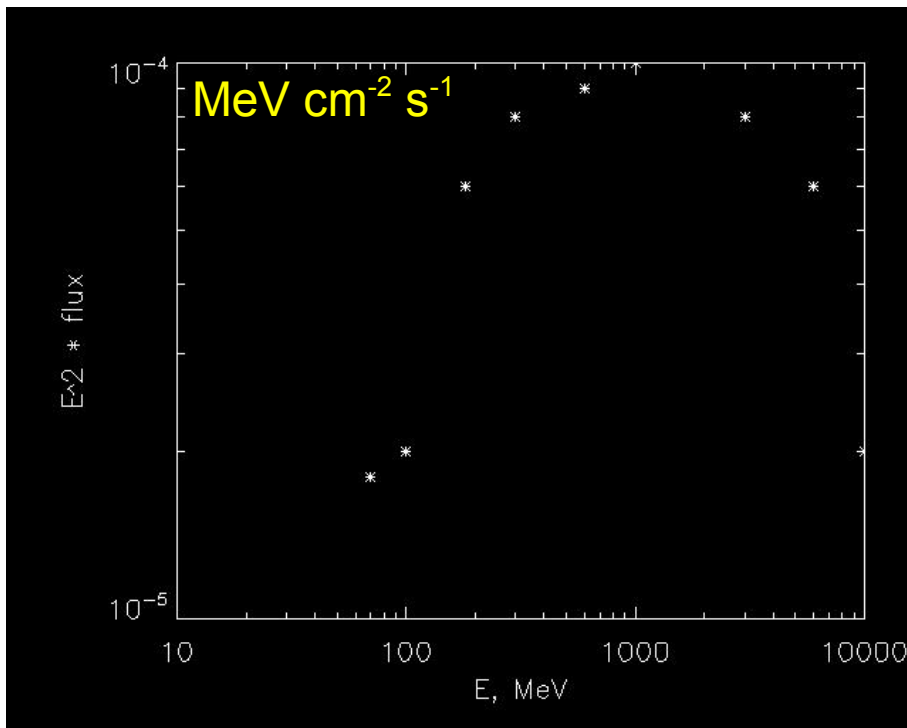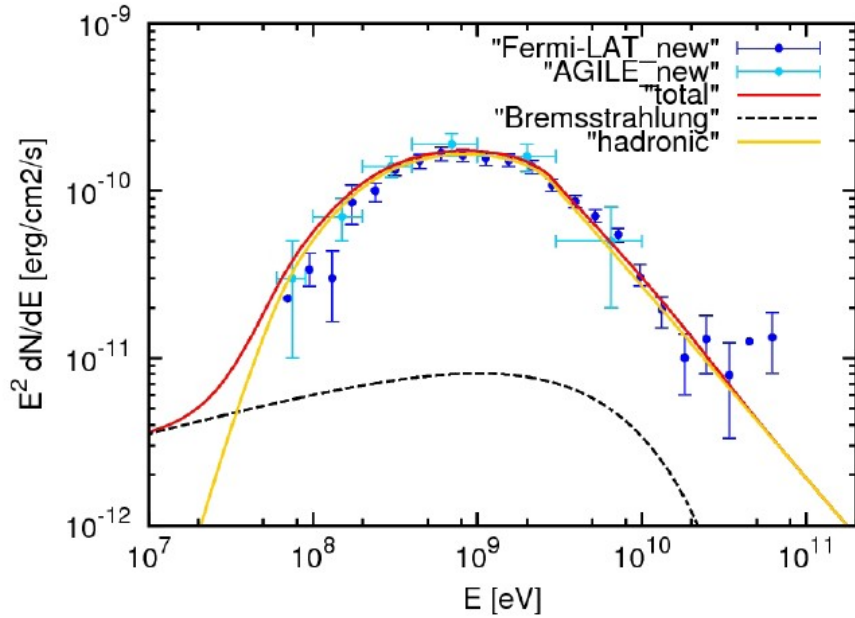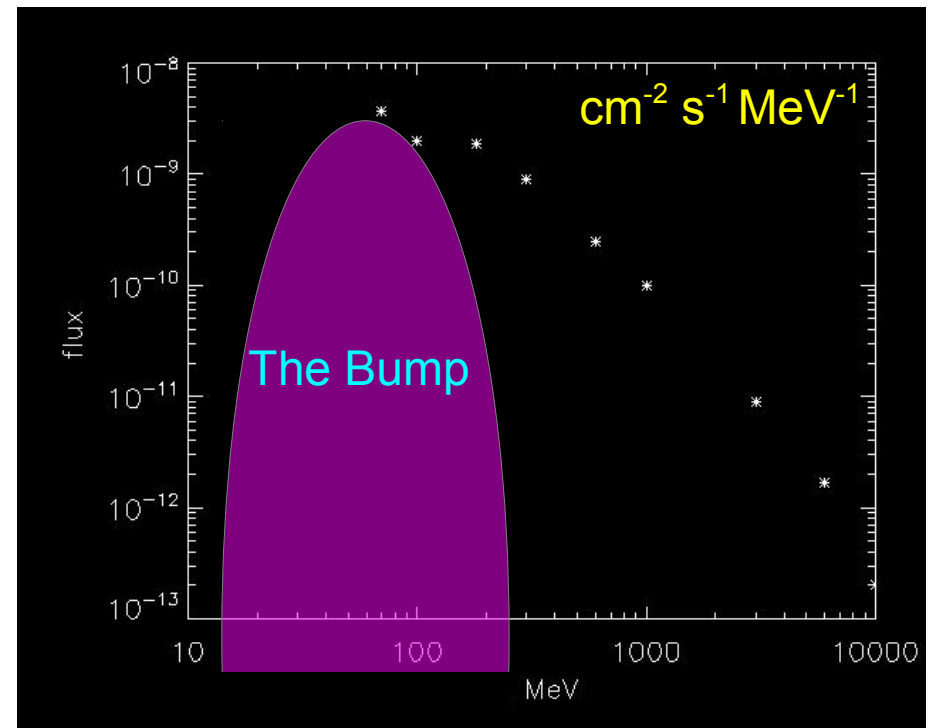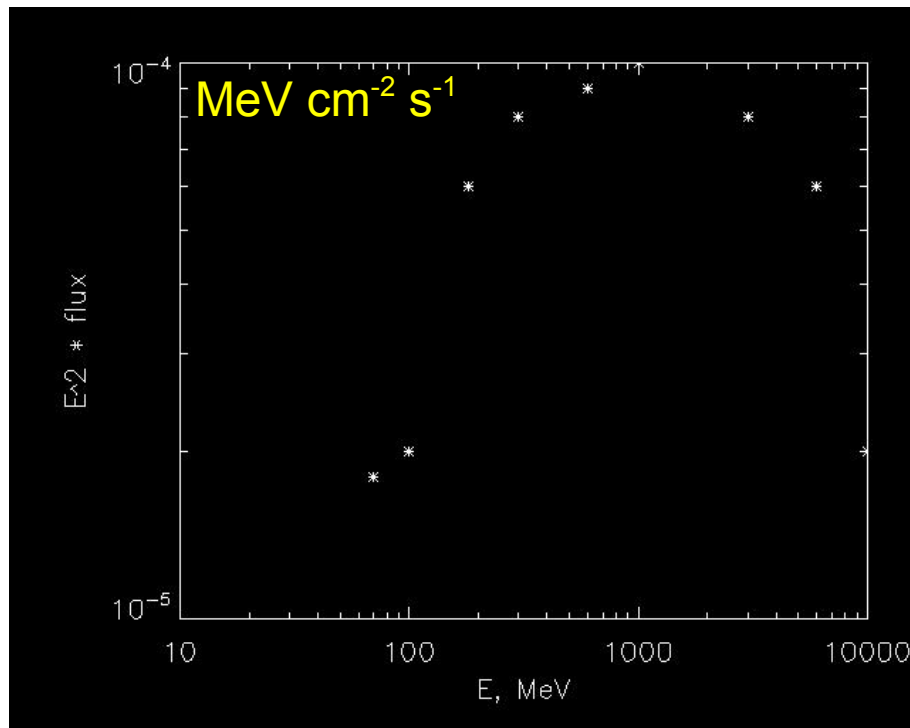


Spectrum X E$^2$

Shifts the peak
to higher energy
but Fermi cannot
see a peak which is
below it's range!

Spectrum times E$^2$

Spectrum without E$^2$



MeV cm$^{-2}$ s$^{-1}$



cm$^{-2}$ s$^{-1}$ MeV$^{-1}$

The Bump

# The supernova remnant W44: a case of Cosmic-Ray reacceleration.

M. Cardillo[1], E. Amato[1], and P. Blasi[1,2]

[1] INAF/Osservatorio Astrofisico di Arcetri, Largo E. Fermi, 5 - 50125 Firenze, Italy
e-mail:martina@arcetri.astro.it
[2] Gran Sasso Science Institute (INFN), viale F. Crispi 7, 67100 L' Aquila, Italy.

## ABSTRACT

Supernova remnants (SNRs) are thought to be the primary sources of Galactic Cosmic Rays (CRs). In the last few years, the wealth of $\gamma$-ray data collected by GeV and TeV instruments has provided important information about particle energisation in these astrophysical sources, allowing us to make progress in assessing their role as CR accelerators. In particular, the spectrum of the $\gamma$-ray emission detected by AGILE and Fermi-LAT from the two middle aged Supernova Remnants (SNRs) W44 and IC443, has been proposed as a proof of CR acceleration in SNRs. Here we discuss the possibility that the radio and $\gamma$-ray spectra from W44 may be explained in terms of re-acceleration and compression of Galactic CRs. The recent measurement of the interstellar CR flux by Voyager I has been instrumental for our work, in that the result of the reprocessing of CRs by the shock in W44 depends on the CR spectrum at energies that are precluded to terrestrial measurement due to solar modulation. We introduce both CR protons and helium nuclei in our calculations, and secondary electrons produced *in situ* are compared with the flux of Galactic CR electrons reprocessed by the slow shock of this SNR. We find that the multi-wavelength spectrum of W44 can be explained by reaccelerated particles with no need of imposing any break on their distribution, but just a high energy cut-off at the maximum energy the accelerator can provide. We also find that a model including both re-acceleration and a very small fraction of freshly accelerated particles may be more satisfactory on physical grounds.

ArXiv:1604.02321  July 2016

# The supernova remnant W44: a case of Cosmic-Ray reacceleration.

M. Cardillo[1], E. Amato[1], and P. Blasi[1,2]

teractions with ambient matter. Indeed the $\gamma$-ray spectrum of W44 showed the pion bump that can be unequivocally linked to CR hadronic interactions, as later confirmed by the Fermi-LAT

**Fig. 3.** **Left**:VLA (red) and Planck (blue) radio data from the whole remnant (Castelletti et al. 2007; Planck collaboration 2014) and VLA radio data from the high-energy emitting region (green), plotted together with primary (cyan dashed line), secondary (magenta dot-dashed line) and total (black line) synchrotron radio emission obtained in our best fit reacceleration model. **Right**: AGILE (green) and Fermi-LAT (red) $\gamma$-ray points (Cardillo et al. 2014; Ackermann et al. 2013) plotted with $\gamma$-ray emission from pion decay (blue dotted line), emission due to bremsstrahlung of primary (cyan dashed line) and secondary (magenta dot-dashed line) electrons, and total emission (black line).

# The supernova remnant W44: a case of Cosmic-Ray reacceleration.

M. Cardillo[1], E. Amato[1], and P. Blasi[1,2]

arXiv: 1604.02321

'bump' is result of break in proton spectrum



**Fig. 2.** Spectra of protons, He nuclei and electrons in the local ISM (solid lines) and after shock reacceleration and compression in the crushed cloud (dashed lines). The change of slope at ~ 10 GeV is associated with the acceleration cutoff. Particles at higher energy are simply compressed in the cloud. Ionisation energy losses affect the spectral slopes at lower energies, synchrotron losses steepen the electron spectrum at higher energies, whereas Bremsstrahlung and pp losses mainly affect the normalization. remnant (Castelletti et al. 2007; Planck collaboration 2014) and VLA radio primary (cyan dashed line), secondary (magenta dot-dashed line) and total leration model. **Right**: AGILE (green) and Fermi-LAT (red) $\gamma$-ray points on from pion decay (blue dotted line), emission due to bremsstrahlung of ectrons, and total emission (black line).
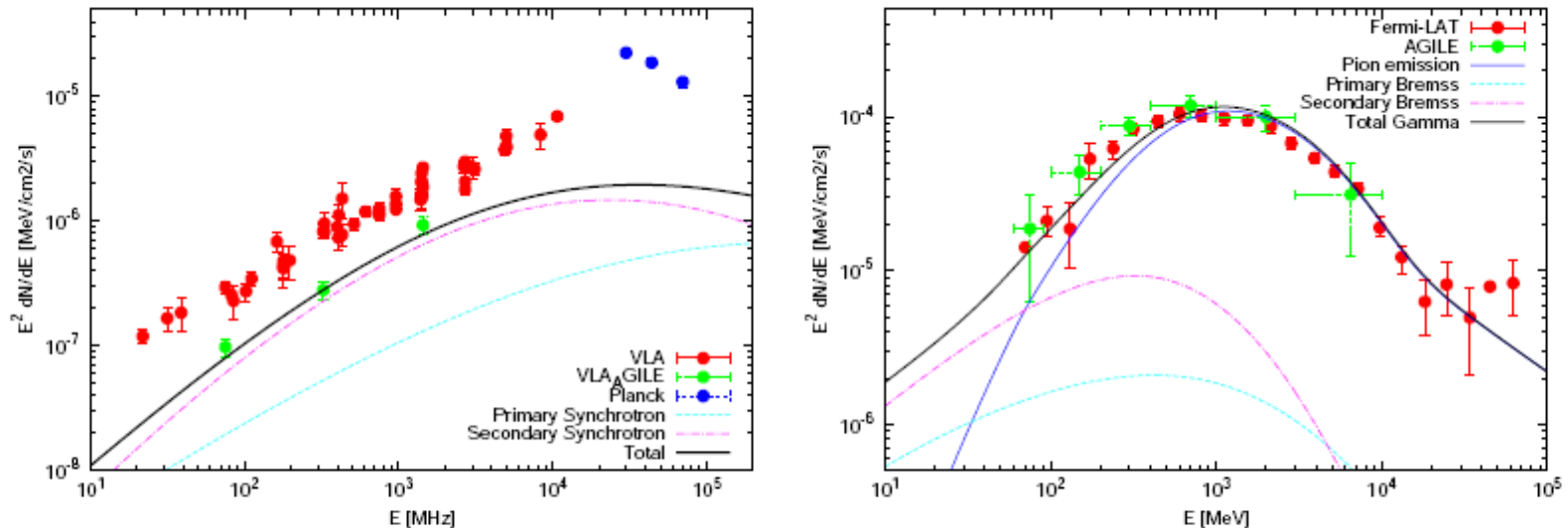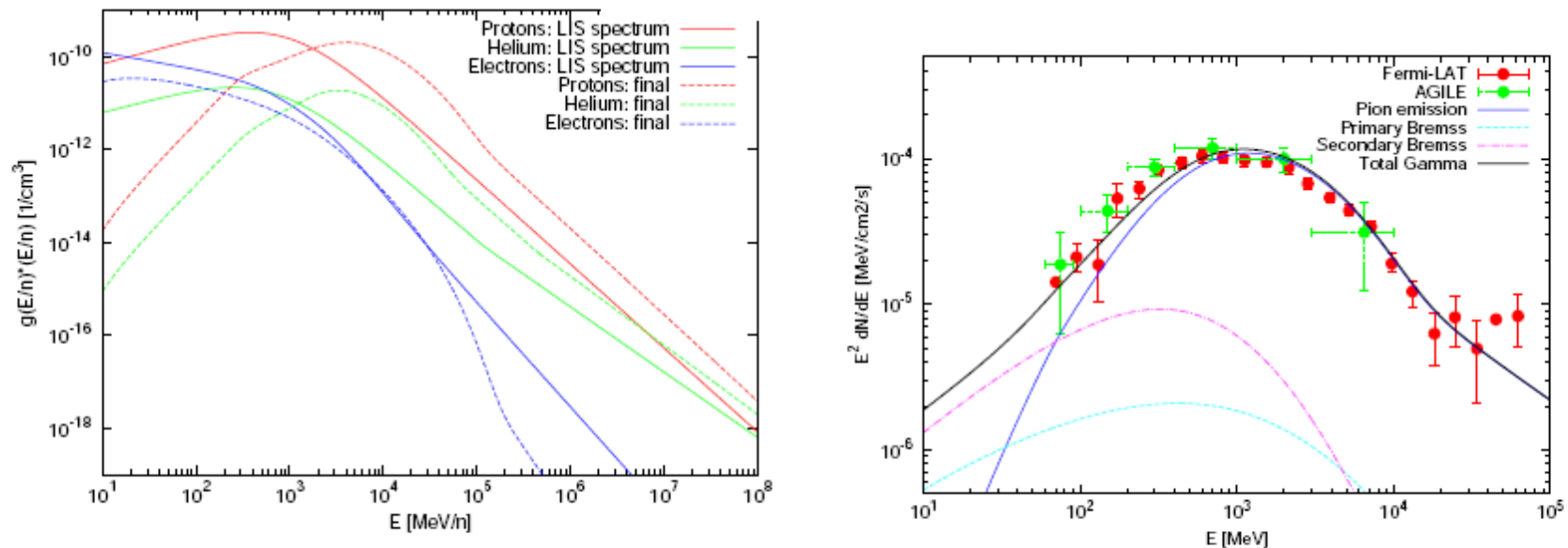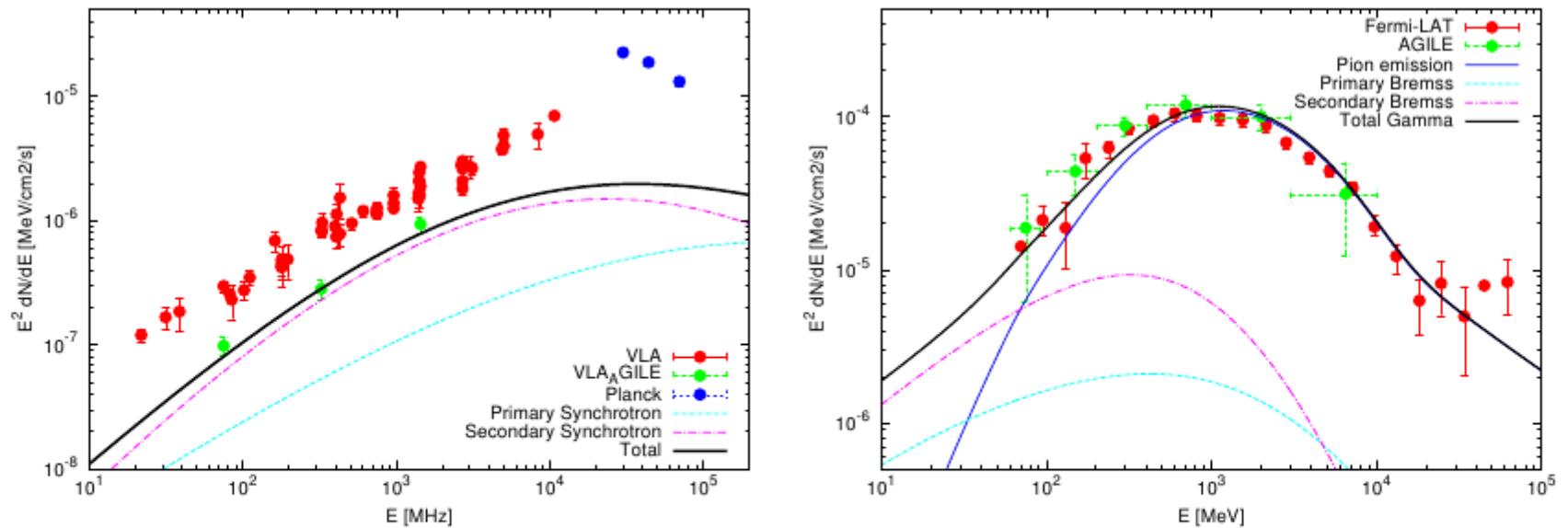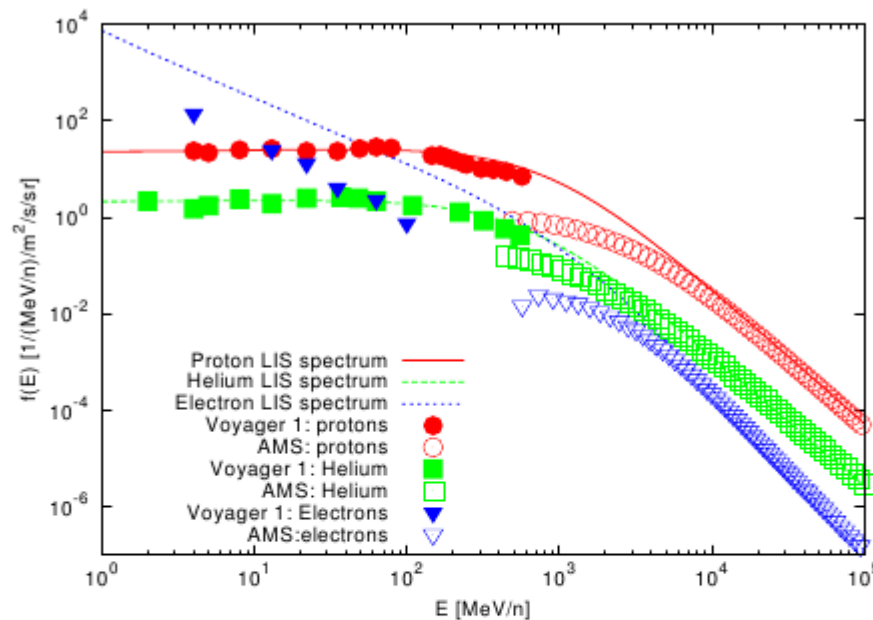
**Fig. 3. Left:** VLA (red) and Planck (blue) radio data from the whole remnant (Castelletti et al. 2007; Planck collaboration 2014) and VLA radio data from the high-energy emitting region (green), plotted together with primary (cyan dashed line), secondary (magenta dot-dashed line) and total (black line) synchrotron radio emission obtained in our best fit reacceleration model. **Right:** AGILE (green) and Fermi-LAT (red) $\gamma$-ray points (Cardillo et al. 2014; Ackermann et al. 2013) plotted with $\gamma$-ray emission from pion decay (blue dotted line), emission due to bremsstrahlung of primary (cyan dashed line) and secondary (magenta dot-dashed line) electrons, and total emission (black line).

Cardillo etal 2016



**Fig. 1.** Protons (red), Helium (green) and electrons (blue) spectra. Cir-
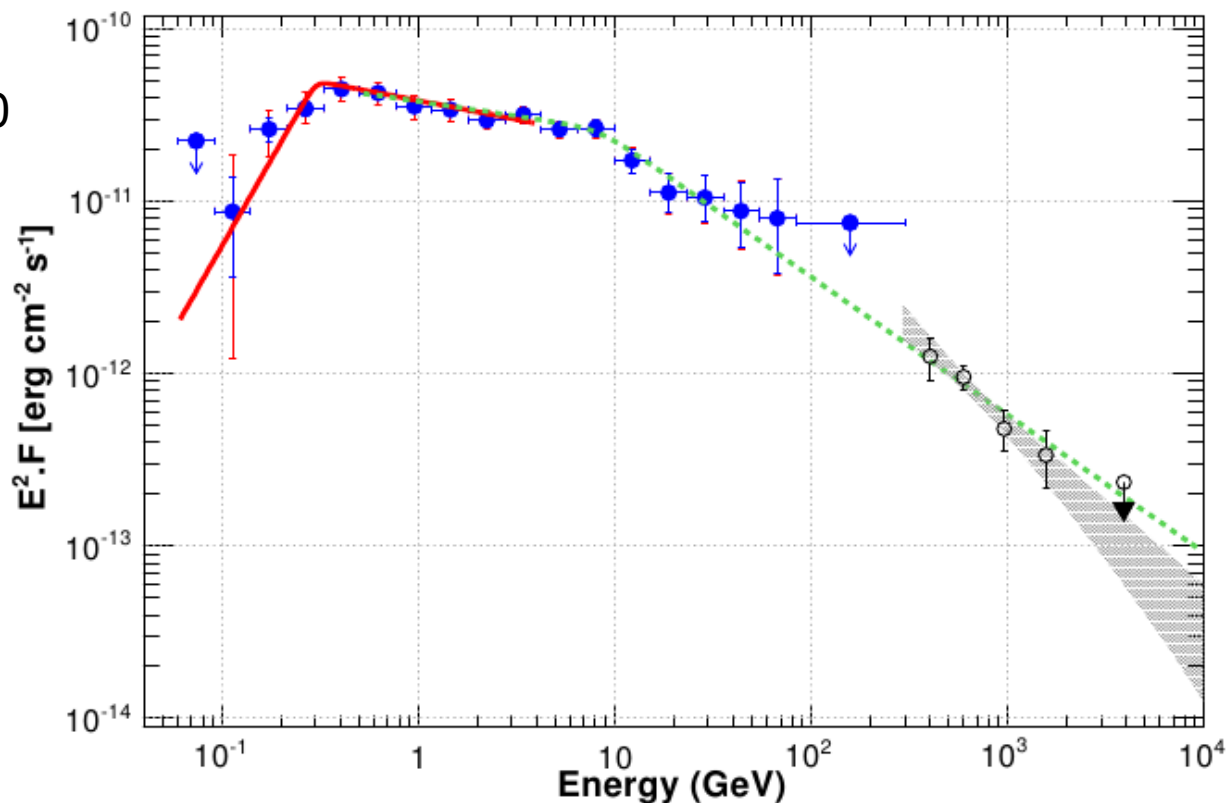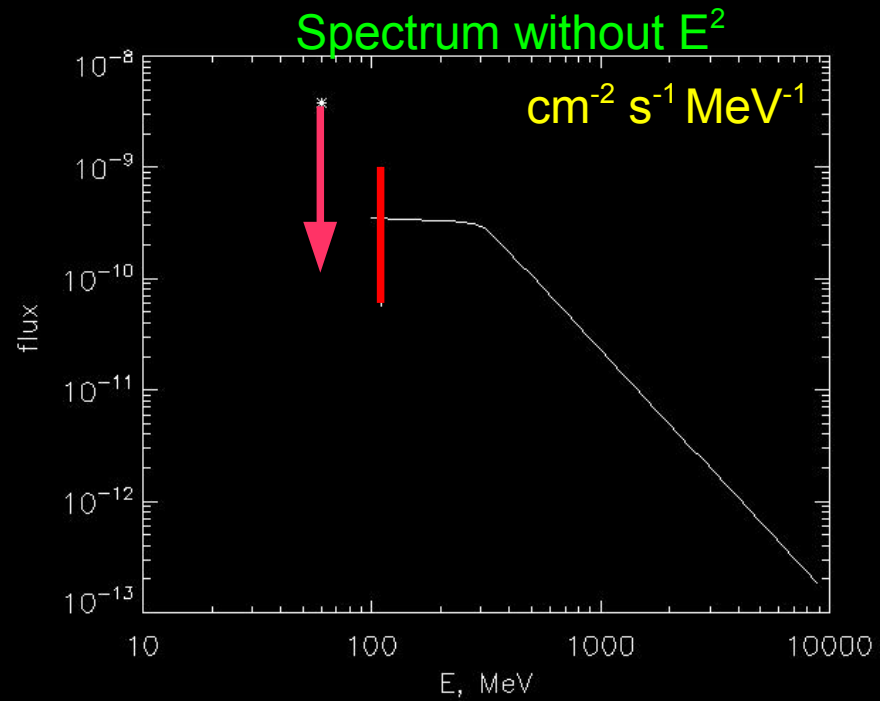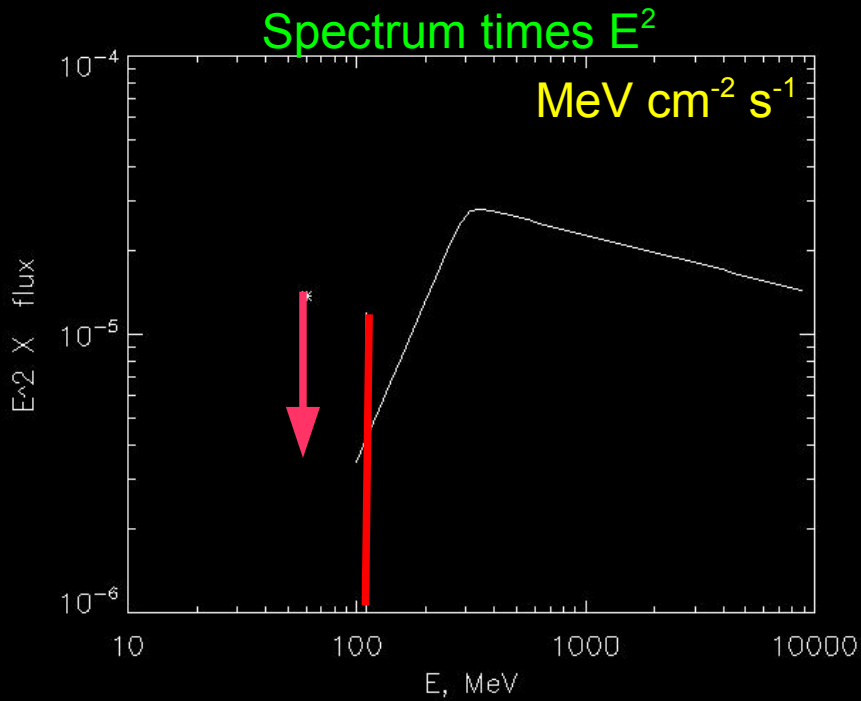
W49B
Fermi + H.E.S.S.
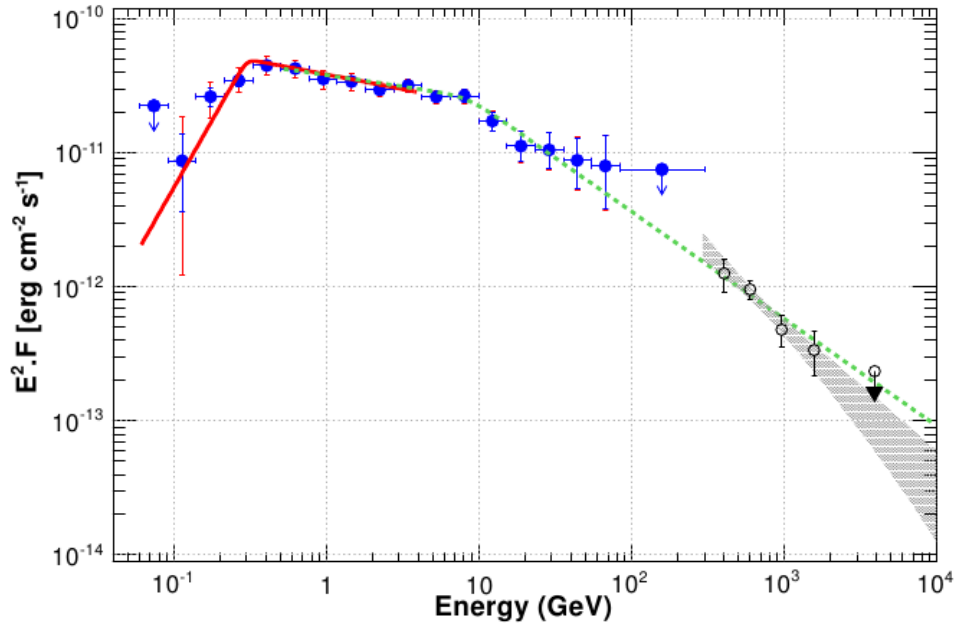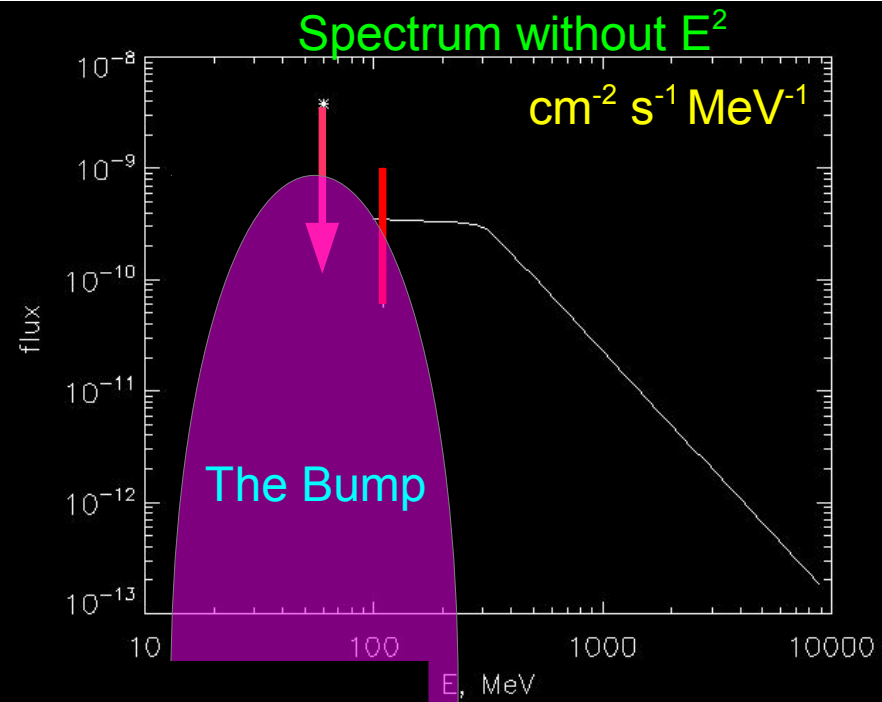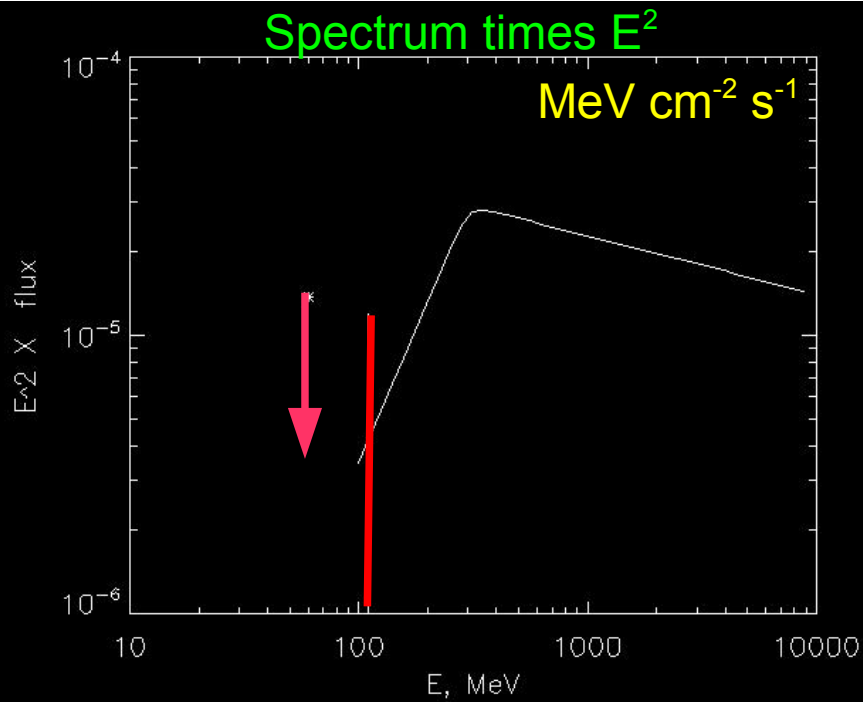arXiv: 1609.00900
2 Sept 2016
A&A in press



**Fig. 3.** *Fermi*-LAT and H.E.S.S. spectrum of W49B. The red line shows the best fit of a smoothly broken power-law derived between 60 MeV and 4 GeV and the blue data points indicate the fluxes measured in each energy bin with the *Fermi*-LAT. The statistical errors are shown in blue, while the red lines take into account both the statistical and systematic errors as discussed in Sect. 2.2.2 The gray band shows the 68% confidence level (CL) uncertainty of the best-fit power-law model with H.E.S.S. The open black circles are the spectral points computed from the forward-folding fit with their statistical errors shown in black. For both instruments, a 95% CL upper limit is computed when the statistical significance is lower than $2\sigma$. The dotted green line shows the best smoothly broken power-law model obtained from the joint fit of the *Fermi*-LAT and H.E.S.S. data between 500 MeV and 10 TeV, as described in Sect. 2.3

W49B

Spectrum times $E^2$

MeV cm$^{-2}$ s$^{-1}$

Spectrum without $E^2$

cm$^{-2}$ s$^{-1}$ MeV$^{-1}$

W49B

Spectrum times E²

MeV cm⁻² s⁻¹

Spectrum without E²

cm⁻² s⁻¹ MeV⁻¹

The Bump
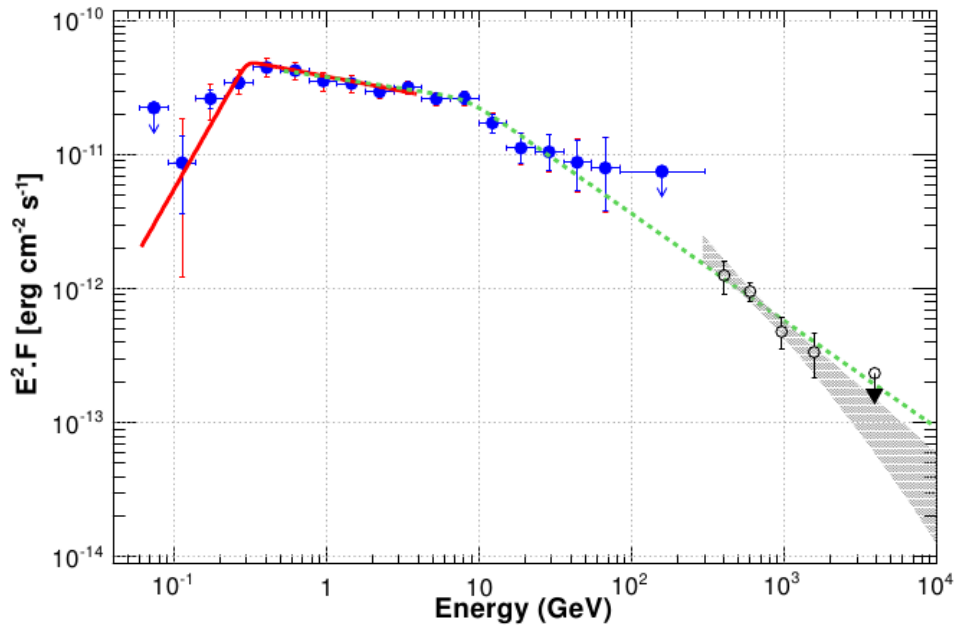
W49B
Fermi + H.E.S.S.
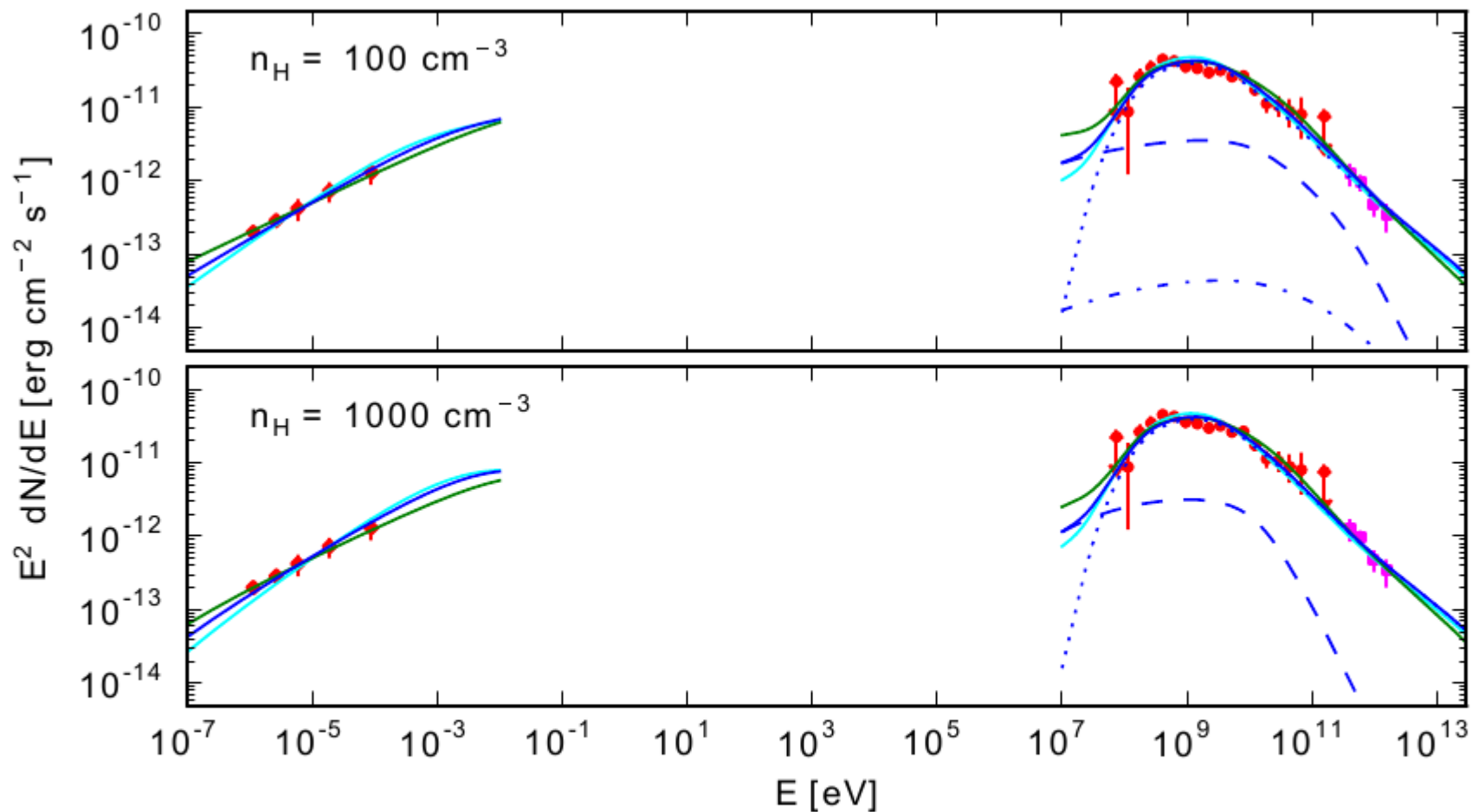arXiv: 1609.00900
2 Sept 2016
A&A in press



**Fig. 5.** SEDs of W49B with model curves for the hadronic-dominant scenario. The upper and the lower panels show (a1–3) and (a4–6) respectively (see Table 2). The red diamonds, red circles, and magenta squares represent observed data in the radio (Moffett & Reynolds 1994), LAT, and H.E.S.S. bands respectively. The radio emission is explained by the synchrotron radiation from the relativistic electrons. The $\gamma$-ray emission can be decomposed into $\pi^0$-decay (dotted line), bremsstrahlung (dashed line), and IC scattering (dot-dashed line). The solid line represents the total flux of the components. The cases (a1)/(a4), (a2)/(a5), and (a3)/(a6) are represented by cyan, blue, and green lines respectively in the upper/lower panel. The decomposed emissions are shown for the cases (a2) and (a5) in the upper and the lower panels respectively.

# DEEP MORPHOLOGICAL AND SPECTRAL STUDY OF THE SNR RCW 86 WITH *FERMI*-LAT

M. Ajello[2], L. Baldini[3,4], G. Barbiellini[5,6], D. Bastieri[7,8], R. Bellazzini[9], E. Bissaldi[10], E. D. Bloom[4],
R. Bonino[11,12], E. Bottacini[4], T. J. Brandt[13], J. Bregeon[14], P. Bruel[15], R. Buehler[16], G. A. Caliandro[4,17],
R. A. Cameron[4], M. Caragiulo[18,10,1], E. Cavazzuti[19], E. Charles[4], A. Chekhtman[20], S. Ciprini[19,21],
J. Cohen-Tanugi[14], B. Condon[22,1], F. Costanza[10], S. Cutini[19,23,21], F. D'Ammando[24,25], F. de Palma[10,26],
R. Desiante[27,11], N. Di Lalla[9], M. Di Mauro[4], L. Di Venere[18,10], P. S. Drell[4], G. Dubner[28], D. Dumora[22],
L. Duvidovich[28], C. Favuzzi[18,10], W. B. Focke[4], P. Fusco[18,10], F. Gargano[10], D. Gasparrini[19,21], E. Giacani[28],
N. Giglietto[18,10], T. Glanzman[4], D. A. Green[29], I. A. Grenier[30], S. Guiriec[13,31], E. Hays[13], J.W. Hewitt[32],
A. B. Hill[33,4], D. Horan[15], T. Jogler[4], G. Jóhannesson[34], I. Jung-Richardt[35], S. Kensei[36], M. Kuss[9],
S. Larsson[37,38], L. Latronico[11], M. Lemoine-Goumard[22,1], J. Li[39], L. Li[37,38], F. Longo[5,6], F. Loparco[18,10],
M. N. Lovellette[40], P. Lubrano[21], J. Magill[41], S. Maldera[11], A. Manfreda[9], M. Mayer[16], M. N. Mazziotta[10],
J. E. McEnery[13,41], P. F. Michelson[4], W. Mitthumsiri[42], T. Mizuno[43], M. E. Monzani[4], A. Morselli[44],
I. V. Moskalenko[4], M. Negro[11,12], E. Nuss[14], M. Orienti[24], E. Orlando[4], J. F. Ormes[45], D. Paneque[46,4],
J. S. Perkins[13], M. Pesce-Rollins[9,4], F. Piron[14], G. Pivato[9], T. A. Porter[4], S. Rainò[18,10], R. Rando[7,8],
M. Razzano[9,47], A. Reimer[48,4], O. Reimer[48,4], T. Reposeur[22], J. Schmid[30], A. Schulz[16], C. Sgrò[9], D. Simone[10],
E. J. Siskind[49], F. Spada[9], G. Spandre[9], P. Spinelli[18,10], J. B. Thayer[4], L. Tibaldo[50], D. F. Torres[39,51],
G. Tosti[21,52], E. Troja[13,41], Y. Uchiyama[53], G. Vianello[4], J. Vink[54], K. S. Wood[40], M. Yassine[14]

## ABSTRACT

RCW 86 is a young supernova remnant (SNR) showing a shell-type structure at several wavelengths and is thought to be an efficient cosmic-ray (CR) accelerator. Earlier *Fermi* Large Area Telescope results reported the detection of $\gamma$-ray emission coincident with the position of RCW 86 but its origin (leptonic or hadronic) remained unclear due to the poor statistics. Thanks to 6.5 years of data acquired by the *Fermi*-LAT and the new event reconstruction Pass 8, we report the significant detection of spatially extended emission coming from RCW 86. The spectrum is described by a power-law function with a very hard photon index ($\Gamma = 1.42 \pm 0.1_{\mathrm{stat}} \pm 0.06_{\mathrm{syst}}$) in the 0.1–500 GeV range and an energy flux above 100 MeV of $(2.91 \pm 0.8_{\mathrm{stat}} \pm 0.12_{\mathrm{syst}}) \times 10^{-11}$ erg cm$^{-2}$ s$^{-1}$. Gathering all the available multiwavelength (MWL) data, we perform a broadband modeling of the nonthermal emission of RCW 86 to constrain parameters of the nearby medium and bring new hints about the origin of the $\gamma$-ray emission. For the whole SNR, the modeling favors a leptonic scenario in the framework of a two-zone model with an average magnetic field of $10.2 \pm 0.7$ $\mu$G and a limit on the maximum energy injected into protons of $2 \times 10^{49}$ erg for a density of 1 cm$^{-3}$. In addition, parameter values are derived for the North-East (NE) and South-West (SW) regions of RCW 86, providing the first indication of a higher magnetic field in the SW region.

## 7.2. *Modeling of the whole SNR*

Here we present the results of two leptonic scenario models. Since a pure hadronic scenario requires unlikely parameter values such as a very hard spectral index for protons (as it was already suggested in Lemoine-Goumard et al. 2012) and a high magnetic field ($B > 100\ \mu$G), we did not consider this case. The presence of a high magnetic field is not excluded in very thin regions, near the shock, but it is very unlikely to have such high values for the whole remnant. Moreover, a spectral index softer than 1.7 is excluded with more than $3\sigma$, as described in Section 3.2. The hadronic model re-
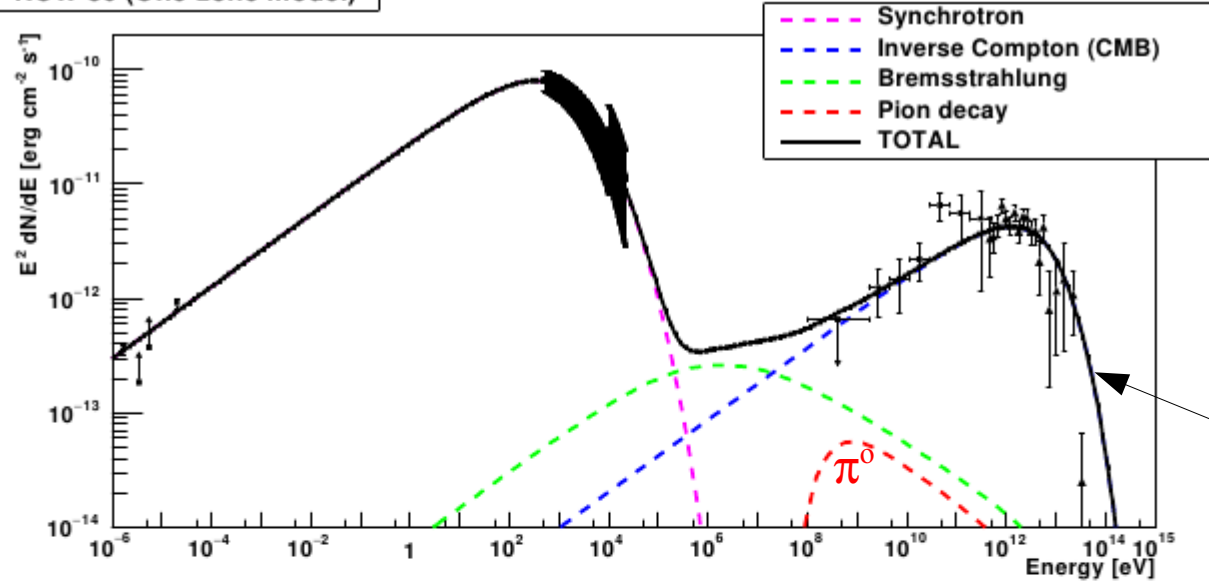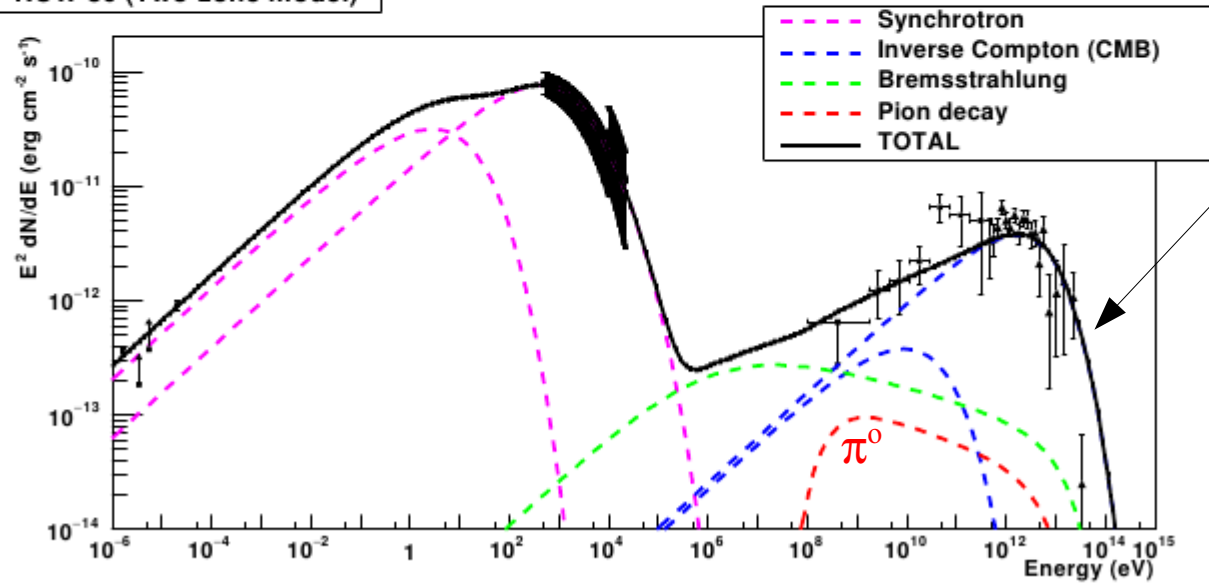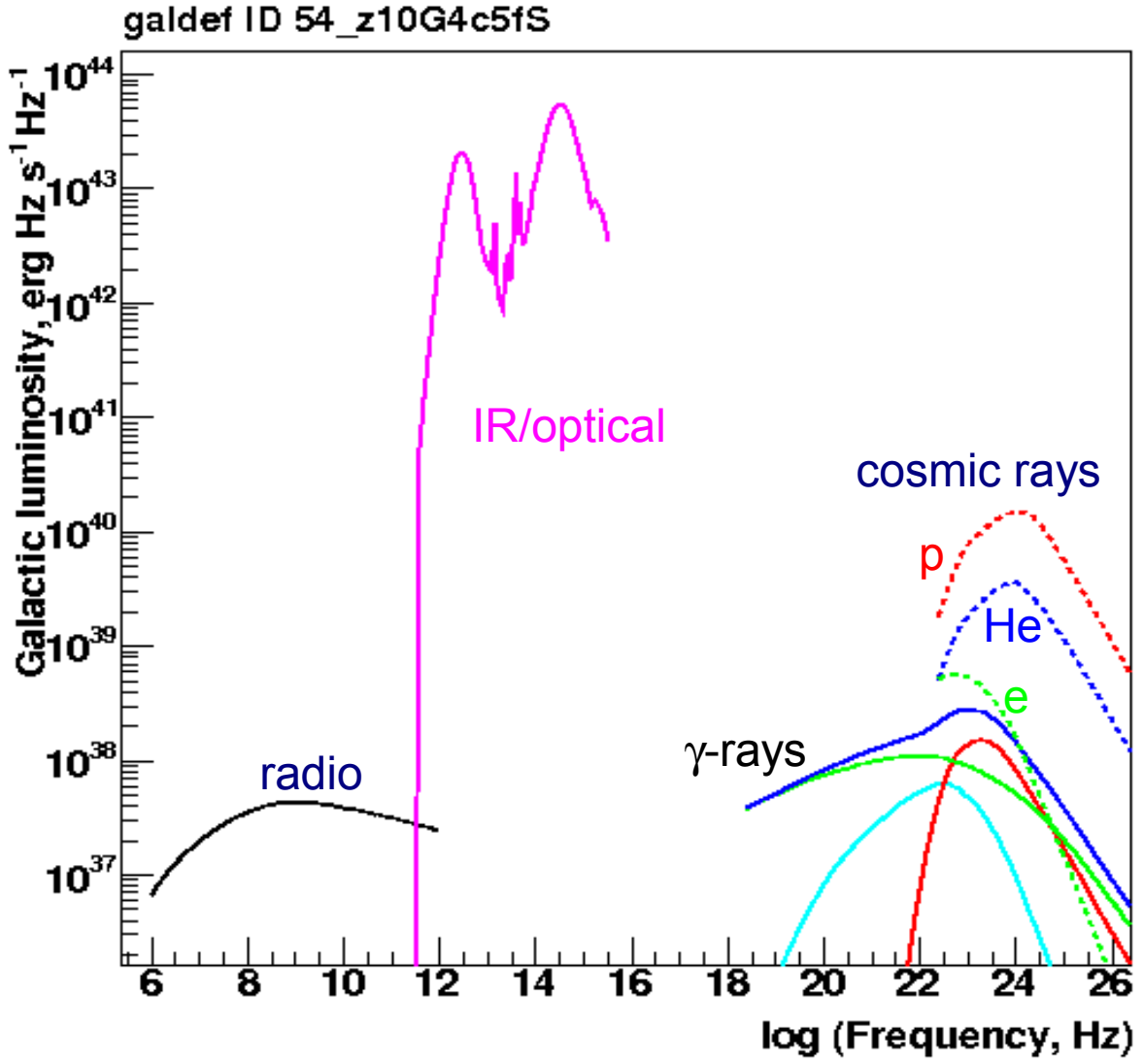
FIG. 9.— Spectral Energy Distribution of RCW 86 with the best-fit leptonic one-zone (top) and two-zone (bottom) models. The radio points are from Molonglo at 408 MHz and Parkes at 5 GHz (Caswell et al. 1975; Lemoine-Goumard et al. 2012) and lower limits from MOST at 843 MHz and ATCA at 1.43 GHz (Whiteoak & Green 1996; Dickel et al. 2001). X-ray spectra from ASCA and RXTE are from Lemoine-Goumard et al. (2012). The *Fermi*-LAT spectral points and upper limits (95% C.L.) derived in Section 3.2 and the H.E.S.S. data points in the VHE γ-ray domain from Abramowski et al. (2015) are also shown.

Moral:

Fit to hadronic models but don't call it the Pion Bump or even Pion Rise!

Need multiwavelength models to show hadronic origin, and this is of course done.

# Galaxy luminosity over 20 decades of energy



galdef ID 54_z10G4c5fS

IR/optical

cosmic rays

p

He

e

γ-rays

radio

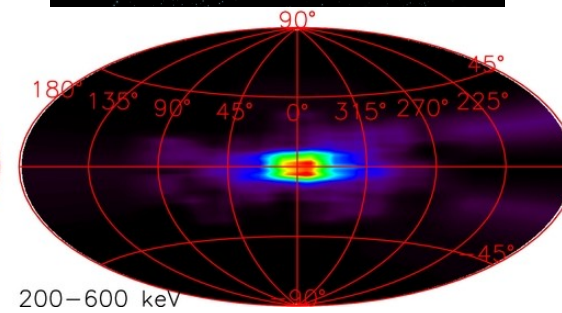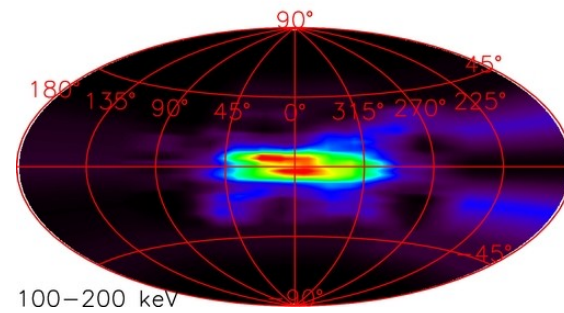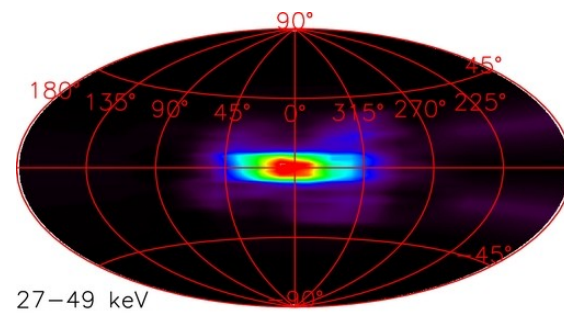Strong et al. (2010), ApJL 722, L58

Interstellar MeV gamma rays
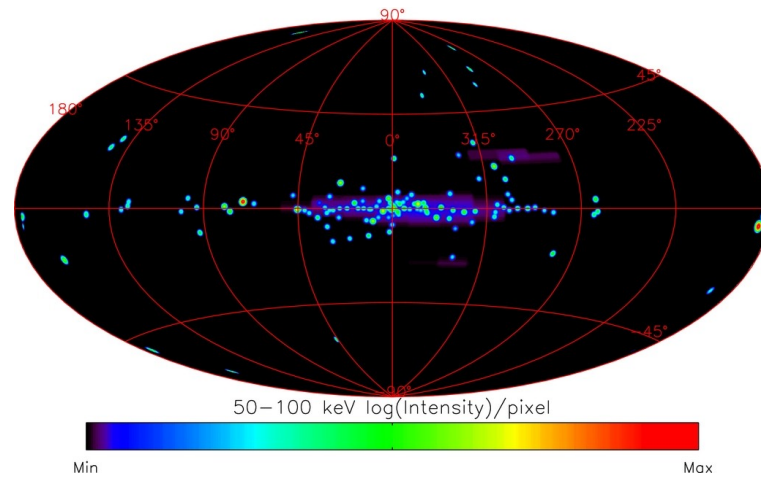
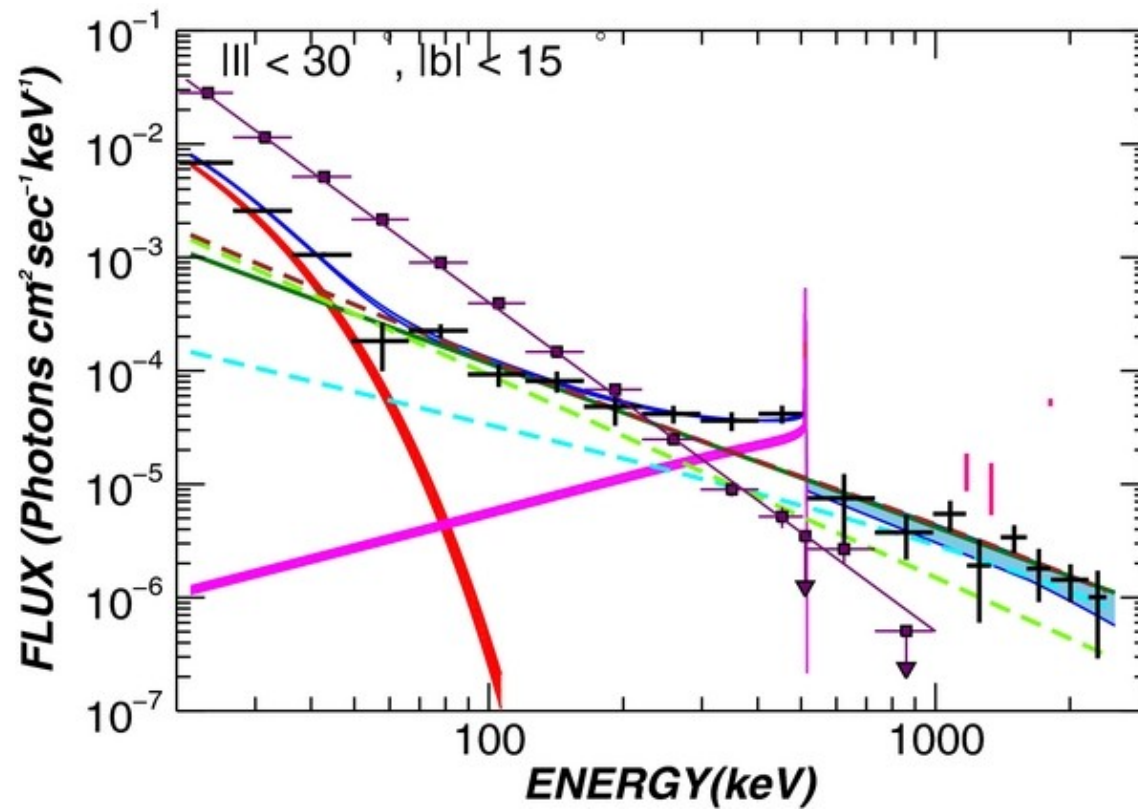the cosmic-ray connection

see talk by Elena Orlando at this conference

Continuum skymaps
INTEGRAL / SPI
Bouchet et al. ApJ 739, 29, 2011



50−100 keV log(Intensity)/pixel
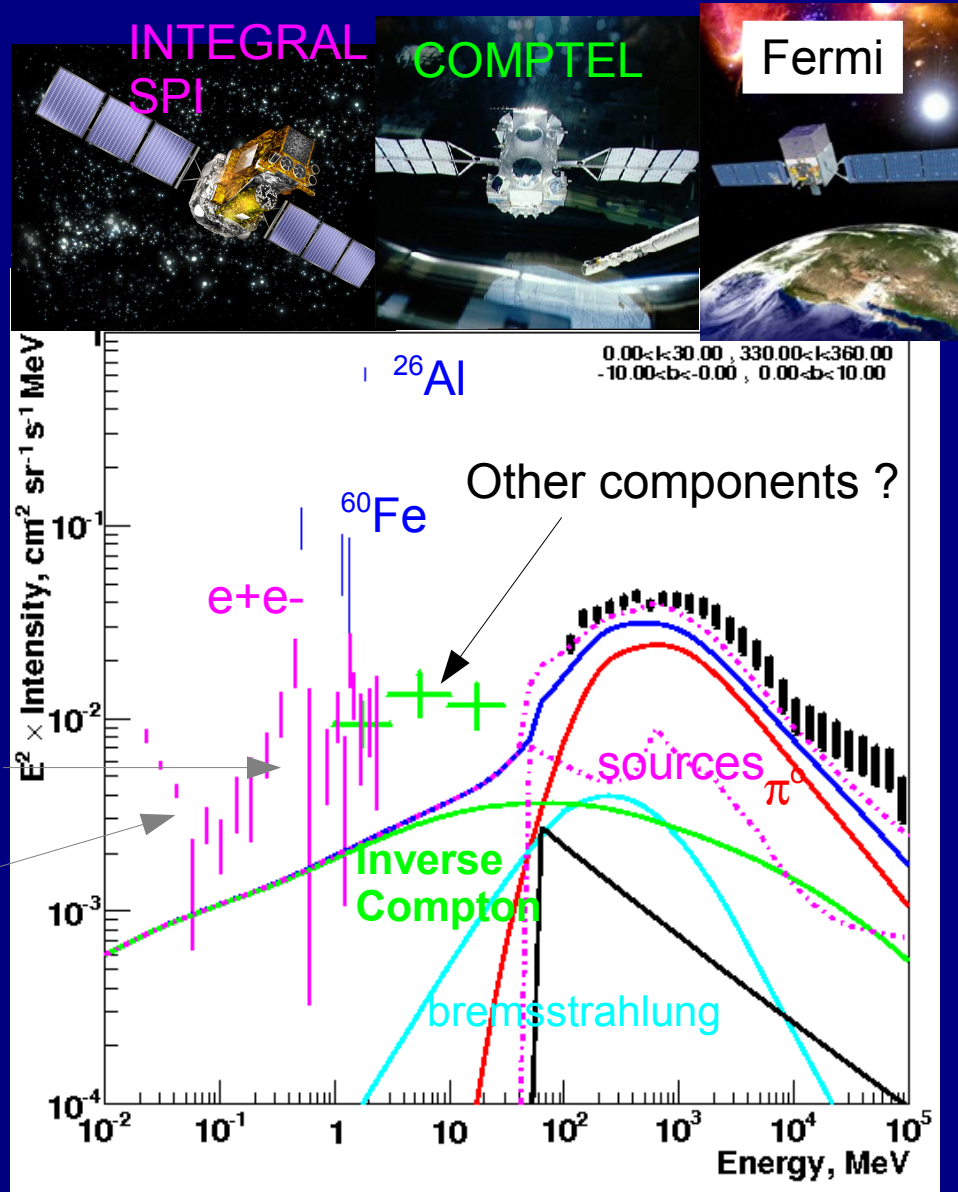
Min                                    Max

27−49 keV

100−200 keV

200−600 keV

Inner Galaxy
INTEGRAL / SPI
Bouchet et al. ApJ 739, 29, 2011

# Inner Galaxy: keV to TeV



GeV electrons – inverse Compton -  important  for MeV gamma rays !

Reminder that Galaxy contains ~50000 gamma-ray sources, mainly pulsars

Fermi-LAT detected only about 250 so far (and more: unassociated sources)

O  The brightest
O  The nearest

Tip of the iceberg!

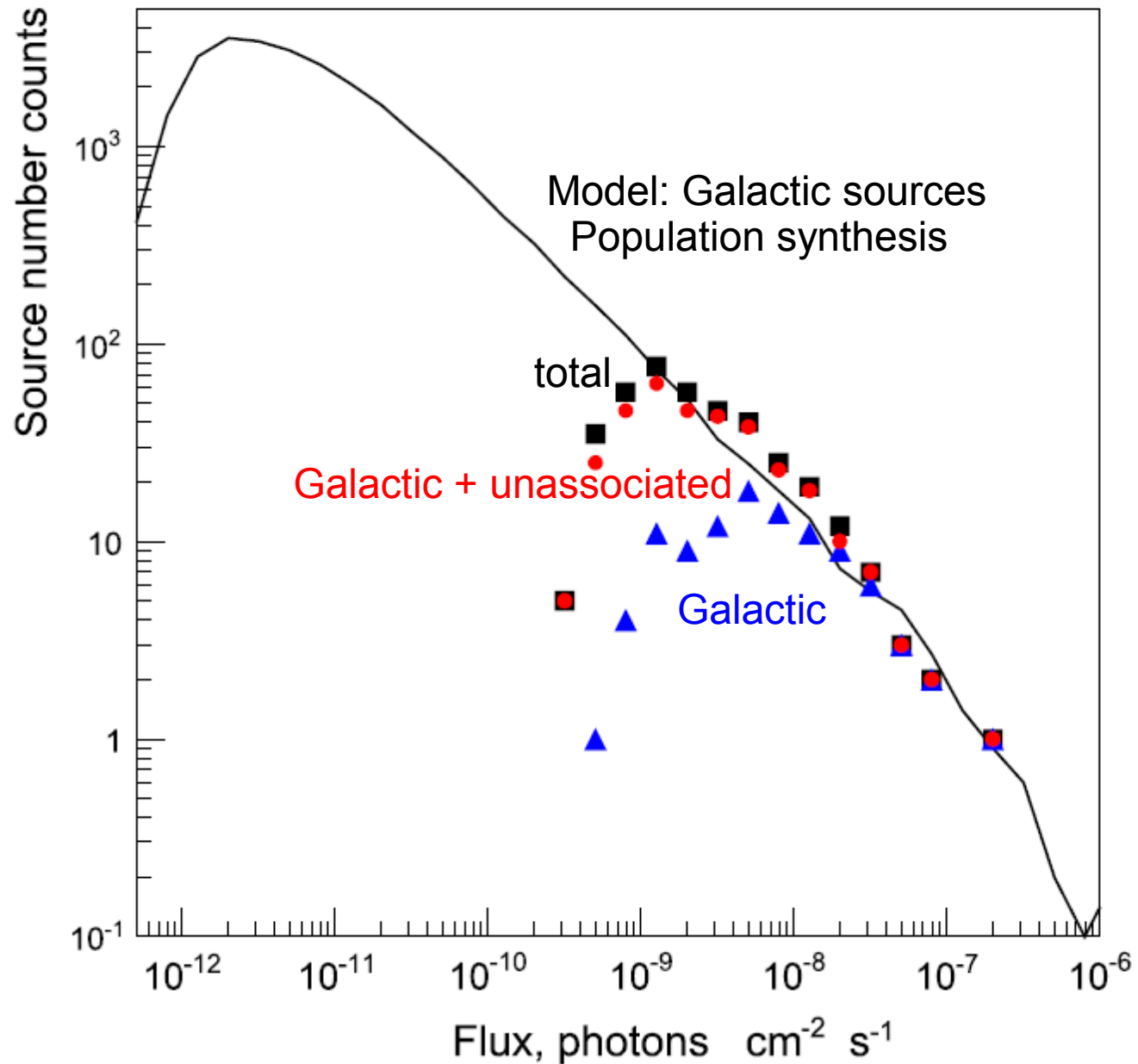Model source population synthesis, Fermi 3FGL paper Section 6.2

(a) Inner Galaxy

Fermi-LAT
3FGL paper
Section 6.2
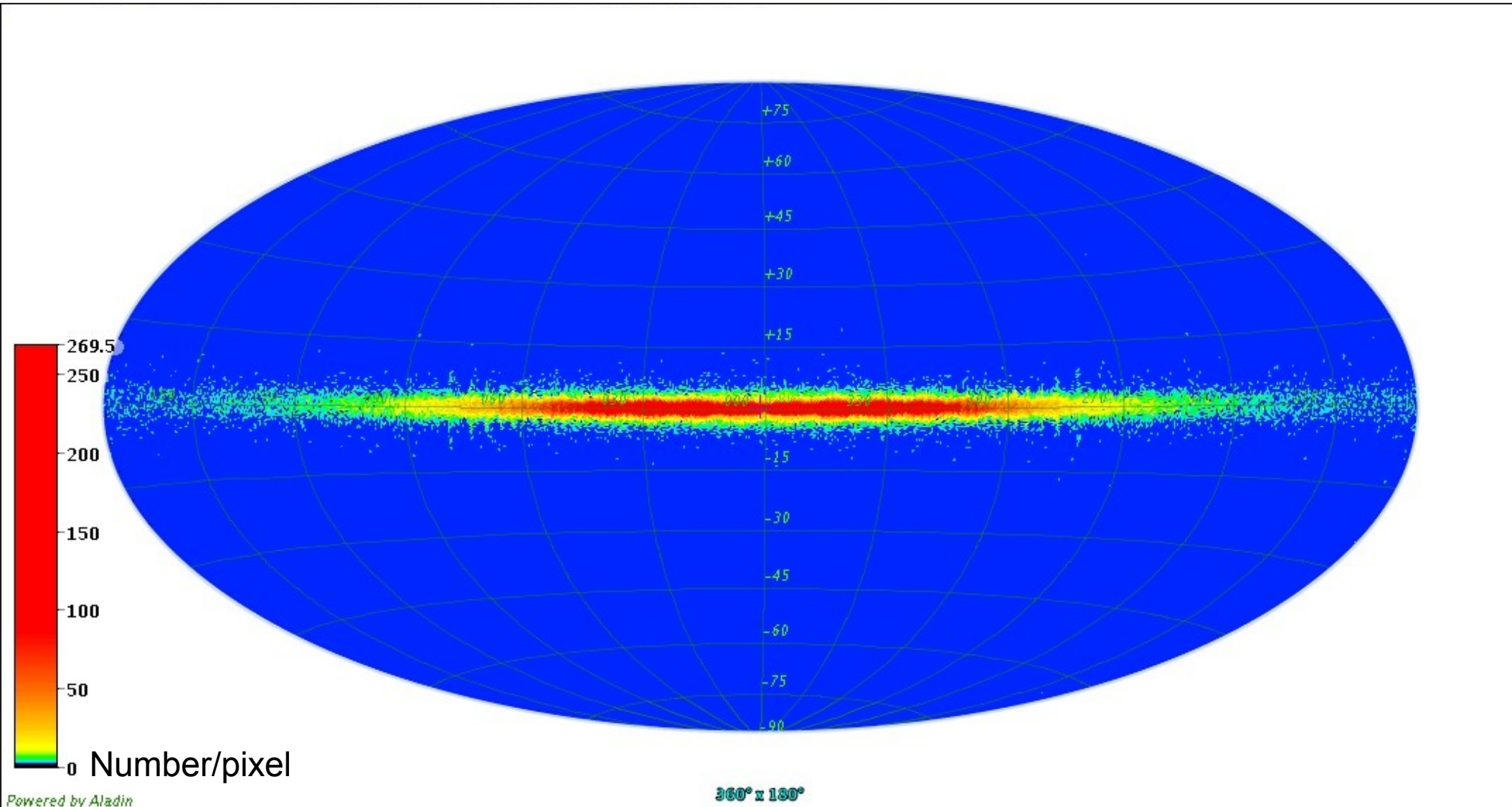
Source
Differential
number
Counts

N(S)

Inner Galaxy

$300° < l < 60°$
$|b| < 10°$

# "All sources in the Galaxy"
## (according to one particular model)



Number/pixel

Powered by Aladin

360° x 180°

END